A NEURAL NETWORK BASED IONOSPHERIC MODEL FOR THE BOTTOMSIDE ELECTRON DENSITY PROFILE OVER GRAHAMSTOWN, SOUTH AFRICA

A thesis submitted in fulfillment of the
requirements for the degree of

DOCTOR OF PHILOSOPHY

of

RHODES UNIVERSITY

by

Lee-Anne McKinnell (née Williscroft)

June 2002

ABSTRACT

This thesis describes the development and application of a neural network based ionospheric model for the bottomside electron density profile over Grahamstown, South Africa. All available ionospheric data from the archives of the Grahamstown (33.32ºS, 26.50ºE) ionospheric station were used for training neural networks (NNs) to predict the parameters required to produce the final profile. Inputs to the model, called the LAM model, are day number, hour, and measures of solar and magnetic activity. The output is a mathematical description of the bottomside electron density profile for that particular input set.

The two main ionospheric layers, the E and F layers, are predicted separately and then combined at the final stage. For each layer, NNs have been trained to predict the individual ionospheric characteristics and coefficients that were required to describe the layer profile. NNs were also applied to the task of determining the hours between which an E layer is measurable by a ground-based ionosonde and the probability of the existence of an F1 layer. The F1 probability NN is innovative in that it provides information on the existence of the F1 layer as well as the probability of that layer being in a L-condition state - the state where an F1 layer is present on an ionogram but it is not possible to record any F1 parameters. In the event of an L-condition state being predicted as probable, an L algorithm has been designed to alter the shape of the profile to reflect this state. A smoothing algorithm has been implemented to remove discontinuities at the F1-F2 boundary and ensure that the profile represents realistic ionospheric behaviour in the F1 region.

Tests show that the LAM model is more successful at predicting Grahamstown electron density profiles for a particular set of inputs than the International Reference Ionosphere (IRI). It is anticipated that the LAM model will be used as a tool in the pin-pointing of hostile HF transmitters, known as single-site location.

ACKNOWLEDGEMENTS

Special thanks to my supervisor, Prof Allon Poole, for inspiring and supporting my interest in this field over many years.

The South African DPS systems are owned and maintained by GrinTek Ewation. I thank them and in particular Hannes Coetzee, for allowing access to the ionospheric data collected from the Grahamstown station and for frequent technical support.

The magnetic data used for this research was obtained from the Hermanus Magnetic Observatory (HMO). I acknowledge the use of this data and thank Louis Loubser of HMO for making access to this data possible.

Thank you to the German Academic Exchange Service (Deutscher Akademischer Austauschdienst/DAAD) for providing financial support in the form of a DAAD scholarship from 1999 to 2001 inclusive.

I thank Althea Coupé and Prof Graham Poole for support and encouragement throughout the preparation of this thesis.

And finally, thank you John, for believing in me and providing support in more ways than can be mentioned.

TABLE OF CONTENTS

LIST OF FIGURES

Chapter 1

Chapter 3

Chapter 4

Chapter 5

Chapter 6

Chapter 7

Chapter 8

Chapter 9

LIST OF TABLES

Chapter 5

Chapter 6

Chapter 1

INTRODUCTION

In this thesis I present research into the development of an ionospheric model for the bottomside electron density profile over Grahamstown, South Africa (33.32°S, 26.50°E). The bottomside ionosphere is that region of the upper atmosphere lying between about 80 km and 350 km. This region of the ionosphere is divided into layers, referred to as E, F1 and F2. The division of the bottomside ionosphere into layers and the physical processes that give rise to these layers are described in detail in *McNamara [1991]* and *Davies [1990]*.

1.1 Ionospheric Data

The behaviour of the ionosphere is monitored by using an ionospheric sounder called an ionosonde. Each sounding produces an ionogram, a graph of virtual height versus frequency that represents the response of the ionosphere to diurnal, seasonal, solar and magnetic variations. These variations are the main variables that need to be considered when developing an ionospheric model. However, there could be other minor variations that induce ionospheric response. The process of interpreting the ionograms and recording ionospheric parameters from the ionograms is called scaling. Each ionogram can be converted into an electron density profile, n(h). This profile represents how the electron density varies with real height. An example of a daytime ionogram with its corresponding electron density profile is shown in figure 1-1.

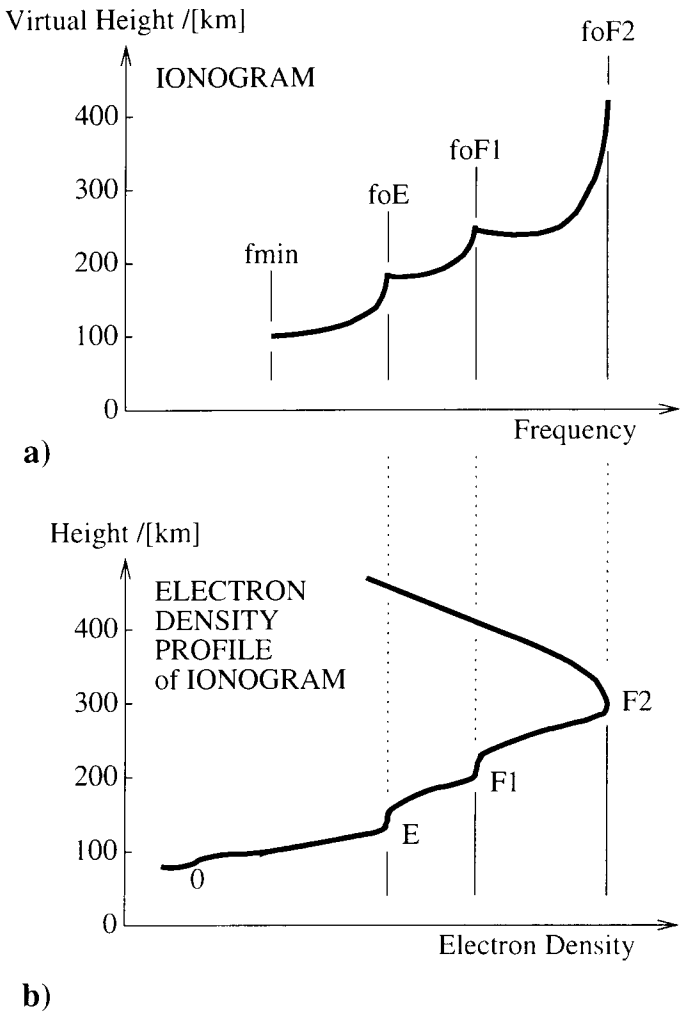

Figure 1-1: a) A daytime ionogram and b) its corresponding electron density profile. The critical frequencies and electron densities for each layer are indicated.

It is often more convenient to work with a frequency versus real height profile, f(h). Electron density is simply related to frequency by the equation:

$$N/m^{-3} = 1.24 \times 10^{10} \left(f/MHz\right)^2 \qquad (1\text{-}1)$$

For the past 29 years vertical incidence ionospheric data has been collected at the Grahamstown ionospheric station. Prior to 1996 a Barry Research Vertical Chirp Sounder (Verti) was used to collect the data, which was then manually scaled. In 1996 a Digital Portable Sounder (DPS) system was installed. This DPS system was designed and built by the University of Massachusetts Lowell Center for Atmospheric Research (UMLCAR). The DPS operates on a pulse sounding technique *(UMLCAR, [1996])*.

The data from the DPS is automatically scaled using UMLCAR software, called **Artist**. The **Artist** scaling software records the ionospheric characteristics and gives a description of the electron density profile. This description can take the form of a listing of real heights with their corresponding electron densities or a set of Chebyshev coefficients and peak heights. The output from **Artist** is recorded in Standard Archiving Output (SAO) format. SAO format has become the international standard format for recording ionospheric data. *Galkin [1998]* gives a full description of the SAO format.

The Grahamstown ionograms that were measured with the Verti sounder were manually scaled. Therefore the ionospheric data for the period January 1973 to April 1996 only has information on the important ionospheric parameters *(Wakai et al., [1985])* and their virtual heights. There is no real height information for this period at all.

Current global ionospheric models, such as the International Reference Ionosphere (IRI), do not perform well in the South African region. This is mostly due to an historic paucity of available data in this area. In South Africa there are now two other ionospheric stations continuously collecting data in addition to the Grahamstown station, namely, Louisvale (28.51°S, 21.24°E) and Madimbo (22.38°S, 30.88°E), which have only been operational for one year.

Grahamstown has the largest archived ionospheric database in the Southern African region, which makes it an excellent base from which to design an ionospheric model.

1.2 Neural Networks

Throughout this thesis neural networks (NNs) are used as a tool for predicting different parameters that make up the ionospheric model. Briefly a NN is a computer program that is trained by presenting to its input any number of multi-dimensional input vectors that correspond to a known measured parameter. The NN learns to identify the relationship between the input vectors and the known output. *Haykin [1994]* and *Fausett [1994]* give detailed information on the concept of NNs.

The NN software package used for training the NNs required for this project was version 4.2 of the Stuttgart Neural Network Simulator (SNNS). SNNS (*SNNS, [1995a])* was developed by the University of Stuttgart Institute for Parallel and Distributed High Performance Systems and is available via the Internet (*SNNS, [1995b])*.

The most important requirement for training NNs is access to a large database. For ionospheric modelling the dataset should ideally span at least 22 years, being 1 solar cycle. In the case of each layer's peak electron density the available Grahamstown data contains more than 22 years worth. For the real height and complete profile information there are only 5 years of data available. However, it is still possible to set up the model and prove that it performs accurately. The advantage of NNs is, that once they are set up and the input space is decided, it will be a relatively simple procedure to retrain when additional data becomes available.

The standard NN architecture that has been used throughout consists of one input layer, one hidden layer and one output layer. Unless stated otherwise the number of nodes in the hidden layer is 15. The input and output nodes are dependent on the parameter the NN is being trained to predict.

Training the NN is an iterative process that starts with randomly chosen weights in the NN model *(Haykin, [1994])*. Identical results for the same training data but different starting conditions are not guaranteed. For each NN required in the development of this model twenty five NNs were trained, all with the same NN

architecture and training sets but with different starting weights. The mean output from these NNs is the output used. This was done to minimize the effects of statistical variability. *McKinnell [1996]* and *Williscroft and Poole [1996]* show how neural networks can be applied to the task of ionospheric modelling.

1.3 An Application

The main application for this new ionospheric model is in the field of Direction Finding (DF) systems. DF systems are used to find the location of a transmitter by measuring the elevation angle and azimuth of the incoming signal. The accuracy of any DF system relies on a good knowledge of the behaviour of the ionosphere and how this behaviour changes over time. With a good ionospheric model the radio waves can be traced back from the DF site to the transmitter and the location of the transmitter determined. This technique is referred to as reverse ray tracing. Both High-Frequency (HF) communicators and DF stations benefit from a reliable ionospheric model.

GrinTek Ewation is a company that designs and builds DF systems. I am investigating with them the possibility of incorporating my model into their DF systems to enable them to improve the accuracy of their current systems.

1.4 Towards a New Ionospheric Model

The ionospheric model required to do ray tracing should take the form of a model for predicting the variation of electron density with height. In my master's thesis, *McKinnell [1996]*, I dealt with the prediction of the peak ionospheric electron density, foF2. I used NNs to predict foF2 for the Grahamstown station given day number, time of day, sunspot number and the magnetic index a_k.

In this thesis I expand upon this method by using NNs to produce a model for the entire bottomside electron density profile. A model f(h) profile is shown in figure 1-2. The f(h) model is split into two main sections, the E layer (fsE to foE,

including the valley) and the F layer (fsF1 to foF2). The contribution of each layer to the final NN based model is developed separately. The model layers are combined to form a smooth f(h) profile that can easily be converted to its equivalent n(h) profile.

During the process of developing this model I show how NNs can be used to determine different ionospheric states such as the presence of a F1 layer. I investigate a solution to the F1 ledge problem and introduce a new technique for smoothing out the electron density profiles to ensure more realistic results.

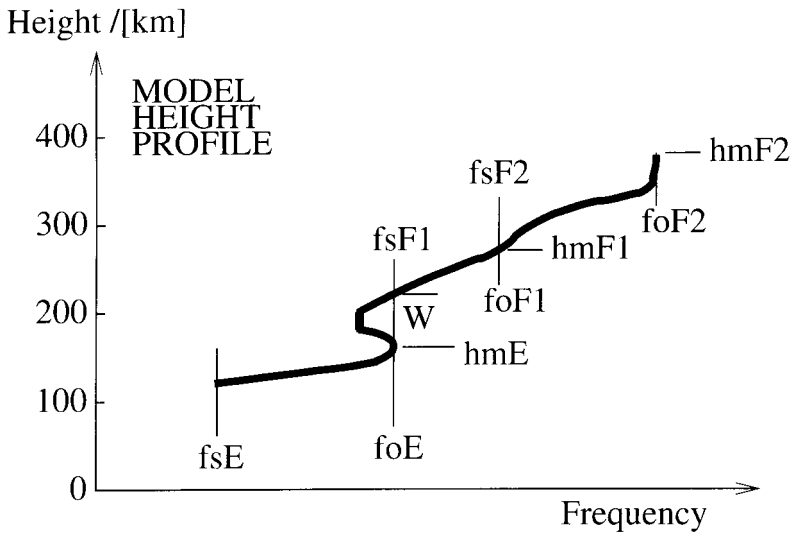

Figure 1-2: A model f(h) profile. The start and end points of each section as well as other required parameters are shown.

The next chapter in this thesis describes existing ionospheric models that I have utilized at different stages in the development of my model. Initial attempts to find a suitable technique are described in chapter 3. The following chapters detail the process of developing each model layer and the final outcome. Finally, I show that I have achieved the aim of producing a model for the ionosphere over Grahamstown, South Africa. This model can be easily expanded and improved to cover the whole of South Africa and all ionospheric events. I also show that this model has an improved accuracy for predicting ionospheric behaviour over the International Reference Ionosphere (IRI), which is the current model used.

Chapter 2

EXISTING MODELS

2.1 Introduction

Various groups have attempted to model the bottomside ionosphere and its parameters. The ionospheric models discussed in this chapter are the International Reference Ionosphere (IRI), the Titheridge model and the University of Massachusetts Lowell Center for Atmospheric Research (UMLCAR) model. These models are used either for comparison or in conjunction with the new NN based ionospheric model.

Mostly due to a lack of data from the Southern African region, global ionospheric models do not in general perform well at predicting ionospheric behaviour at these latitudes. It is possible that the South African NN based model developed in this thesis can be used to assist with improving these global models.

2.2 The International Reference Ionosphere

The International Reference Ionosphere (IRI) is an international project jointly sponsored by the Committee on Space Research (COSPAR) and the International Union of Radio Science (URSI). These organizations formed a Working Group in the late nineteen sixties to produce an empirical standard model of the ionosphere, based on all available data sources. This Working Group meets on an annual basis to discuss and implement improvements to the IRI model.

For a given location, time and date, IRI describes the electron density, electron temperature, ion temperature, and ion composition in the altitude range from about 50 km to about 2000 km, as well as the electron content. It provides monthly averages of these parameters for magnetically quiet conditions.

Since inception several improved versions of the IRI have been released. The latest three versions are referred to as IRI 90, IRI 95 and IRI 2001. *Bilitza [1990]* gives a detailed description of the IRI 90 model while *Bilitza [1997]* and *Bilitza [2001]* provide details of the subsequent improvements. In *McKinnell [1996]* I discussed the IRI with reference to predicting ionospheric characteristics for Grahamstown and made some comparisons with the foF2 value. Some details on the IRI's prediction method will be provided in the relevant chapters of this thesis as required, but for full details the reader is referred to the abovementioned publications.

Although the IRI is based on all major ionospheric data sources, no Southern African data was used and, therefore, the IRI does not do particularly well at predicting ionospheric conditions in South Africa. Despite this, up until now, the IRI has been the best empirical ionospheric model available in the Southern African region. I will use the IRI to make comparisons with the NN based model. Part of the aim in developing this model is to provide a better ionospheric model for South Africa.

The National Space Science Data Center (NSSDC) provided the IRI 2001 model in the form of Fortran subroutines. I wrote a front-end Fortran program to take year, day number and hour and use those subroutines to produce an electron density profile for comparison purposes. In predicting the bottomside profile, the IRI 2001 version has only improved on previous versions in the F1 region.

2.3 The UMLCAR Model

The University of Massachusetts Lowell Center for Atmospheric Research (UMLCAR) is the birthplace of the DPS, the equipment currently gathering data at the three South African stations. The software that controls the DPS and scales the data is also a product of UMLCAR. Artist, the scaling software, scales the ionogram and inverts it to produce an electron density profile. This inversion technique is the basis of the UMLCAR model, and details of this procedure can be found in *Huang and Reinisch [1996]*. More information on the scaling procedure plus the inversion process can be found in *Reinisch and Huang [1983]*.

This section describes the part of the UMLCAR model that approximates the E layer. The UMLCAR model for the E layer assumes a parabolic profile shape. For the section of the profile leading up to the peak of the E layer, hmE, the frequency, f, at each height, h, can be calculated as follows *(Huang and Reinisch, [1996])*:

$$f^2 = foE^2 \times \left[1 - \left(\frac{h - hmE}{y}\right)^2\right] \qquad (2\text{-}1)$$

where y is the layer half-thickness at f = 0.0 MHz, foE is the E layer critical frequency and hmE is the peak height. The layer half-thickness is the difference between hmE and the height at f = 0.0 MHz. When a measurement is possible, the DPS measured values of foE and hmE are used otherwise predicted values are used. UMLCAR uses the same method as the IRI for predicting foE. This method takes the form of an analytical equation, which has four terms. These terms are made up of a solar activity factor, a seasonal factor, a latitude factor and a time of day factor. The full form of this expression appears in *Bilitza, [1990]*. For hmE a constant value of 110 km is used when no measured value is available.

The UMLCAR model for the E layer is used in conjunction with the NN based model for the E layer. The details of this appear in chapter 4. Details of other parts of the UMLCAR model will appear as required.

2.4 The Titheridge Model

Dr John Titheridge is the author of the generalized program POLAN *(Titheridge, [1985])*. POLAN is an ionogram analysis software package that takes raw ionograms, scales them and inverts them to produce a n(h) profile in a similar way to the task that the ARTIST software performs.

Dr Titheridge has completed extensive research into modelling the E layer peak *(Titheridge, [2000])*, using a chemical analysis of the atmospheric processes at work as the electron density at the peak (NmE) changes. It is this part of his model that will be used in this thesis. *Titheridge [2000]* presents analytical equations for the calculation of NmE and hmE. The predicted values for NmE and hmE are calculated as functions of latitude, season, hour and solar flux. These equations are valid for all conditions, nighttime and daytime.

The foE value is calculated from the NmE value using equation 1-1 and is much better behaved in the Titheridge model than in the IRI. A simple equation for calculating the hmE value is preferred over the constant value quoted by the IRI. Fortran programs for calculating NmE and hmE were obtained from Dr Titheridge, and these were converted to C programs to use in conjunction with the NN based model for foE and hmE. This combination of the models will be discussed in chapter 4.

2.5 Conclusion

The IRI is currently the best available global ionospheric model, however, as will be shown later in this thesis, the IRI does not predict the ionosphere over South Africa very well. A disadvantage of the IRI is that it only gives monthly median values; the actual values can deviate by up to 30% due to large day-to-day variations. Also, the IRI takes the 12-month running mean sunspot number as an input. I shall use NNs to show that this is not the optimum solar activity input for predicting ionospheric characteristics. However, the IRI has undergone extensive international critical review and is constantly being improved. Hopefully, the NN based South African model will assist in the further improvement of the IRI.

The major advantage of the Titheridge model is that an attempt has been made to predict the value of hmE under all conditions. Most ionospheric models adopt the IRI's fixed hmE value of 110 km or a similar fixed value. Since measured hmE values have proven that hmE is variable, this area has been identified *(Bilitza, [1998])* as requiring further work.

The development of a new empirical ionospheric model for the prediction of the electron density profile including ionospheric parameters is presented in this thesis. This model will initially be a single station model that takes easily acquired input parameters and allows the description of the electron density profile to be available in different formats. I will name this new model the **LAM model,** and the presentation on the development of this model will begin in the next chapter.

Chapter 3

LAM MODEL: INITIAL ATTEMPTS

3.1 Introduction

Various groups (*Altinay et al [1997]*, *Williscroft and Poole [1996]*, *Wintoft and Cander [1999])* have used NNs for predicting the non-linear behaviour of the ionosphere. Mostly these groups have concentrated their efforts on predicting the critical frequency of the F2 layer, foF2, which is related to the peak ionospheric electron density by equation 1-1. *Stanislawska [2000]* has made an attempt at forecasting n(h) profiles at a single station by using NNs to predict the ionogram and then using the POLAN *(Titheridge, [1985])* inversion technique to determine the n(h) profile. The method of NNs has been shown to be successful in modelling the behaviour of the ionosphere over Grahamstown (*Williscroft and Poole [1996]*, *McKinnell [1996]*, *Poole and McKinnell [2000])*.

The requirements for the LAM model include (i) that the inputs should be easily acquired parameters, and (ii) that the predictions should be an improvement on similar predictions made by the IRI. This chapter describes the preliminary investigation into the use of NNs to produce a bottomside ionospheric electron density profile for Grahamstown, South Africa - the LAM model. This preliminary investigation was undertaken with the aim of proving the method in order to justify further research.

The contents of this chapter were presented at the 1999 International Reference Ionosphere (IRI) Workshop and were published in *McKinnell and Poole [2001]*.

3.2 The Data

This preliminary investigation was carried out in 1999. At that time only three years of electron density profile data was available for Grahamstown and the other two South African stations were not operational. The available data range spanned the period April 1996 to May 1999 inclusive. Although there is additional ionospheric data archived from before April 1996, this data does not contain any real height information. Therefore initial attempts excluded it.

The Artist scaling software that runs on the DPS can provide, on request and specification, electron density profile information as a set of (n, h) points, where n is the electron density in m^{-3} and h is the height in km. The height increments must be specified.

All the available electron density profile points were extracted from the Artist SAO format files. The n(h) profiles start at the height corresponding to an electron density of 4.96×10^8 m^{-3} and end at the peak height of the F2 layer, hmF2, proceeding in height increments of 5.0 km. The number of data points available exceeded 900 000 and were made up as follows: 1156 days (April 1996 to May 1999), 24 hours per day, 1 profile per hour, and approximately 35 points per profile.

3.3 The Inputs

The electron density in the ionosphere varies diurnally and seasonally. There can also be a response in the electron density to changes in solar activity and magnetic activity. In *McKinnell [1996]*, I showed that the peak electron density (foF2) is dependent on day number, hour, solar activity and magnetic activity. For these initial attempts at predicting the electron density at other heights I will make use of this information. As a requirement for training a NN, input parameters representing the variables that the output responds to are required.

Day number (DN), $1 \leq DN \leq 365$, represents the seasonal variation and hour (HR), $0 \leq HR \leq 23$, the diurnal variation. The HR input is in Universal Time (UT).

As explained in *Poole and McKinnell [2000]* the DN and HR inputs are split into their cyclic components and presented to the NN as four inputs, two for DN and two for HR. These four inputs are calculated as follows:

$$DNS = \sin\left(\frac{2\pi \times DN}{365}\right) \tag{3-1}$$

$$DNC = \cos\left(\frac{2\pi \times DN}{365}\right) \tag{3-2}$$

$$HS = \sin\left(\frac{2\pi \times HR}{24}\right) \tag{3-3}$$

$$HC = \cos\left(\frac{2\pi \times HR}{24}\right) \tag{3-4}$$

As a measure of solar activity a two month running mean value of the daily sunspot number, R2, was used. At this stage I chose not to investigate the solar activity input further, but to use the R2 value, which previously proved to be the optimum value for predicting the peak electron density (*Williscroft and Poole [1996]*, *McKinnell [1996])*. The range of R2 from April 1996 to May 1999 is on the increasing slope of the sunspot cycle, and varies in value from 0 to 100. This limits the input space to this range of R2.

In addition, for this preliminary stage, I restricted the dataset to 12 noon South African Standard Time (SAST) data only, therefore, the hour inputs were withdrawn from the input space. Magnetic influences were also excluded here.

3.4 The Electron Density at 150 km

An initial idea was to train separate NNs to predict the electron density at each height required to make up the profile. To investigate this idea, one height was initially selected and a NN was trained to predict the electron density at that height. For this first attempt, the dataset was limited to all 12h00 South Africa Standard Time (SAST) data. A height that lay well away from any peculiarities at that hour (e.g. the valley region) was chosen. This height was 150 km and the dataset was further limited to contain only those points at that height.

The range of electron density in any one profile can cover up to four orders of magnitude. Although this was not a problem when dealing with only one height at a time, the log of the electron density was used as the output. The inputs to the NN were DNS, DNC and R2, and the output was the log of the electron density, Log(n), at 150 km. The total number of input vectors that the NN was trained with was 983, 70% of which was used for training and 30% for testing the NN. Figure 3-1 illustrates the inputs and output to this NN, using a block diagram.

The nature of NNs is to provide an average output for a given input set. Figure 3-2 shows the dataset of 12h00 SAST measured values for Log(n) at 150 km. A predicted Log(n) at 150 km was obtained from the NN for every input vector, training and testing sets, and these values are also shown in figure 3-2. It can be seen from this graph that the NN has learnt the relationship between the input parameters and the output. Although the NN trained well, this would not be an ideal method for predicting the entire bottomside profile. Several NNs would need to be trained for every height required in the profile, and the number of points in a profile is not a fixed value and is very user dependent. It would be difficult to build in mechanisms to deal with the many different aspects of the profile (e.g. valley and F1 regions). Altogether this is an inelegant way of tackling the problem and it was abandoned at this stage. Therefore, an alternative method is presented next.

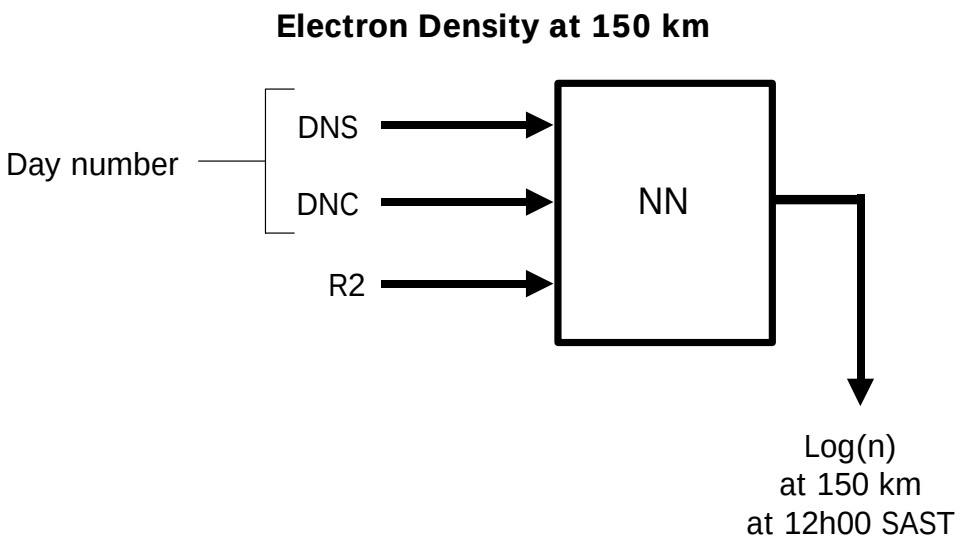

Figure 3-1: An illustration of the inputs and output to the NN that was trained to predict the electron density, n, at a height of 150 km at 12h00 SAST.

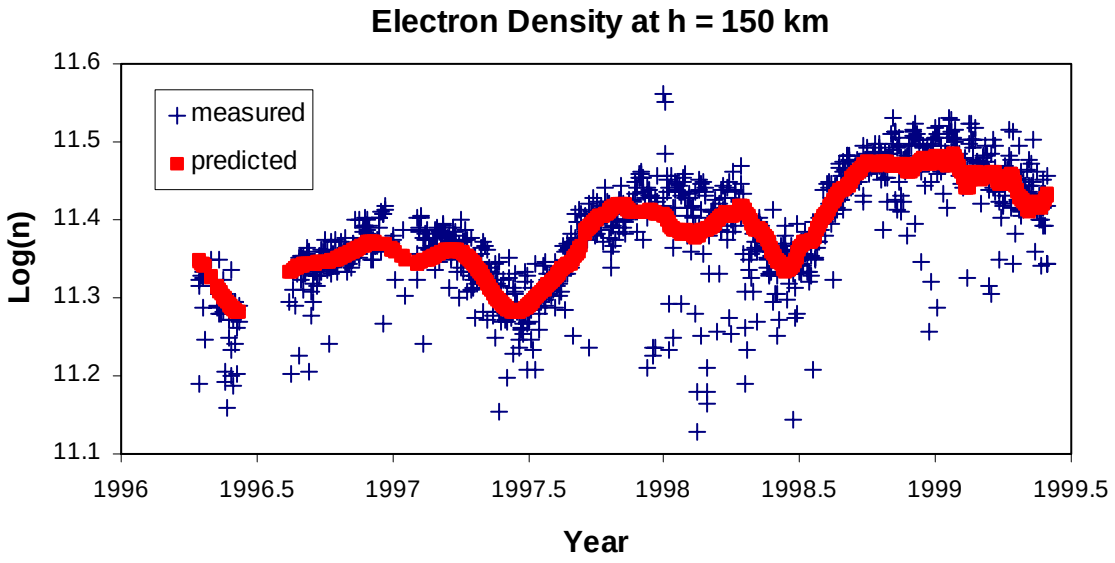

Figure 3-2: A graph of the measured and predicted values of the log of the electron density, Log(n), at a height of 150 km. These values are the 12h00 SAST values for Grahamstown for the period April 1996 to May 1999.

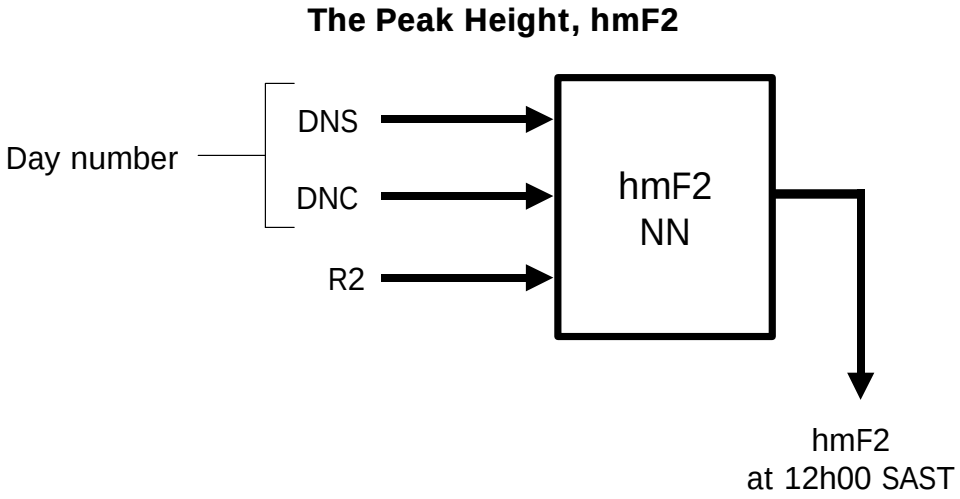

Figure 3-3: The hmF2 NN has three inputs and one output, which is the hmF2 value at 12h00 SAST.

3.5 The peak height, hmF2

The real height at which the critical frequency of the F2 layer, foF2, occurs is hmF2. The value of hmF2 indicates the peak height of the bottomside electron density profile, and is required if the entire profile is to be predicted. In this section I discuss an initial attempt to predict an hmF2 value that could be used when predicting the rest of the profile.

The value of hmF2 varies in a similar manner to foF2, in that it depends on day number (DN), hour (HR) and solar activity. The hour was again restricted to 12 noon SAST, and R2 was used as the measure of solar activity. A NN was then trained to predict the 12h00 SAST value of hmF2. The input vectors spanned three years from April 1996 to May 1999. Figure 3-3 shows a block diagram of the inputs and output for this initial hmF2 NN.

Figure 3-4 shows a distribution of hmF2 over the three year period. The predicted hmF2 values show that the NN produces an average value of hmF2 for each set of input data.

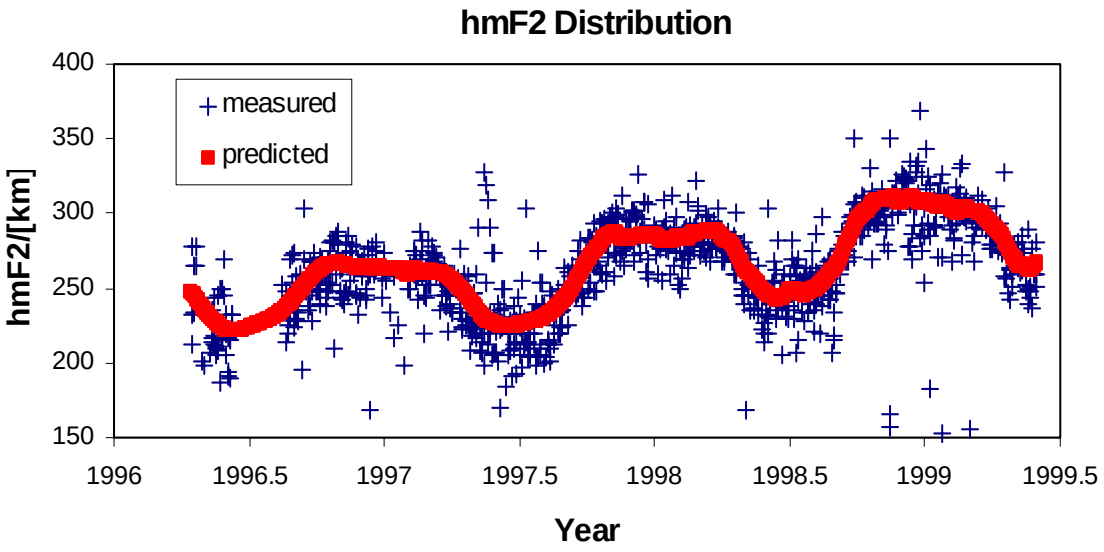

Figure 3-4: The distribution of the 12h00 SAST measured and predicted hmF2 values for Grahamstown for the period April 1996 to May 1999.

3.6 Electron Density Profile Prediction

In this section I make an attempt to predict the entire bottomside profile with one NN. As this was still a preliminary investigation, I again used inputs that had previously been shown to be optimal for the prediction of ionospheric characteristics (*Williscroft and Poole, [1996]*).

Inputs to the NN included DNS, DNC and R2, but excluded magnetic influences. Again only the 12h00 SAST profiles were used for training this initial NN and so the HS and HC inputs were excluded. Real height was included as an input and the output was the log of the electron density, Log(n), at that input height. Figure 3-5 shows the block diagram of the inputs and output of the initial profile prediction NN.

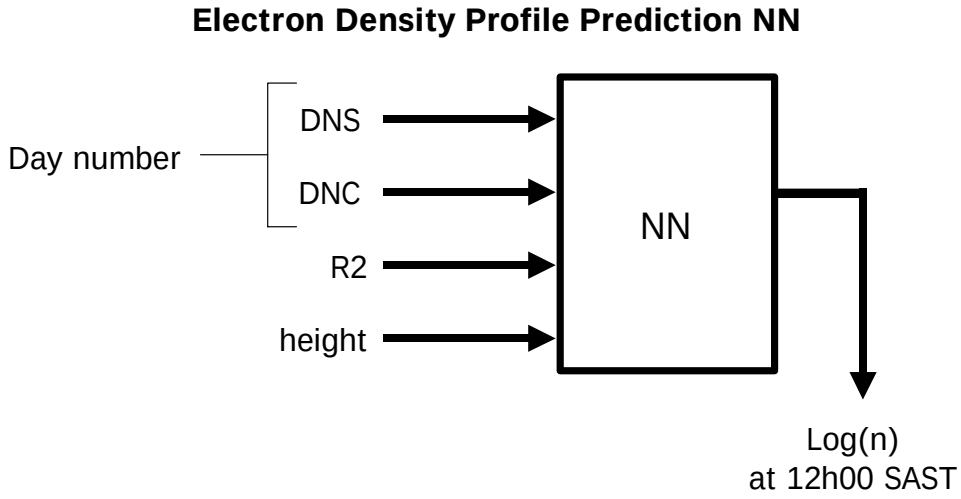

Figure 3-5: The electron density NN inputs and output. This NN predicts the log of the electron density, Log(n), at 12h00 SAST for the selected input set.

As a test of the NN's ability to predict the bottomside electron density profile, the NN was presented with input data corresponding to summer (DN = 1) and winter (DN = 180) at low, medium and high levels of R2. The low, medium and high values of R2 were chosen according to the percentage of R2 values (90%, 50% and 10% respectively) that lay above the value chosen. For example, the low R2 value was chosen such that 90% of all R2 values lay above that value. The R2 values that were used to determine these levels were those that appeared in the original dataset with which the NN was trained.

The hmF2 NN was used to predict an hmF2 value which provided the cut off height for the profile. Then the profile prediction NN predicted the electron density at input heights from 90.0 km to hmF2 in steps of 5.0 km. An average electron density profile was then predicted for each set of input data. These profiles are shown in figure 3-6.

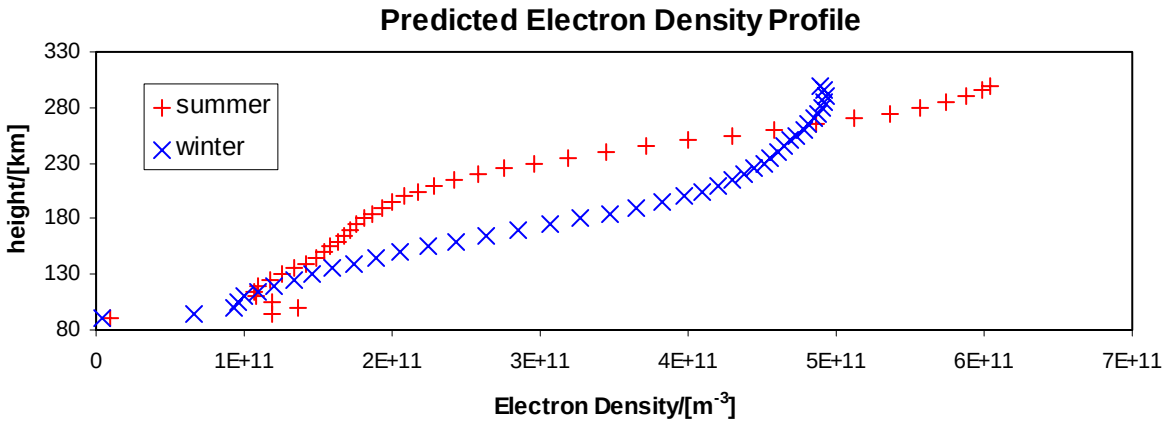

(a)

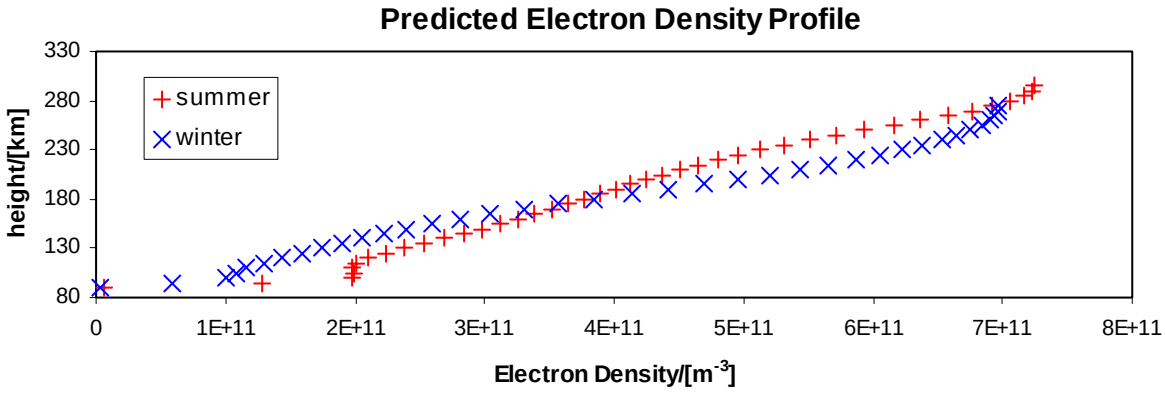

(b)

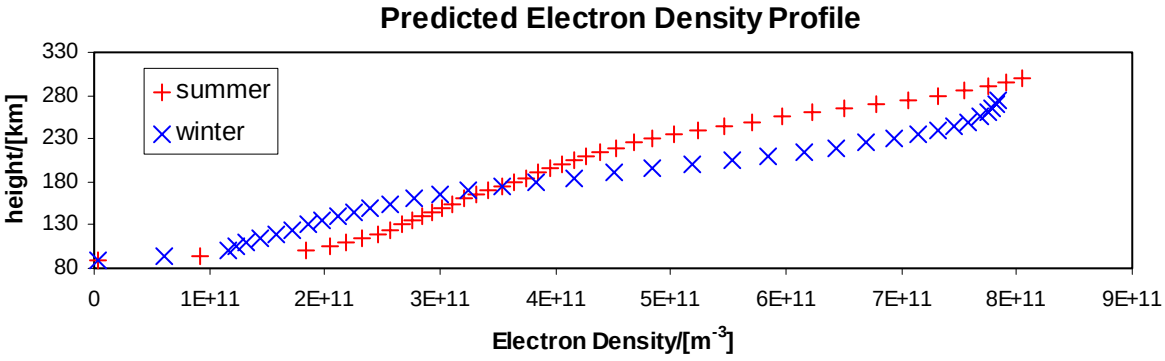

(c)

Figure 3-6: The average 12h00 SAST Grahamstown electron density profiles at (a) low R2 (R2=20), (b) medium R2 (R2=45) and (c) high R2 (R2=60) as determined by the NN for a test input set.

NNs interpolate well through the input space, therefore, although the NN was trained with a height increment of 5.0 km, the predicted profiles could have different height increments and the NN would still predict reasonable average profiles.

3.7 Conclusion

This chapter discussed preliminary investigations into the use of NNs for the prediction of bottomside profiles. As can be seen, from figures 3-2, 3-4 and 3-6, the NNs have successfully predicted the average shape and location of the electron density profiles. The ease with which NNs have gained the knowledge that allows for successful prediction shows that it will almost certainly be possible to produce a NN based electron density profile model.

For this investigation, DN and R2 were used as inputs to all the NNs. R2 was used as a measure of the solar activity because it has proved to be optimal for the prediction of foF2. Another solar time series may be more effective in predicting the shape of the entire profile, or different solar time series may be needed for different parts of the profile. The effect of magnetic influences was excluded from the initial attempts. A magnetic time series, A16, was shown to be required for the prediction of foF2 to allow for variations in magnetic activity (*Williscroft and Poole [1996]*, *McKinnell [1996])*. This requirement will need to be investigated for the entire profile. There may be other measurable and easily accessible parameters upon which the profile is dependent and, which could be used for improving the prediction.

The HS and HC inputs (equations 3-3 and 3-4) were also excluded as only 12h00 SAST data were considered. In future developments the NNs will need to be expanded to include all hours. Some thought is required here as different parts of the profile are not measurable at all hours, and a mechanism for handling those times will need to be developed.

Ideally one solar cycle (approximately 22 years) of ionospheric data is required in order to train a NN to its full potential. The dataset used for these initial attempts was severely limited in that it only spanned three years. This limited dataset can still be used to develop the model. It will be a relatively simple procedure to re-train the NNs once more data becomes available. The NN based model will be useable even if developed with a limited dataset, however, the user must be made aware of the limitations of the input space.

The larger archived data base that came from data measured by the Verti sounder (previously operational at Grahamstown) will be used for developing the critical frequency sections of the model while the smaller data base from measurements made with the DPS sounder will be used when real height information is required.

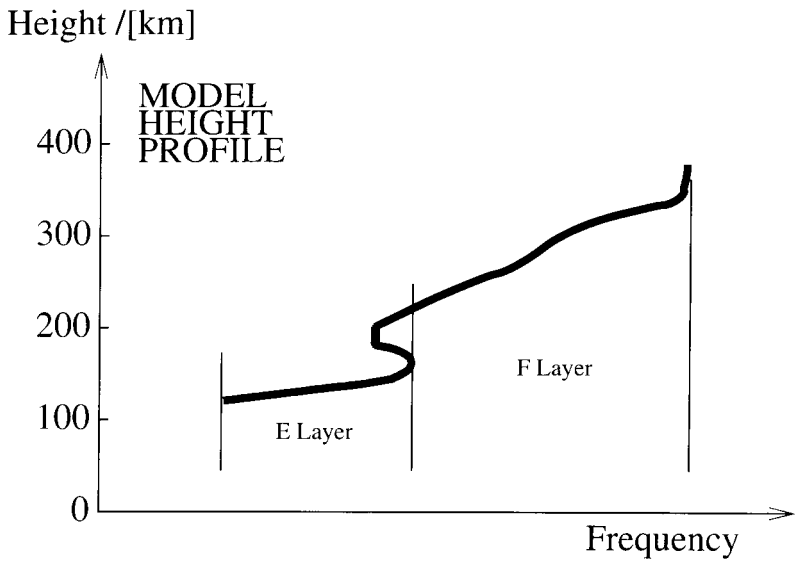

Figure 3-7: The model frequency versus height profile will be divided into two sections, the E layer and F layer, for the purposes of developing the LAM model.

The lower parts of the bottomside electron density profile, the E layer including the valley, were not predicted particularly well by these first NNs. It is possible that there were not enough data points available to adequately describe the shape of the profile in that region. In that case there would not have been sufficient examples available from which the NN could learn. The solution here would be to either train a separate NN to predict the E layer or to obtain more data points for that layer.

At this point I made the decision to develop the LAM model in two main sections, combining them at the end. Therefore, the model was split into the E layer and the F layer, which are shown in figure 3-7 and discussed in the following two chapters. Although NNs have been shown to successfully predict foF2 (*Williscroft and Poole [1996]*, *McKinnell [1996])*, these initial attempts inspire further confidence in the use of NNs as a tool for ionospheric prediction in the South African region.

Chapter 4

LAM MODEL: E LAYER

4.1 Introduction

In this chapter I present the development of the LAM model for the E layer. The subject of this chapter formed the basis of a paper that was presented at the 2001 International Reference Ionosphere (IRI) Workshop, (*McKinnell and Poole [2002]*).

The E layer is that region of the ionosphere from 85 km to about 150 km. Below the E layer is the D layer. The ionosonde is not able to take measurements from the D layer and, therefore, the lowest region for which South African data exists is the E layer.

An example of the E layer of a model electron density profile for Grahamstown, midday South African Standard Time (SAST), is shown in figure 4-1. This profile is shown as a height versus frequency profile, where the x-axis variable is frequency in MHz instead of electron density. Electron density is proportional to the frequency squared, as shown in equation (1-1), therefore, frequency will be used throughout this thesis, reserving the option to convert to electron density in the final model if required. In figure 4-1 the ionospheric characteristics that are important for defining the start and end points of the profile are indicated.

Several neural networks (NNs) have been designed to predict the parameters needed to describe the electron density profile in the E layer.

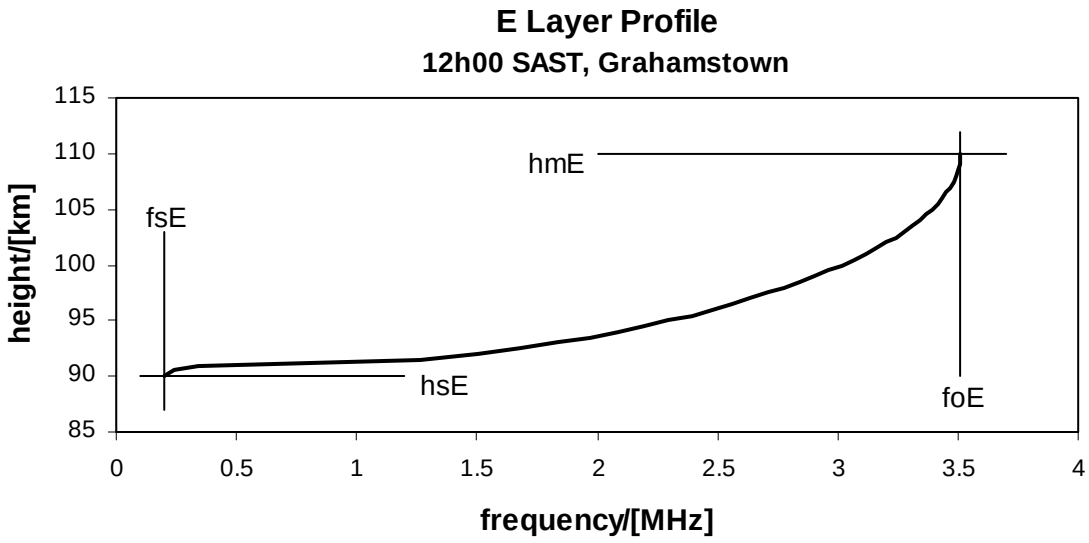

Figure 4-1: An example of a Grahamstown E layer profile for 12h00 SAST. The start and end points of the profile are labeled.

4.2 The Inputs

It is well known that the ionospheric E layer responds to seasonal, diurnal and solar changes (*Muggleton [1975]*, *Titheridge [2000])*. There is also a dependence on geographic position, but initially the LAM model will be a single station model and, therefore, geographic position is not considered as an input at this stage.

DNS, DNC, HS and HC represent seasonal and diurnal variations in the input space. These four inputs are defined in chapter 3 by equations (3-1) to (3-4).

The other inputs required were determined by using the peak characteristics to investigate the response of the E layer to various variables. Therefore, these inputs are discussed in the E layer peak section of this chapter.

4.3 The E Layer Peak

The maximum electron density in the ionospheric E layer is measured in terms of the critical frequency of that layer, foE, which is an easily measurable quantity. The peak height of the E layer, hmE, is the real height that corresponds to foE. These values, foE and hmE, have the units MHz and km respectively. The peak of the E layer is required in order to determine the profile. Therefore, the first step is to establish a model for foE and hmE.

4.3.1 foE

The IRI (*Bilitza [1990])* uses an analytical model for the prediction of foE developed by *Kouris and Muggleton [1973]* for the International Radio Consultative Committee (CCIR model). This model predicts the monthly median value of foE as a function of season, time, solar activity and geographic position. As a measure of solar activity the 12-month running mean value of the 10.7 cm solar radio flux is used. The contributions to this model are explained in detail in *Muggleton [1975]*. UMLCAR use the same CCIR model in the Artist scaling software to predict foE at times when no E layer measurements are possible (*Huang and Reinisch [1996])*. The IRI will be used as a comparison for predictions made by the LAM model.

Titheridge [2000] has developed a global analytical model for the peak of the E layer that is much simpler than the CCIR model used by the IRI. This model will be referred to as the JET model. The JET model prediction for foE depends on geographic latitude, season, local time and solar activity. At times when the LAM model is unable to make an E layer peak (foE, hmE) prediction, the JET model will be used.

The ionospheric data archive for the Grahamstown station contains 28 years of measured foE values. These values span more than one solar cycle and make an ideal dataset for using NNs to develop an empirical model for predicting foE.

4.3.1.1 Determining the inputs

As a measure of the solar activity the sunspot number (SSN) was considered. Most ionospheric models have adopted the procedure of using a 12-month running mean value of the daily SSN (R12) as the solar activity input. In particular the IRI requires R12 as an input (*Bilitza [1990])*. *Williscroft and Poole [1996]* and *McKinnell [1996]* show that a 2-month running mean value of the SSN (R2) is an optimum input for predicting the peak ionospheric electron density (foF2). In *McKinnell [1996]* I used NNs to determine the optimum length of time over which the daily value of the SSN should be averaged in order to predict the noon value of foF2. The same method is used here to determine the SSN input required for predicting foE.

Eight different NNs were trained and tested with five inputs and one output. The first four inputs were DNS, DNC, HS, and HC, for all eight NNs. Running means of the daily sunspot number over the preceding $^1/_{30}$, $^1/_2$, 1, 2, 4, 8, 12 and 16 months made up the fifth input for the corresponding NN. The output was the foE value in MHz.

The root mean square (rms) error between the measured and predicted values of foE was used as a criterion for determining the optimum solar activity index.

Figure 4-2 shows the rms errors obtained for each of the eight NNs. From this graph it can be seen that R1 (1-month running mean value of the daily SSN) gave the lowest rms error.

Other models use the 10.7 cm solar radio flux (SF) as a measure of solar activity. No significant difference was found when comparing the rms errors obtained from using the SF index with those from using the SSN index. As the daily SSN value is more readily available than the daily SF value, R1 will be used as the solar activity input for predicting the foE value.

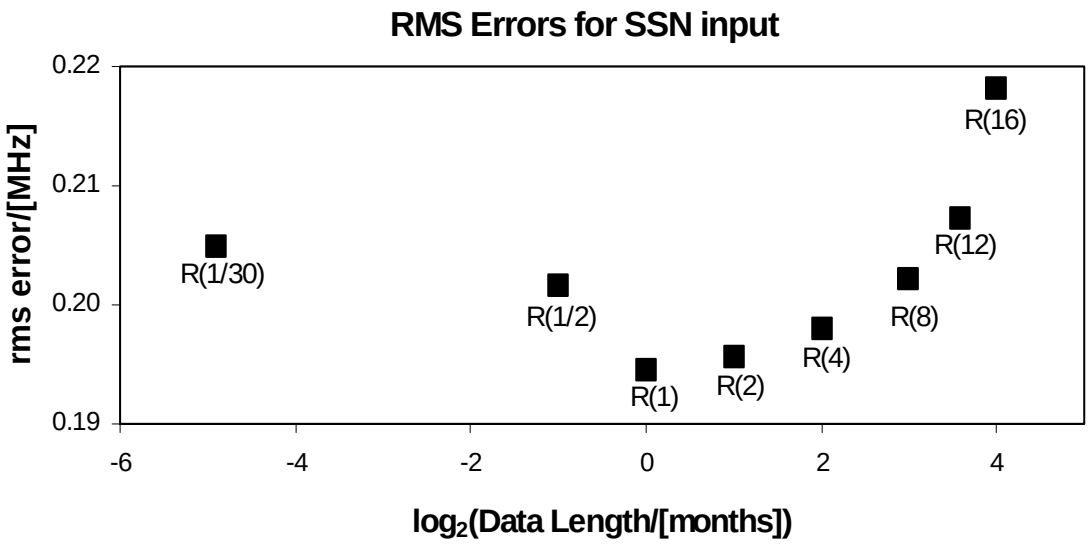

Figure 4-2: This graph shows the rms errors between the measured and predicted foE values. The rms errors apply to eight different NNs, each trained with a different time length of daily SSN as the solar activity input. The optimum time length appears to be near one month.

Another variable that could be used as an input to the foE NN is the zenith angle (ZA), which can be calculated analytically if the year, day number and hour are known. To find the response of foE to ZA, a NN was trained with R1 and ZA as inputs. The rms error between the measured and predicted foE values increased slightly when using ZA instead of the DN and HR inputs. It made no difference to the rms error when ZA was included with DN, HR and R1. The ZA input was providing no additional information to the input space that could improve the prediction of foE.

McKinnell [1996] and *Williscroft and Poole [1996]* show how foF2 responds to a magnetic activity input. The procedure for determining the optimum magnetic activity index is the same as the procedure for determining the optimum solar activity index and is reported in full in both of these publications. A similar procedure was carried out to determine the response of foE to magnetic activity.

The addition of a magnetic activity input resulted in an improvement in the rms error of 0.5%. This was considered not significant enough to warrant the addition of another input and, therefore, the magnetic activity input was excluded from the training of the E layer NNs.

4.3.1.2 Training the foE NN

The architecture of the NN that was trained to predict the foE value was made up of one input layer with 5 nodes, one hidden layer with 15 nodes and one output layer with 1 node. A block diagram of the inputs that were presented to the NN (DNS, DNC, HS, HC, and R1) and the corresponding output (foE in MHz) is shown in figure 4-3. The dataset consisted of all measured data from 1973 to 2000 inclusive and totalled 88443 input vectors. Of that dataset, 70% was used for training and 30% for testing.

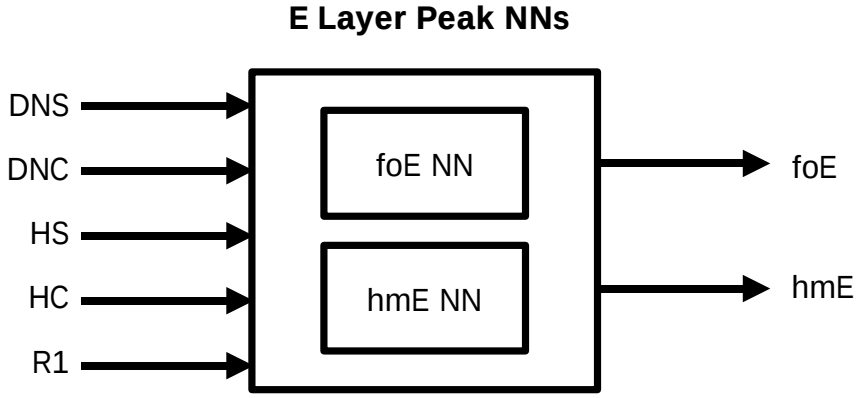

Figure 4-3: This block diagram shows the inputs used for training the NNs that predict the peak characteristics of the E layer, foE and hmE.

4.3.2 hmE

The IRI does not use a model to predict hmE but assumes a constant height of 105 km in the IRI 90 version and 110 km in the IRI 95 and IRI 2001 versions (*Bilitza [1990]*, *Bilitza [1998])*, under all conditions. It has been recognized (*Bilitza [1998])* that this is not a good assumption for the hmE value since available data shows a dependence of hmE on latitude, season, time and solar activity. A few groups have attempted to provide a model for hmE.

Titheridge [2000] has developed a simple analytical model for the hmE value that estimates variations of hmE with latitude, season, local time and solar flux.

Ivanov-Kholodny et al. [1998] have used data from a mid latitude incoherent scatter radar to establish an empirical hmE model. They predict hmE at this latitude using seasonal, diurnal and solar inputs and then extend their model to other latitudes using the solar zenith angle.

The procedure followed in the development of the LAM model for predicting the hmE parameter is similar to that employed in developing the LAM model for predicting foE. I shall refer back to the foE section of this chapter for procedures that were discussed earlier but are also relevant here, and use this section to describe items that are unique to the hmE model.

Almost five years of hourly measured hmE values are available for the Grahamstown station. This dataset spans the period April 1996 to December 2000 inclusive and covers the solar cycle from minimum to maximum. Although this is not a comprehensive dataset, there is still enough available data for a NN to be set up and trained to predict hmE to suitable accuracy.

4.3.2.1 Determining the inputs

The seasonal and diurnal changes are discussed in chapter 3 and the inputs representing these changes are as shown in equations (3-1) to (3-4).

To determine the solar dependence of hmE the SSN was used and a similar procedure to that for foE was followed. Eight NNs were trained each with the DN

and HR inputs plus an input representing the level of solar activity. This solar activity input took the form of running means of daily SSN over the preceding $^{1}/_{30}$, $^{1}/_{2}$, 1, 2, 4, 8, 12 and 16 months. As was the case for the prediction of foE, the 1-month running mean SSN value (R1) was found to be an optimum measure of the solar activity for predicting hmE.

The solar zenith angle (ZA) was also considered as an input parameter here, but it did not contribute any further information towards improving the prediction of hmE. Therefore DNS, DNC, HS, HC, and R1 were used as inputs.

The available hmE data are restricted to five years, which imposes limitations on the input space with which the NN is trained. Figure 4-4 shows a graph of R1 versus DN that illustrates these restrictions. The R1 values in this graph are from 1996 to 2000, which covers solar minimum to the recent solar maximum, but there are still parts of the input space that are not sufficiently covered by the dataset. Although NNs interpolate reasonably well, they do not extrapolate well. The green squares in figure 4-4 represent examples of areas of the input space for which the NN is not sufficiently trained, and which should be avoided when interrogating the model. It is reasonably easy to re-train a NN, and a future plan is to re-train as soon as more data becomes available.

4.3.2.2 Training the hmE NN

A NN was trained to predict hmE using the available five years of measured hmE data and the same set of input parameters as for foE. A block diagram of the inputs that were presented to the NN (DNS, DNC, HS, HC, and R1) and the corresponding output (hmE in km) is shown in figure 4-3. The dataset consisted of all measured data from 1996 to 2000 inclusive, and totalled 10422 input vectors. Of that dataset, 70% was used for training and 30% for testing.

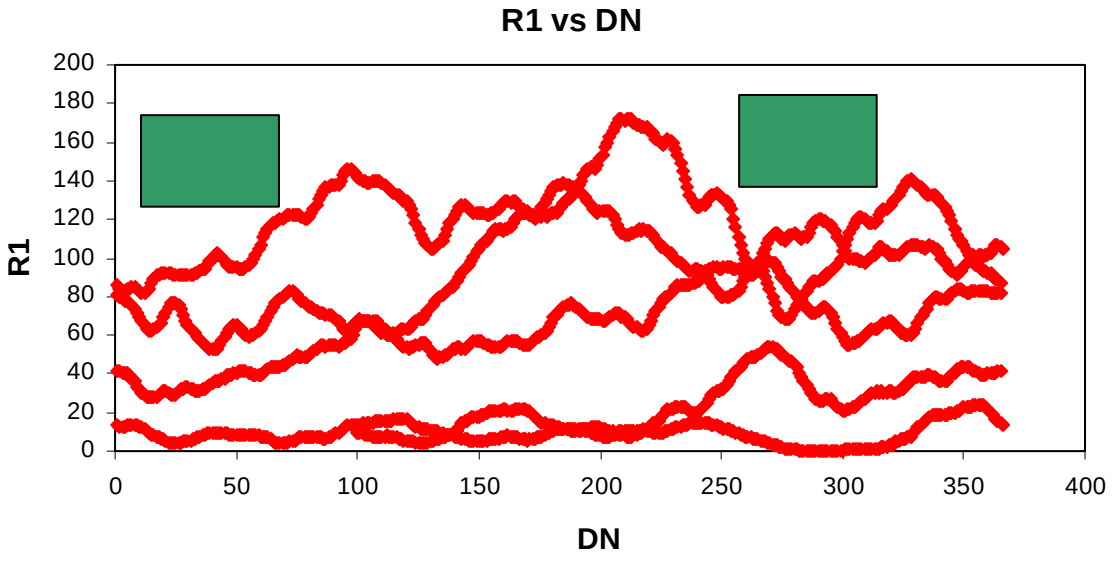

Figure 4-4: This graph illustrates the extent to which the input space (R1, DN) is covered by the limited available dataset. The green boxes indicate examples of areas that should be avoided when interrogating the NNs.

4.4 The E Limits NN

Another restriction on the E layer dataset is that the NN is only trained with data that is measured or derived from measured data. Measurements of the E layer are only available for the hours between sunrise and sunset. These hours vary with season and solar activity. Therefore, a mechanism is needed for determining those hours between which an E layer could be measured, and thus successfully predicted by a NN.

Using the foE dataset, the start and end hours for measured E characteristics were extracted. With DNS, DNC, and R1 as inputs a NN was trained to predict the start hour (SH) and end hour (EH) for measured E characteristics. This NN will be referred to as the "E limits NN". Determining these limits this way means that the danger of interrogating the E layer NNs with input parameters with which they have not been trained is avoided.

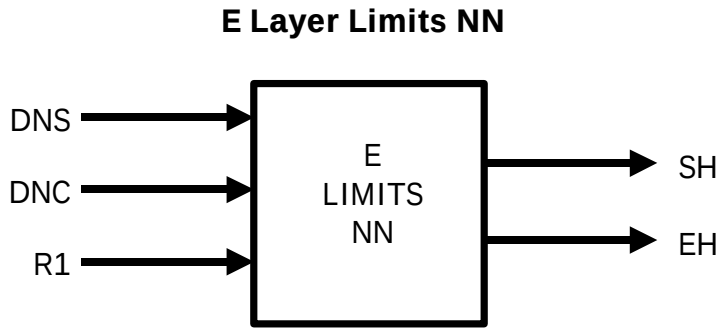

Figure 4-5: A block diagram that shows the inputs and outputs of the E limits NN.

To check the dependence of the outputs on R1 a NN was trained with only the DN inputs. Using the rms error criterion a dependence on R1 was found. Therefore, R1 will be included as an input for this NN.

Figure 4-5 shows a diagram depicting the inputs and outputs to the E limits NN.

For the hours that fall outside of the E limits SH and EH, existing models will be used to determine the E layer description. In the case of the peak characteristics, foE and hmE, the JET E layer peak model (*Titheridge [2000])* is used, and for the profile description the UMLCAR model (*Huang and Reinisch [1996])* is used.

4.5 Describing the Profile

The IRI applies an exponential function to connect the D layer profile with the E layer peak (*Bilitza [1990])*. The D layer profile is determined from empirical relationships that have been defined by using rocket measurements. It has been recognized by the IRI community that a data based description of the E layer profile shape is required for use in the IRI model (*Bilitza [1998])*.

Hafner et al. [2001] use a combination of cubic spline fitting to known E layer profiles and then linear interpolation to deal with latitudinal and solar dependences.

4.5.1 The Data

There are five years of profile data available for the Grahamstown station. Ionograms from the DPS are automatically scaled using the Artist scaling software. Artist reports the electron density profile description in two formats. The first format is a set of Chebyshev coefficients for each individual layer. For the E layer there are three Chebyshev coefficients that, together with the peak characteristics (foE, hmE), are used to determine the height at each frequency analytically. In this case the frequency is the independent variable with an increment of 0.02 MHz. The second format is a listing of frequencies at given heights where the height is the independent variable and the user decides what height increment will be used. These formats are equivalent since they are derived from the same model. Thus there are two methods that can be adopted for setting up the NN to provide a model description of the profile. The “cheby method” uses the data as presented in the first format while the “direct method” uses the data as presented in the second format. Both methods are explained here and then compared.

4.5.2 Direct Method

For this method the data is available as a set of height, frequency points provided directly by Artist. The height is the independent variable here with a height increment chosen to be 0.5 km. The E layer profile data was extracted in this format for all measured profiles from 1996 to 2000. This amounted to 443551 input vectors.

Five NNs were trained to predict the frequency in MHz at a particular height. Each NN used different combinations of the input parameters DNS, DNC, HS, HC, R1, ZA and height to make up the input vector for training the NN. The lowest

rms error was obtained for the NN that was trained with an input vector made up of all seven of these parameters. However, the difference between the rms errors for the NN trained with the solar zenith angle (ZA), and the NN trained without, was hardly significant. The improvement in the rms error was not worth the complexity of adding another dimension to the input space. Therefore ZA was excluded and the NN was trained with DNS, DNC, HS, HC, R1 and height as the inputs. The output was the frequency in MHz at the corresponding input height. The visual representation of the direct method NN is shown in figure 4-6. The lowest height presented to the NN for training was the height at a frequency of 0.2 MHz, which is the starting frequency of the Artist profile output. A lot of effort was expended in an attempt to find a convenient height with which to start interrogating the NN. For a prediction with the direct method a starting height is required as part of the first input set. An analysis of all available heights corresponding to a frequency of 0.2 MHz revealed that 87.4% reported a height of 90.0 km at 0.2 MHz. Therefore, when interrogating the direct method NN to predict the E layer profile, the first input height will be 90.0 km.

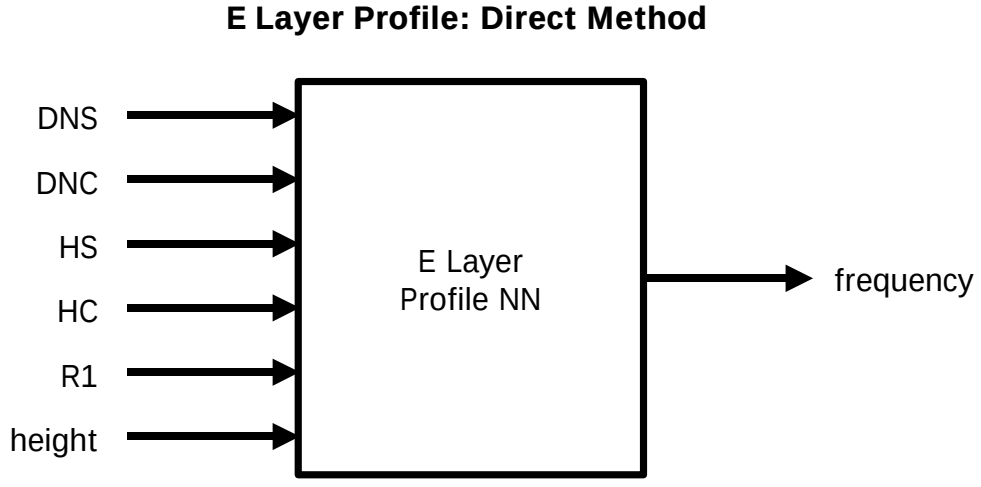

Figure 4-6: A block diagram of the inputs and output to the E layer profile NN using the direct method.

4.5.3 Cheby Method

An alternative method for describing the E layer profile in the LAM model is to train a NN to predict the three Chebyshev coefficients, A0, A1 and A2. Artist provides a set of these coefficients for every ionogram. The three coefficients are used in an analytical equation to provide the real height in km for a given frequency in MHz. These equations are described in *Huang and Reinisch [1996]* but are reproduced here for ease of reference. To calculate the height, h, in km at a frequency, f, in MHz:

$$h = hmE + \sqrt{g} \times \sum_{i=0}^{n} A_i T_i^*(g) \tag{4-1}$$

where

$$g = \frac{\ln\left(\frac{f}{fmE}\right)}{\ln\left(\frac{f_s}{fmE}\right)}; 0 \le g \le 1 \tag{4-2}$$

$$\left.\begin{aligned} T_0^* &= 1 \\ T_1^* &= 2g - 1 \\ T_j^* &= 2 \times T_1^* \times T_{j-1}^* - T_{j-2}^* \; ; \; j = 2..n \end{aligned}\right\} \tag{4-3}$$

In the above equations f is the given frequency and f_s is the start frequency of the E layer, which was fixed at 0.2 MHz. The T_i^* are the shifted Chebyshev polynomials which are functions of g. The value of n in the summation of equation (4-1) is 2 for the E layer.

Reliable predictions for the three Chebyshev coefficients (A0, A1 and A2) can be used in conjunction with the peak parameter predictions (foE, hmE) in the above equations to obtain the real height as a function of frequency.

Initially, using DNS, DNC, HS, HC and R1 as inputs and the three Chebyshev coefficients as outputs, a NN was trained with data derived from measured ionograms for the period 1996 to 2000 inclusive. Although this NN contained enough information about the relationship between the coefficients, it did not contain any knowledge of how the coefficients were related to the peak characteristics. There are five variables required to calculate the profile from equation (4-1).

The outputs of the NN were then changed to foE, hmE, A0, A1 and A2. The inputs remained the same. Thus the predictions of the coefficients are based on all the available information required to obtain the entire profile. The individual NNs trained to predict foE and hmE are not wasted, as they will be used to predict those characteristics. A more accurate prediction of foE would be expected from the foE NN than from the profile NN, as the input space used to train the foE NN was more comprehensive.

This E layer profile NN is used when the hour for which a profile is required falls between SH and EH as determined by the E limits NN (section 4.4). If the input hour falls outside of this range the UMLCAR model (*Huang and Reinisch [1996])* is used to determine the profile. The UMLCAR model is used with hmE and foE as determined by the JET model (*Titheridge [2000])*, and an E layer half thickness of 28 km. The layer half thickness, y, is the difference between the peak height, hmE, and the height at a frequency of 0.0 MHz.

Figure 4-7 is a block diagram of the process used in determining the E layer profile description.

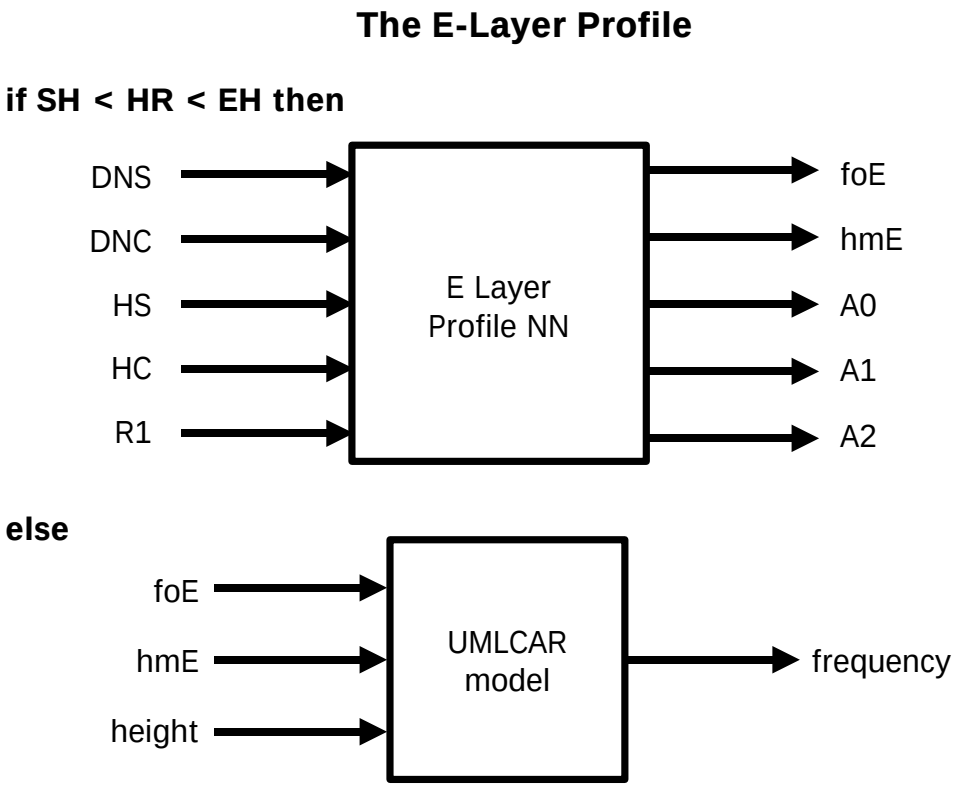

Figure 4-7: A diagram depicting the process for determining the E layer profile. The inputs and outputs are shown for the cheby method NN.

4.5.4 Direct vs Cheby

An advantage of the cheby method is that only five outputs for one input set are required in order to obtain the entire E layer profile. With the direct method an output is required for every height in the profile.

With the cheby method, the predicted coefficients contain all the information required to produce the profile from 0.2 MHz up to the E layer peak. Also, the requirement for a starting input height is eliminated. This makes the cheby method an elegant way in which to obtain a description of a profile for a particular input set. Therefore, for the development of the LAM model, my preference is for the cheby method over the direct method and all further LAM model development, as described in this thesis, uses the cheby method.

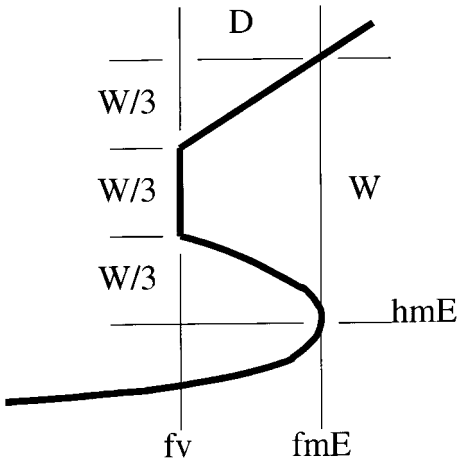

Figure 4-8: The shape of the model valley region used in the UMLCAR model and adopted in the LAM model.

4.6 The E-F Valley

At the top of the E layer an ionization valley exists which forms the transition from the E layer to the F layer. It is not possible to determine the valley shape from the ordinary ray of an ionogram. A way to resolve this problem is to assume a general shape for the profile within the valley and then use the observed virtual heights from the ionogram to determine the details. However, usually there is not enough information on the ionogram to provide any details.

Titheridge [1985] has covered the valley area in detail for his electron density profile model, POLAN. However, since the Grahamstown ionograms are measured with a DPS and scaled with Artist, the valley shape assumed by the UMLCAR model (*Huang and Reinisch [1996])* will be adopted by the LAM model. This valley region shape is shown in figure 4-8.

The only information required to construct this valley shape is the width of the valley, W, which has the units km. There exists a data base of W values, which have been determined by the Artist scaling software. This data base shows that

the W values respond to changes in DN, HR and R1. A NN was trained to predict the W values for times when it is possible to measure an E layer. At times that fall outside of the boundaries set by the E limits NN, the F layer is determined first and the W value is taken to be the difference between hmE and the start of the F layer, hsF. Since the shape of the valley layer is based on an assumption, and not on actual measured ionograms, there is some room to adjust the W value to ensure a smooth transition from E to F layer.

The shape of the valley consists of three parts, a parabolic section at the top of the E layer followed by a slab of constant frequency (the valley bottom frequency, f_v) and then an upper section where the frequency increases linearly with height. Once the W value is determined the rest of the valley can be described by using equations (4-4) to (4-7) (*Huang and Reinisch [1996]*).

First, define dp from W

$$dp = 0.49 + 0.46 \times \frac{e^{(59.45 - W)/14.63} - 1}{e^{(59.45 - W)/14.63} + 1} \tag{4-4}$$

then,

$$D/[MHz] = \left(1 - \sqrt{dp}\right) \times fmE \tag{4-5}$$

and,

$$f_v/[MHz] = fmE - D = \sqrt{dp} \times fmE \tag{4-6}$$

so

$$h/[km] = hmE + \frac{W}{3} \times \sqrt{\frac{(fmE - f_n)}{D}};\ \ f_v \le f_n \le fmE \tag{4-7}$$

4.7 Results

There are two different methods that can be used for presenting the results from a NN based model. The first is a comparison between the measured and predicted values, using the input set associated with the measured value to obtain the predicted value. The second is by varying each input variable individually while keeping the other inputs constant and observing the effect on the output. Both of these methods are used here to present the results obtained from the E layer contribution to the LAM model.

For the E layer model the input parameters were DN, HR and R1. To investigate the relationship between the E layer description and the inputs the second method is used.

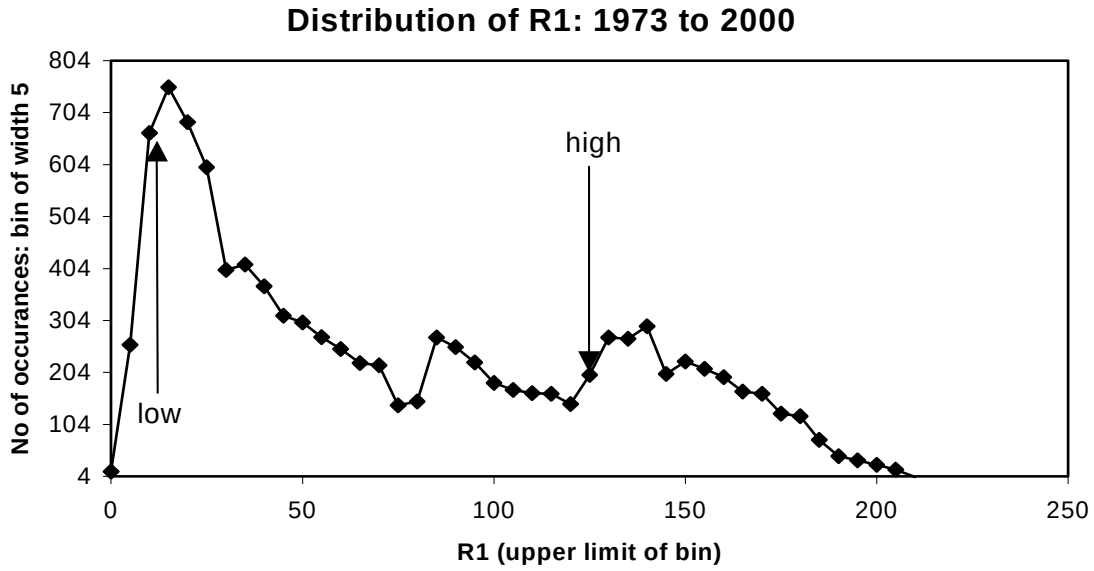

Figure 4-9: The distribution of R1 values, for the years 1973 to 2000 inclusive, that was used to determine typical low and high values of R1.

Typical high and low values were chosen for each of these inputs. The values of DN were arbitrarily chosen as follows: 20 being typical for the summer months, and 180 typical for the winter months. A value of 10h00 UT (12h00 SAST) was chosen for the HR input when a fixed value was required. For R1, values of 10 and 125 were chosen as typical indicators of low and high solar activity, shown in figure 4-9. These values were selected such that approximately 70% of the data lay between the low and high values, 10% at the low end and 20% at the high end. The same high and low R1 values were used when interrogating all E layer NNs; those that were trained with the 28-year dataset (foE and E limits) as well as the 5-year dataset (hmE and E profile). The difference is that with the 5-year dataset approximately 78% of the data lay symmetrically between the low and high values. The distribution of R1 for the 28-year dataset is shown in figure 4-9 and illustrates the selected low and high values of R1. For this results section, these values remain as described here, unless otherwise indicated.

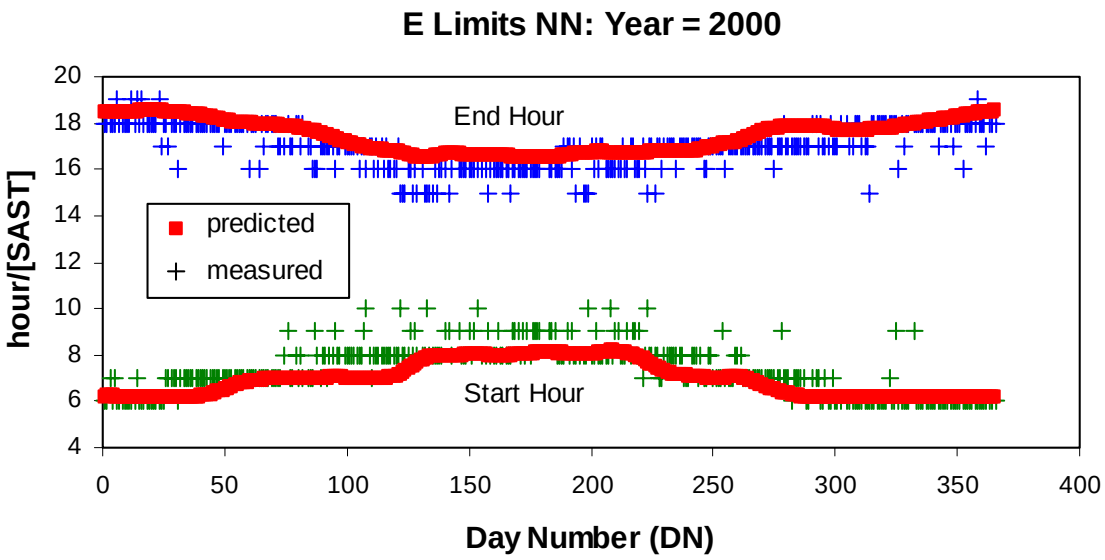

Figure 4-10: Results from the E limits NN for the year 2000.

4.7.1 E Limits NN:

The E limits NN was trained to predict the hours between which the E layer is measurable by our ground based ionosonde. The outputs from this NN are the start hour (SH) and the end hour (EH). In figure 4-10 the graph of hour versus day number is shown for the year 2000, which corresponds to high R1.

The E limits NN was trained with data from 1973 to 1999 inclusive. As the dataset already covered more than a solar cycle, the year 2000 was reserved to use for testing how successfully the NN could determine the E layer limits when presented with unseen data.

4.7.2 The E Layer Peak – foE

The foE NN was trained to predict the critical frequency of the E layer using DN, HR and R1 as inputs. For hours that fall outside of the SH and EH limits set by the E limits NN, the JET model (*Titheridge [2000]*) is used. At the SH and EH boundaries the two models, JET and LAM, merge in a realistic manner.

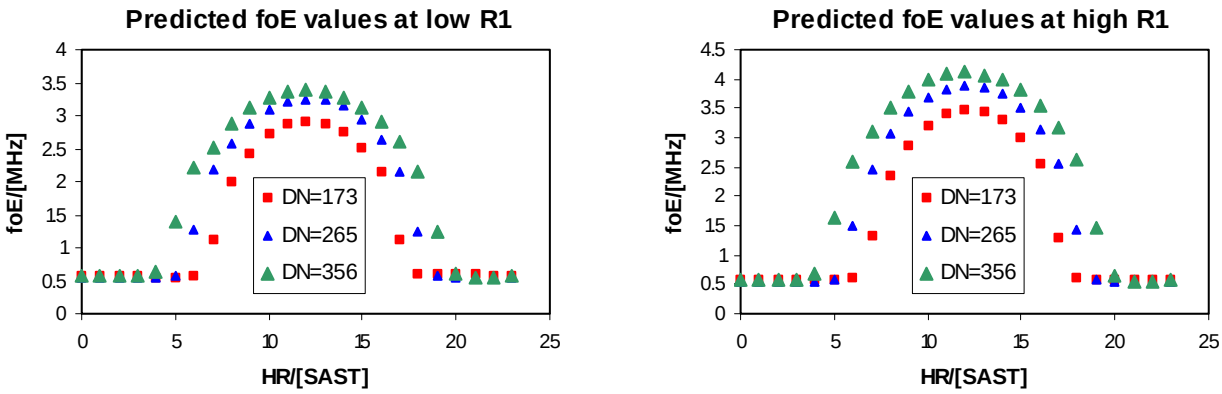

(a) (b)

Figure 4-11: Graphs of the predicted foE values over one day for three days of the year (winter solstice, spring equinox, summer solstice) at (a) low R1 (R1=10) and (b) high R1 (R1=125). The LAM model was used for the daytime values and the JET model for the nighttime.

Figure 4-11 shows graphs of foE values predicted over one day for three days of a year for low and high R1. The three days were chosen to coincide with the winter solstice, spring equinox and summer solstice. In figure 4-12 the measured and predicted foE values for two years, 1989 and 1995, taken from the original dataset are graphed. These values are for 12h00 SAST only. The rms error between the measured and predicted values is 0.25 MHz for 1989 and 0.13 MHz for 1995.

To investigate the relationship between R1, DN and foE the DN was varied from 1 to 365, the hour was fixed at 12h00 SAST and the R1 value varied from 10 to 130 in steps of 20. The result is the graph shown in figure 4-13. This graph shows that the foE NN has learnt the relationship between the inputs and output. NNs can also be used in the same way to discover new relationships between parameters.

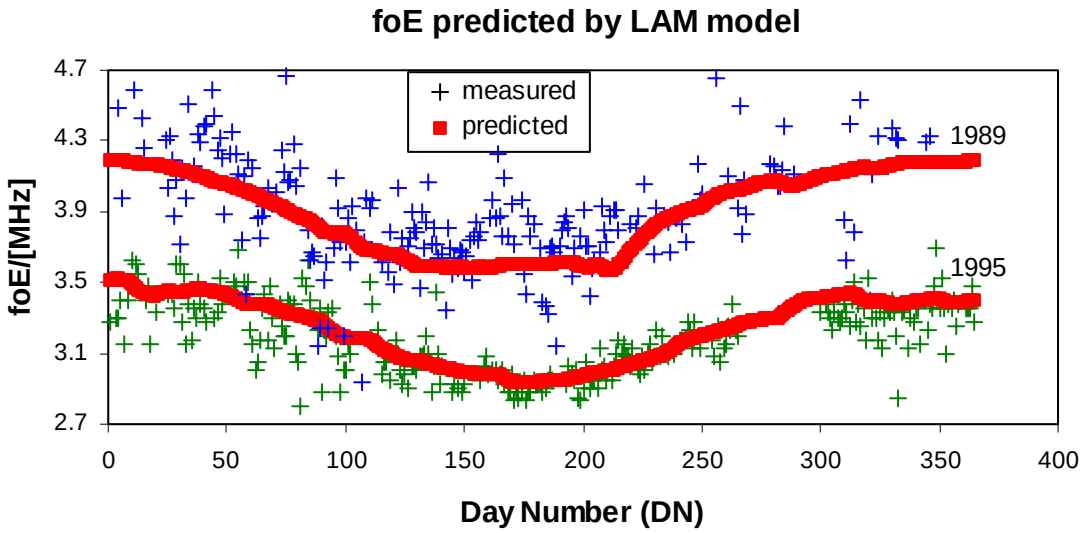

Figure 4-12: This graph shows the measured and predicted 12h00 SAST foE values for 1989 (a year of high R1) and 1995 (a year of low R1). The rms errors were 0.25 MHz and 0.13 MHz respectively.

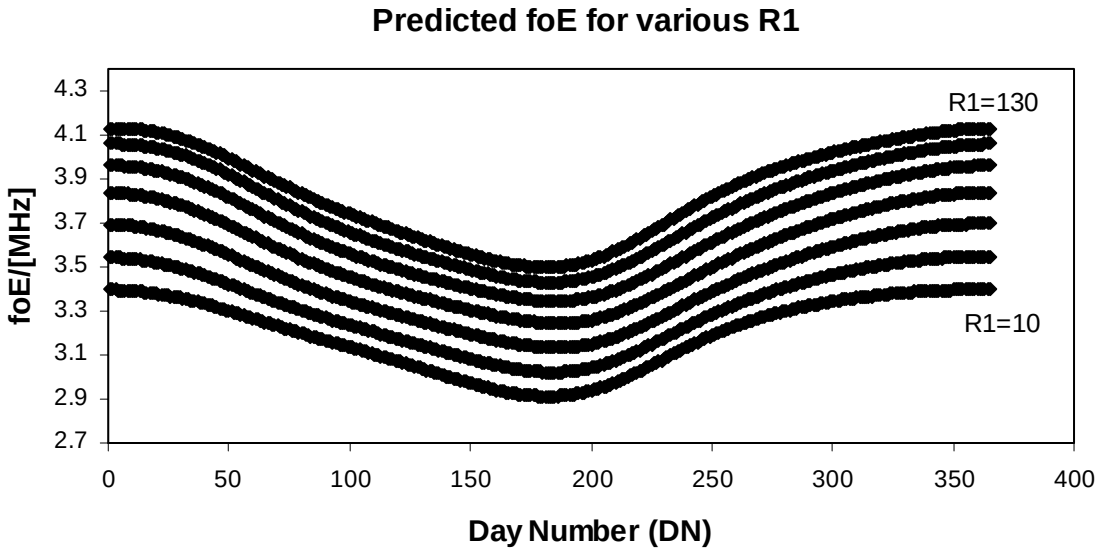

Figure 4-13: A graph of the variation of foE with DN and R1. The hour is fixed at 12h00 SAST and R1 is varied from 10 to 130 in steps of 20.

4.7.3 The E Layer Peak - hmE

The hmE NN was trained to predict hmE using DN, HR and R1 as inputs. As a limited dataset was used for training the NN, the NN was only interrogated with input data for which it had been trained.

As before, the NN is only used for predictions at hours that fall inside the boundaries set by the E limits NN. Outside of these boundaries the JET model (*Titheridge [2000])* is used. In figure 4-14 the predicted values of hmE are shown for two days coinciding with the summer and winter solstice, at low and high R1. The daytime behaviour of hmE predicted by the NN and illustrated in these graphs is identical to the daytime behaviour of hmE reported in *Titheridge [2000]*.

The relationship between DN, R1 and hmE was investigated and is illustrated in figure 4-15. R1 is varied from 10 to 130 in steps of 20 and the hour is fixed at 12h00 SAST.

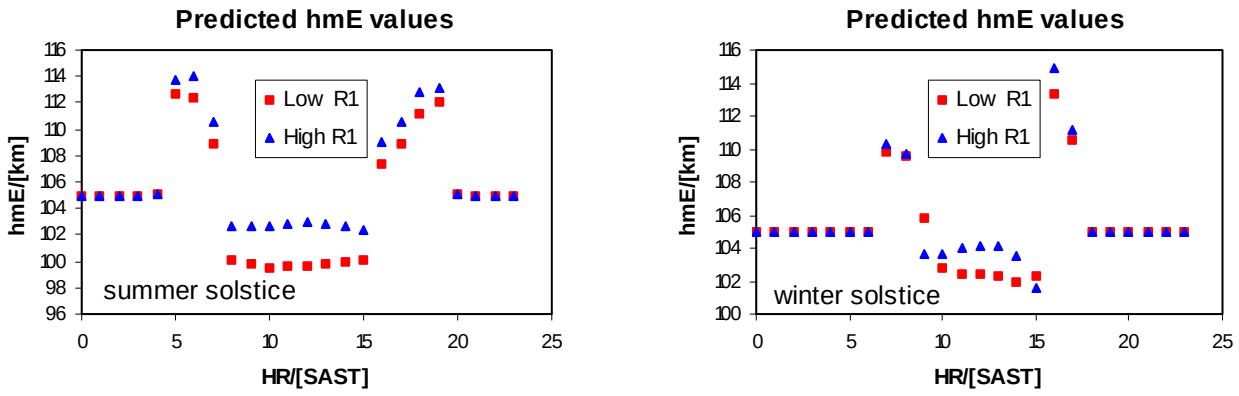

(a) (b)

Figure 4-14: The hmE values over one day at low and high R1 are shown for (a) summer solstice (DN=356) and (b) winter solstice (DN=173).

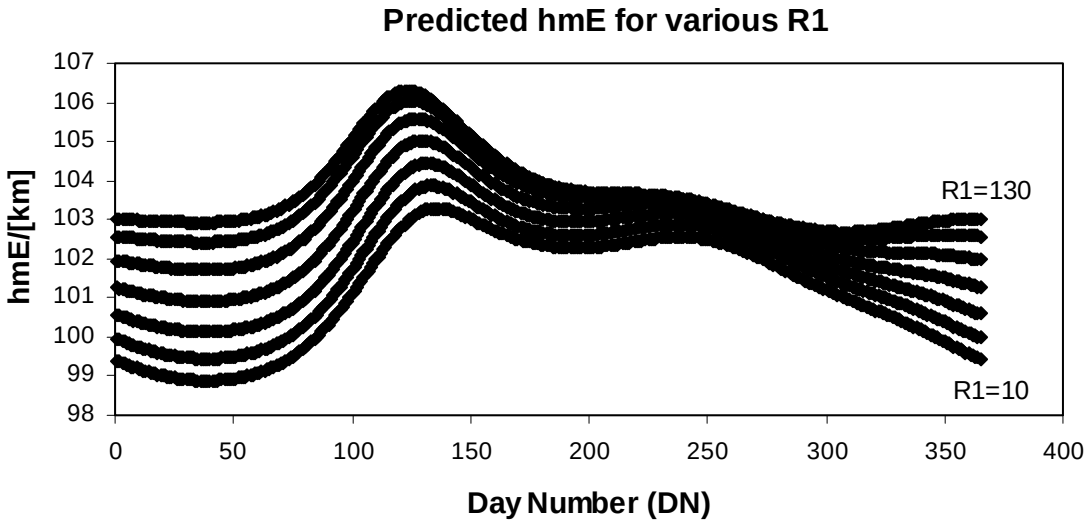

Figure 4-15: A graph of the variation of hmE with DN and R1. The hour is fixed at 12h00 SAST and R1 is varied from 10 to 130 in steps of 20.

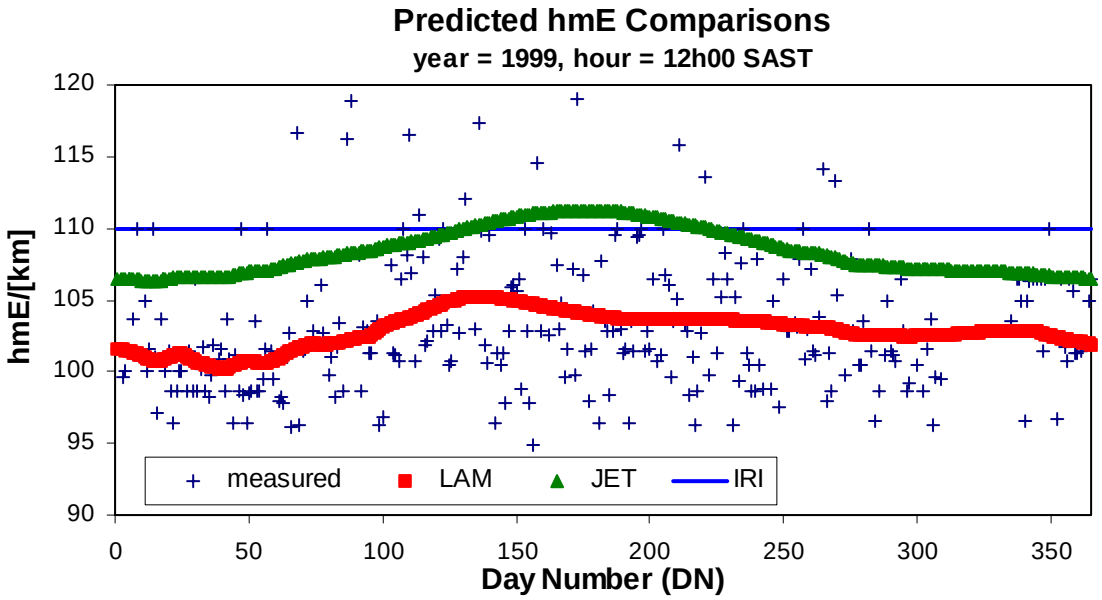

Figure 4-16: Comparisons of measured and predicted values of hmE. The LAM model is compared to the JET model and the IRI for 1999 at 12h00 SAST.

Figure 4-16 illustrates the differences in the predicted hmE values of the three models, LAM, IRI and JET. This comparison was done for one year, 1999, at 12h00 SAST. As can be seen from this graph the IRI fixed value of 110 km is not optimal for these prediction purposes. The JET model appears to overestimate the actual values while the LAM model provides a better average prediction.

4.7.4 E Layer Profile Results

The first results from the LAM model's E layer profile are shown in figure 4-17. These graphs show the predicted E layer profiles for four days, one day for each season, at low R1 and high R1. The hour input was fixed at 12h00 SAST.

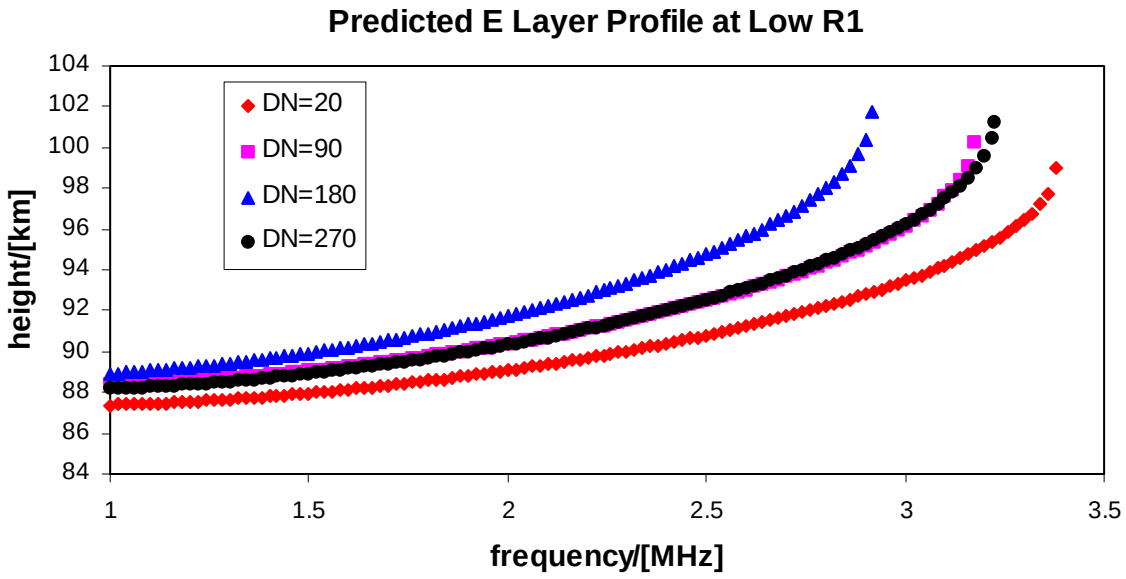

(a)

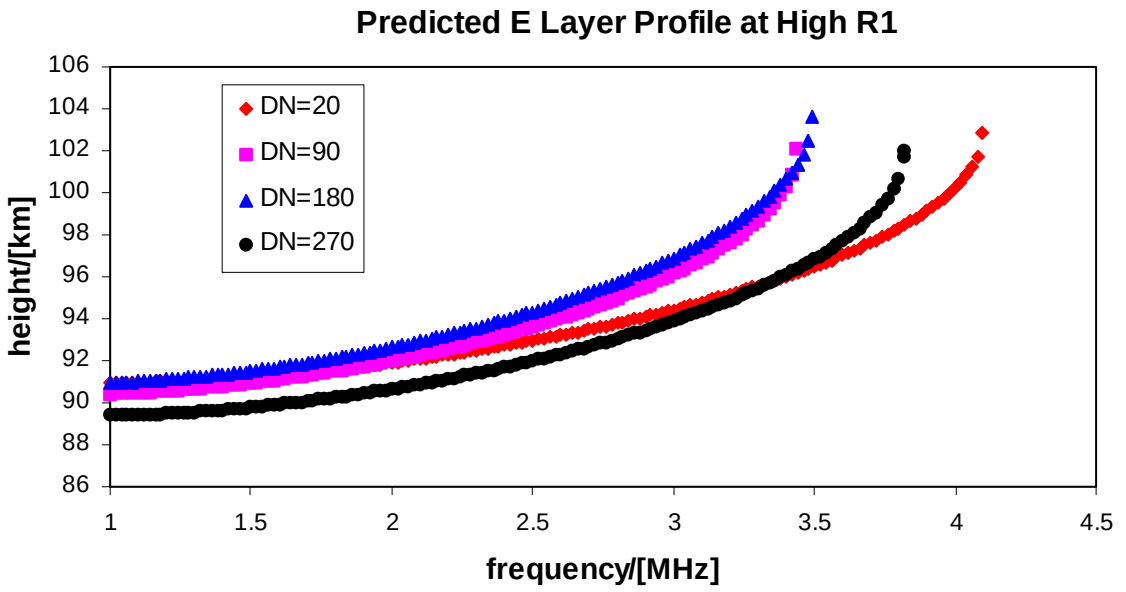

(b)

Figure 4-17: These graphs show the LAM model E layer profile predictions. The profiles are for 12h00 SAST at (a) low R1 (R1=10) and (b) high R1 (R1=125).

To illustrate the variation of the profile shape during the course of one day, the predicted E layer profiles were determined for a summer day at low R1. These profiles are shown in figure 4-18a and figure 4-18b. The first graph shows the profiles leading up to 12h00 SAST and the second graph the profiles at later times.

The nature of NNs is to give the best average output for a particular set of inputs. Six examples have been selected to demonstrate the performance of the E layer model. In each example input sets have been chosen for which actual profiles exist in the original dataset. The LAM model has produced predicted profiles for each set of inputs to the best of its ability, which is determined by the NNs that make up the model. Best and worst case scenarios have been deliberately chosen for this demonstration. As an added comparison profiles predicted by the IRI 2001 are shown for each of the input sets.

These examples are shown in figure 4-19. Two profiles from three different solar activity levels are presented. The profiles were chosen from the original dataset and then the LAM model and the IRI 2001 were used with the actual profile's input set. Therefore, the DN and R1 inputs differ for each profile shown. The first two profiles, figures 4-19(a) and 4-19(b), are for summer and autumn at high R1. Figures 4-19(e) and 4-19(f) show the profiles for summer and winter at low R1. The two middle profiles, figures 4-19(c) and 4-19(d), are for summer and spring at an R1 level that falls between the high and low levels.

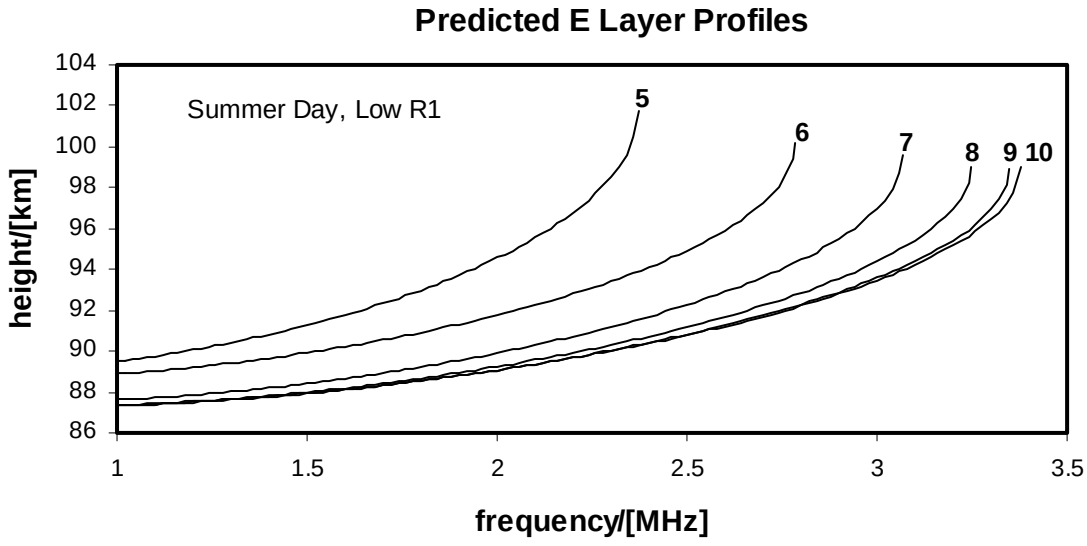

(a)

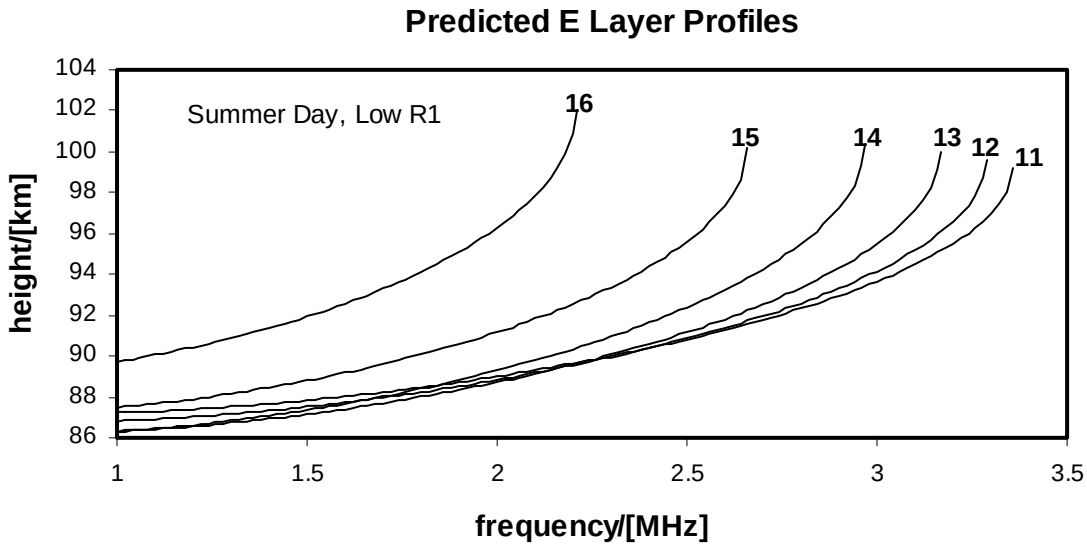

(b)

Figure 4-18: These graphs show the predicted E layer profiles at different hours for one summer day (DN=20) at low R1 (R1=10). The profiles are labeled according to the hour of the day in UT that the profile represents. For this example the E limits NN determined SH as 05h00 UT and EH as 16h00 UT.

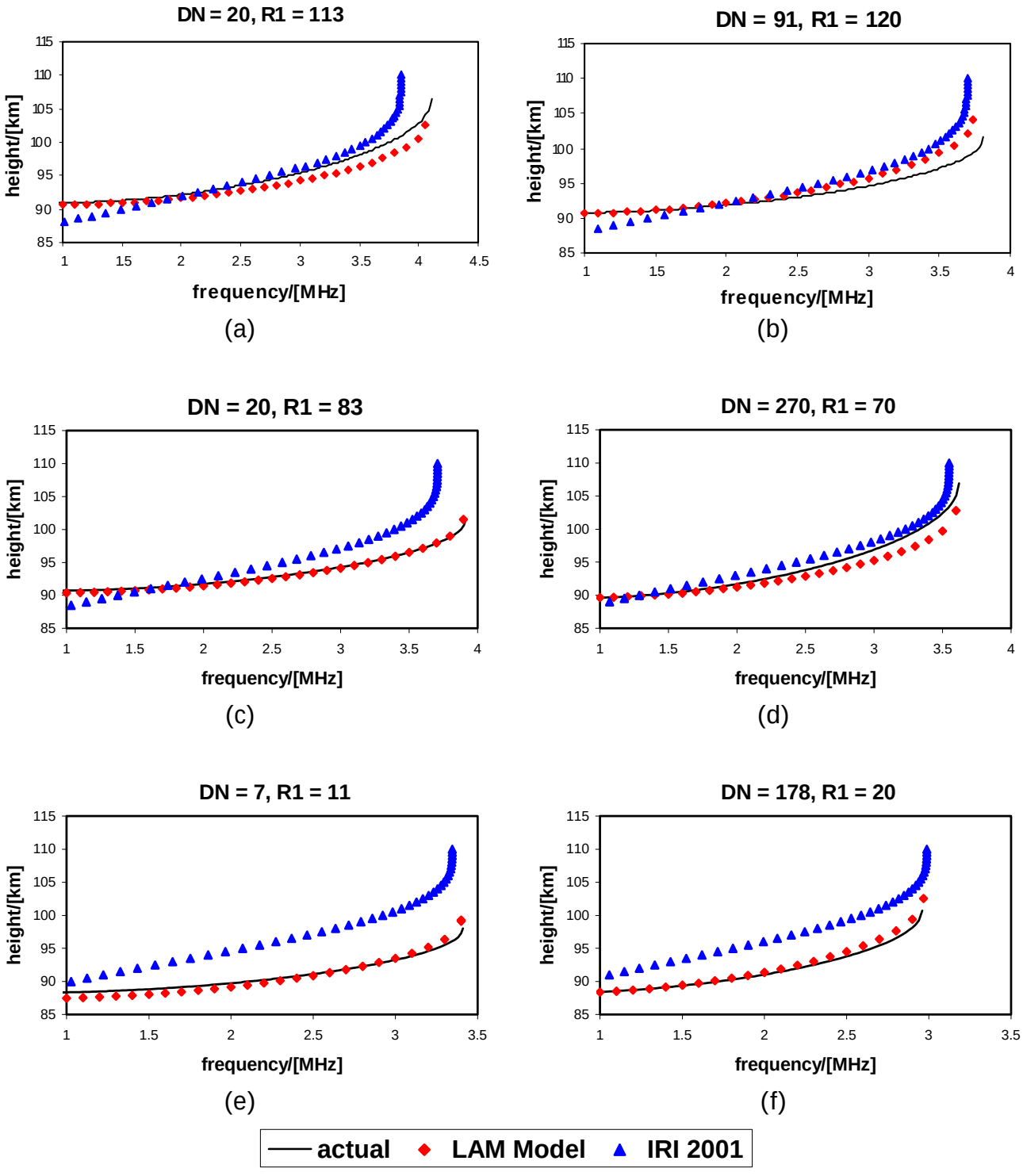

Figure 4-19: Comparisons of the LAM model for the E layer with the IRI 2001 and actual DPS profiles. These comparisons are shown for midday local time at three levels of solar activity.

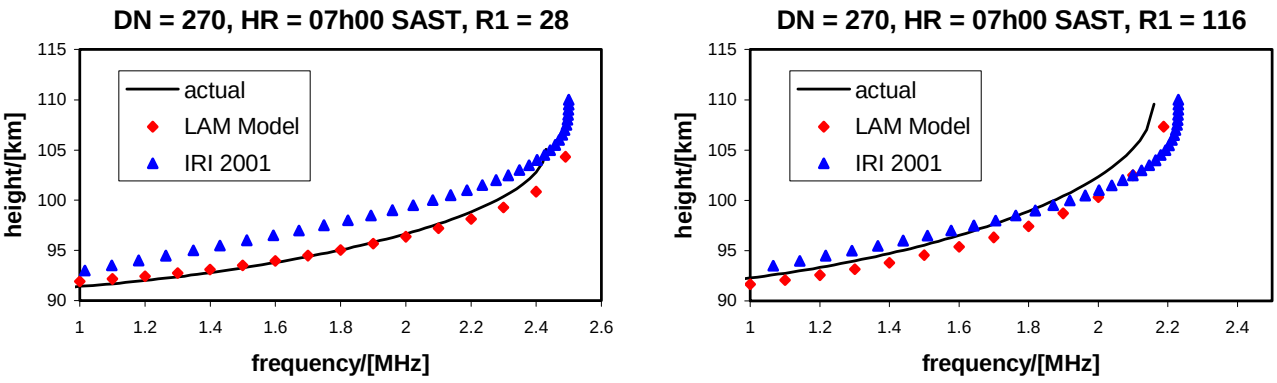

(a) (b)

Figure 4-20: Comparisons of the LAM model for the E layer with actual and IRI 2001 predicted profiles. The input dataset was DN=270, HR=07h00 SAST at (a) R1=28 and (b) R1=116.

From figure 4-19 it can be seen that in some cases the LAM model profile fits the actual profile particularly well while in other cases the LAM model profile deviates from the actual profile. This deviation usually falls well within the estimated profile uncertainty, which is discussed in the next section of this chapter. In addition, the dataset from which the hmE and profile NNs were trained is limited. The predictions from these NNs will improve as more data becomes available and the NNs are re-trained.

The comparisons with the IRI 2001 illustrates in all cases that the LAM model is an improved predictor of the E layer profile compared to the IRI for the Grahamstown ionosphere.

Figure 4-20 shows more of the same comparisons as in figure 4-19 but for a different hour of the day, 07h00 SAST. Profiles for a spring day (DN=270) at low R1 (R1=28) and high R1 (R1=116) are predicted with the LAM model and compared to actual and IRI 2001 predicted profiles.

4.7.5 Estimating the Uncertainty

In *Poole and McKinnell [2000]* a technique for finding the uncertainty in the prediction of a NN based model is described. This technique was employed to investigate the uncertainty in the prediction of the E layer contribution to the LAM model.

An uncertainty can be determined by finding a statistical measure of the differences between the predicted and measured values. For each input vector of the original dataset used to train the NN (NN1), the difference between the predicted and measured output value is evaluated and squared. A second NN (NN2) is then trained with the same input data as NN1 but with the squared differences as the output. Since it is the nature of NNs to find the mean predicted value, the square root of the output of NN2 is a root mean squared (rms) difference. This difference represents a measure of the variation that can be expected between any predicted and measured value. More details of this technique and how it was applied to foF2 can be found in *Poole and McKinnell [2000]*.

Determining the uncertainty in the LAM model prediction of the E layer profile requires applying the above technique to all the relevant datasets. For the peak characteristics, foE and hmE, the uncertainty in each prediction is directly the square root of the output of the relevant squared differences NN. However, for the E layer profile it seemed that a complicated propagation of errors calculation was required to determine the uncertainty on each of the heights that make up the profile.

The E layer profile NN has five outputs (as shown in figure 4-7) each of which plays a role in determining the final shape of the profile. The three Chebyshev coefficients (A0, A1 and A2) are not independent of each other, which is the reason it is not a simple mathematical procedure to find the uncertainty on heights calculated with equation (4-1). However, for the E layer, the relationship between the coefficients can be approximated using linear regression techniques. Figure 4-21 illustrates the dependence of A1 and A2 on A0. These graphs were

plotted using all available Grahamstown data and then linear regression was applied to fit a straight line to the data. For A1 versus A0, the slope of the fitted straight line was – 0.41 and for A2 versus A0 the slope of the fitted straight line was 0.09. Therefore, straight line equations can be written to approximate the values of A1 and A2 given A0.

Using this linear approximation, the estimated uncertainty in the start height of the E layer, hsE, can be determined. The uncertainty in hsE is evaluated in terms of the uncertainty in A0, which is predicted by the squared differences NN corresponding to the E profile NN. Under normal conditions, the minimum frequency the Grahamstown DPS sounds at is set to 2.0 MHz and therefore the height corresponding to 2.0 MHz is taken to be hsE.

The estimated uncertainty in the peak height of the E layer, hmE, is not dependent on the Chebyshev coefficients and provides an indication of the maximum uncertainty in the E layer for a given input set.

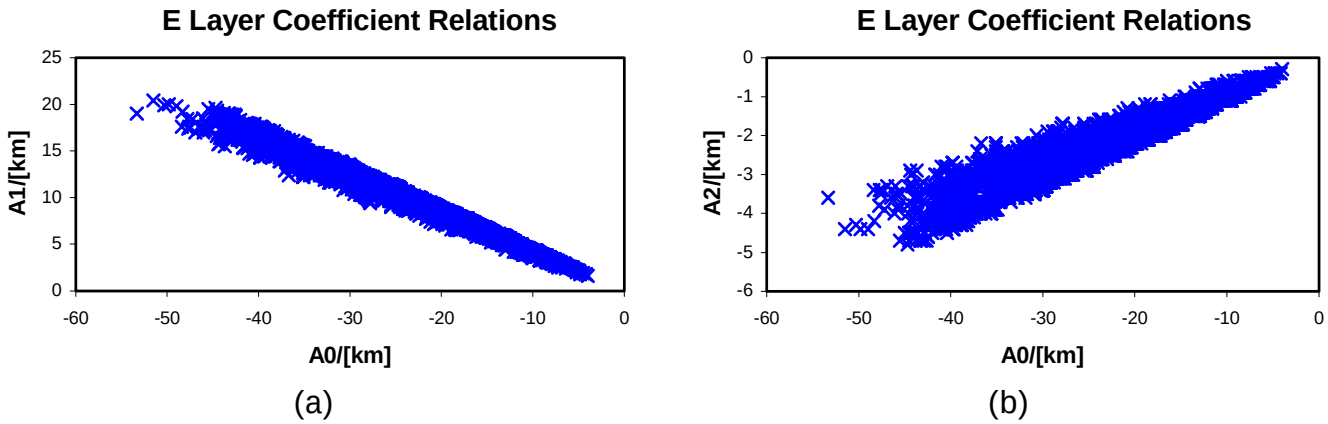

(a) (b)

Figure 4-21: The relationships between the three coefficients that describe the E layer profile are illustrated here. An approximation of the functions that relate A1 and A2 to A0 was determined using linear regression.

Therefore, the estimated uncertainties in hsE and hmE are known and can be used to determine the uncertainty profiles in the E layer. Using these uncertainties, hsE and hmE were adjusted by adding and subtracting the uncertainty from the predicted value to determine the maximum and minimum values respectively. The maximum uncertainty profile was determined by interpolating between hsE+hsE(error) and hmE+hmE(error) in such a way that the profile shape was retained. Similarly, the minimum uncertainty profile was determined by interpolating between hsE-hsE(error) and hmE-hmE(error). The uncertainties due to hsE and hmE are referred to as hsE(error) and hmE(error) respectively.

The examples of figures 4-19(c) and 4-19(d) are shown again in figure 4-22 with their corresponding uncertainty profiles. These estimated uncertainty profiles represent the maximum possible statistical variation of the average predicted E layer profile for a given input set.

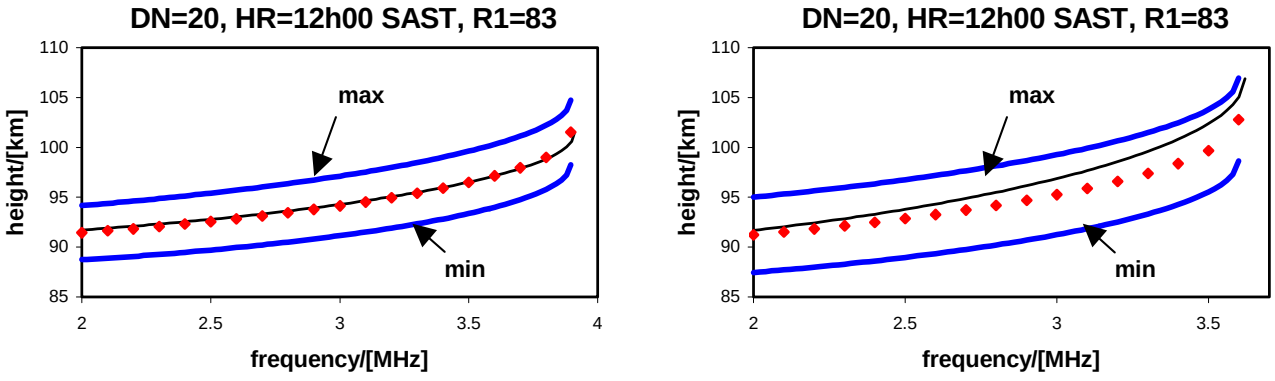

Figure 4-22: These are the same profiles as shown in figures 4-19(c) and 4-19(d) with their uncertainty profiles. The solid black line is the actual profile and the red diamond shape points are the LAM model profile. The solid blue lines are the maximum and minimum uncertainty profiles.

4.8 Conclusion

This chapter has presented the development of the E layer contribution to the LAM model. NNs have been used to provide information on all aspects of the E layer profile, including reasonable times of day to expect a measurable E layer and the variability limits that can be placed on the profile.

The discussions in this chapter have also set the scene for the development of the other contributions to the LAM model, which will be discussed in the following chapters. The cheby method for setting up the profile NN was introduced in this chapter and will now be my preferred method for setting up NNs to predict the other sections of the entire bottomside profile.

As mentioned before the dataset used to train the hmE and profile NNs was limited to only five years. When this dataset has been increased the NNs will be re-trained, thereby improving the LAM model's ability to find the profile.

In spite of this limited dataset, the LAM model is still an improved predictor of the ionospheric E layer description when compared to the IRI. The IRI has acknowledged the need for improvements in the E layer predictions, especially for hmE, and it is possible that the LAM model could be useful in assisting the IRI in making the necessary improvements.

Chapter 5

LAM MODEL: F LAYER

5.1 Introduction

This chapter discusses the F layer contribution to the LAM model. The F layer of the bottomside ionosphere falls in the region from about 150 km to 350 km and is divided into two sections, the F1 and F2 layers. Details on the physical processes that give rise to the distinction between F1 and F2 can be found in *McNamara [1991]*. For the purposes of HF propagation the most important layer in the ionosphere is the F2 layer, since this layer is always present and measurable. There are specific conditions under which an F1 layer is not present at all. In particular, the F1 layer is never present at night.

For the development of a model for the F layer, three points on the electron density profile need to be identified. Firstly, there is the peak of the F layer corresponding to the point of maximum electron density in the ionosphere, which is described by the ionospheric characteristics, foF2 and hmF2. Secondly, the starting point of the F layer is identified by the characteristics fsF and hsF, which are determined by the E layer model. The third point is identified by the ionospheric characteristics foF1 and hmF1, which define the peak of the F1 layer. An example of the F layer profile for the daytime ionosphere over Grahamstown, showing both an F1 and F2 layer, is illustrated in figure 5-1, in which the important points, as mentioned above, are shown.

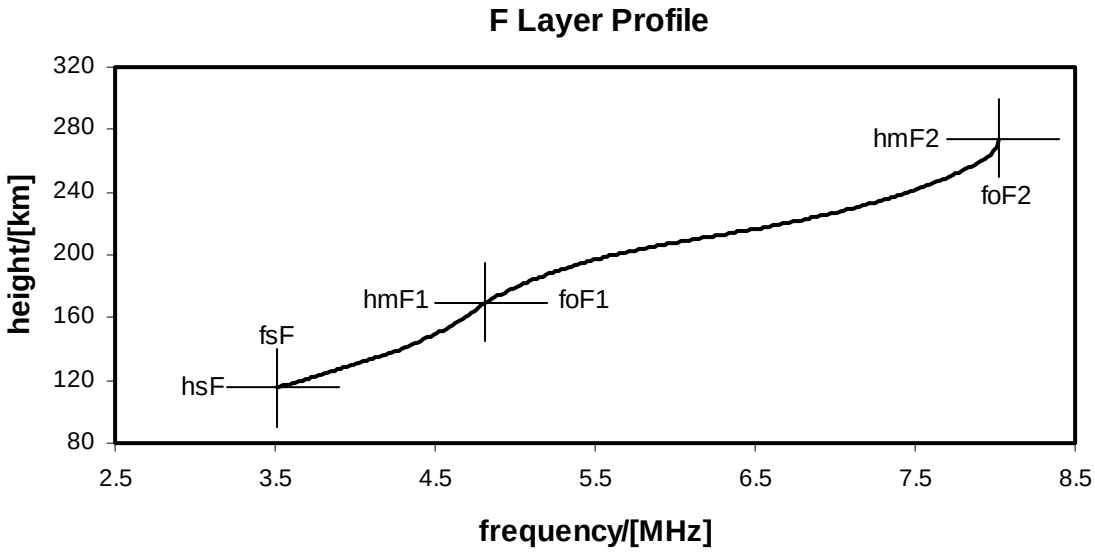

Figure 5-1: An example F layer profile for Grahamstown, showing both an F1 and F2 layer, and indicating the required ionospheric characteristics.

A model of the F layer would need to predict all six of the ionospheric characteristics mentioned above as well as a description of the shape in between the defining points. There would also need to be some mechanism for identifying the conditions required for an F1 layer to exist. This chapter discusses how these considerations were addressed for the LAM model.

5.2 The F2 Peak

An important parameter in ionospheric modelling is the maximum ionospheric electron density, which is quantified by the critical frequency of the F2 layer, foF2. foF2 is a measurable quantity that is directly related to the maximum electron density via equation (1-1). The real height at which foF2 occurs is hmF2, the peak height of the F2 layer.

An initial attempt at predicting hmF2 was discussed in chapter 3. Over the years several groups have successfully predicted the ionospheric parameter foF2, and

there are analytical and empirical models available that predict foF2 under any conditions. In this section the models that predict foF2 and hmF2 for the LAM model are discussed.

5.2.1 foF2

The maximum ionospheric electron density is quantified by the measurable ionospheric parameter, foF2, which is, therefore, of fundamental importance in ionospheric modelling. Much international effort has gone into producing an accurate prediction and forecasting tool for foF2.

The IRI (*Bilitza [1990])* offers two choices for predicting foF2; both are mathematical descriptions. The first is based on Fourier Analysis using monthly median values, while the second is based on worldwide values of foF2 described in terms of Legendre functions. Sets of coefficients are provided for predicting foF2 at high and low solar activity, while foF2 values at intermediate levels are found by linear interpolation. The 12-month running mean of the daily SSN (R12) is used as an input to the IRI and the predicted foF2 value is identical for all input sets where R12 levels are greater than 150.

Although a large global data base of foF2 values is available, one of the largest data sparse areas is that of the Southern Africa region. Most of the available models, including the IRI, that are based on this data base, use mathematical construction techniques to determine the description of foF2 in these data sparse areas. As a result, the predictions of foF2 are often not particularly accurate in the Southern African region.

In recent years a number of groups have developed models for the prediction of foF2 using NNs (*Williscroft and Poole [1996]*, *Altinay et al. [1997]*, *Wintoft and Cander [1999])*. In *McKinnell [1996]* I demonstrated the use of NNs for predicting the 12h00 SAST foF2 value for Grahamstown. This work was expanded to include all hours and the results are presented in *Poole and McKinnell [2000]*, where a section on the use of NNs to develop a short-term

foF2 forecasting program has been included. As well as providing a foF2 prediction tool, NNs have provided a means to discover new ways in which an output is dependent on different inputs. This is demonstrated in the abovementioned publications.

5.2.1.1 The Inputs

It has been shown previously (*Poole and McKinnell [2000])* that the optimum input variables for predicting foF2 are geophysical parameters representing season, time, solar cycle and magnetic activity. The requirement for the LAM model to predict foF2 is identical to that reported in *Poole and McKinnell [2000]* and, therefore, the same input variables will be used here without reporting the techniques involved in obtaining them.

DN and HR represent the seasonal and diurnal variations as defined in chapter 3 equations (3-1) to (3-4). A 2-month running mean value of the daily SSN (R2) and a 2-day running mean value of the hourly magnetic a_k index (A16) were found to be the optimum parameters for representing the solar cycle and magnetic variations respectively. The magnetic indices were obtained from the Hermanus Magnetic Observatory. Full details on determining the A16 index can be found in *McKinnell [1996]*. At this stage the LAM model is a single station model and therefore any latitudinal dependence was excluded at this point.

5.2.1.2 Training the foF2 NN

A NN was trained to predict the foF2 value for Grahamstown. The input vector consisted of six parameters, DNS, DNC, HS, HC, R2 and A16 and the output vector was the foF2 value in MHz. A block diagram depicting these inputs and output is shown in figure 5-2.

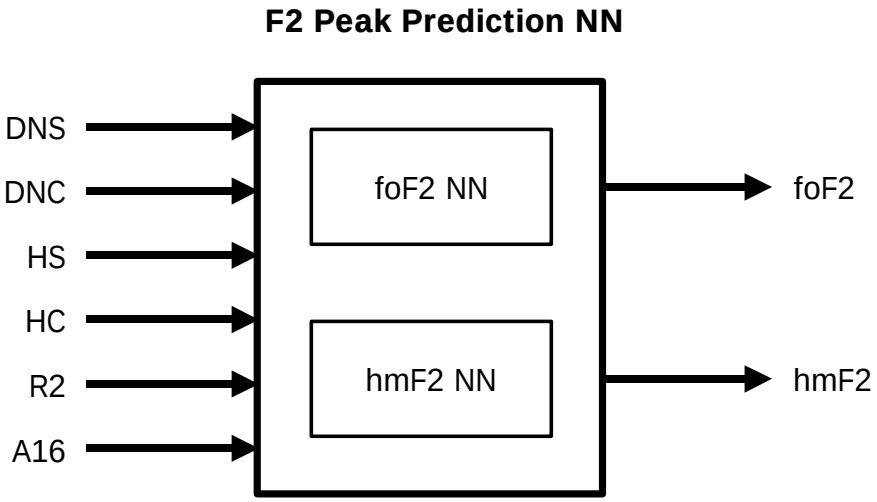

Figure 5-2: A block diagram of the inputs and outputs to the F2 peak NNs. R2 is the 2-month running mean of the daily SSN and A16 is the 2-day running mean of the hourly a_k magnetic index.

All Grahamstown foF2 data from January 1973 to December 2000 inclusive were used for training the NN. This amounted to 192491 vectors, 70% of which were used for training and 30% for testing.

5.2.2 hmF2

The hmF2 value is obtained from the MUF(3000) value, which is the maximum usable frequency that will be reflected by the ionosphere at oblique incidence over a path of 3000 km (*Bradley and Dudeney [1973]*). The MUF value has been routinely scaled from ionograms, and numerical maps of these values have been established. These maps are used by the IRI in conjunction with an analytical equation to calculate hmF2 (*Bilitza [1990]*). The R12 value and the magnetic dip latitude are required as inputs for this equation. Recent versions of the IRI have incorporated improvements to the hmF2 prediction by using incoherent scatter radar data.

Grahamstown ionograms that have been scaled with the Artist scaling software of the DPS report the hmF2 value as part of the SAO format. In chapter 3 an initial attempt to predict the 12h00 SAST hmF2 value was discussed. That procedure is expanded on in this section.

5.2.2.1 The Inputs

The hmF2 value has a similar variation to that of foF2. Seasonal and diurnal variations are represented by the quadrature components of DN and HR as defined in chapter 3, equations (3-1) to (3-4).

A similar investigation to that used to determine the optimum solar input for foF2 (*McKinnell [1996])* and foE (Chapter 4) was used to determine the solar input for hmF2. Seven NNs were trained to predict hmF2 using DNS, DNC, HS, HC and a solar activity index as the inputs. The solar activity index was determined by a running mean of the daily SSN over the preceding $^1/_{30}$, $^1/_2$, 1, 2, 4, 8, and 16 months. The rms error between the measured and predicted values was the lowest for the NN that used R2 as the solar activity input. Therefore, as for the foF2 NN, R2 will be used as the optimum solar activity input for predicting hmF2.

A slight improvement in the rms error was detected when a magnetic activity index was added to the input vector. Four NNs were trained, each with a different magnetic activity input that was determined from the running mean of the hourly magnetic a_k index over the 12 (A4), 24 (A8), 48 (A16) and 96 (A32) preceding hours. The rms error for the NN trained with the A4 index was the lowest. However, the improvement in the rms error when using the A4 index compared to using the A16 index was only 1.5%. Therefore, for simplicity, the A16 index will be used as the optimum magnetic activity input for predicting hmF2, as in the case of predicting foF2.

5.2.2.2 Training the hmF2 NN

The inputs (DNS, DNC, HS, HC, R2, A16) and output (hmF2 in km) to the hmF2 NN are shown in figure 5-2. A NN was trained with these inputs to predict the Grahamstown hmF2 value. All hmF2 values from April 1996 to December 2000 inclusive were used for training. The total number of vectors was 32377, 70% for training and 30% for testing.

5.3 The F1 Peak

The critical frequency of the F1 layer is foF1, and the real height at which the bottomside profile reaches foF1 is hmF1. This point has been poorly represented in ionospheric modelling in the past, due to a paucity of accurately scaled F1 layer data. The F1 peak models developed for the LAM model represent an attempt to provide an empirical model for predicting foF1 and hmF1 with improved accuracy over current global models such as the IRI.

5.3.1 foF1

The IRI (*Bilitza [1990])* predicts foF1 using an analytical equation that is a function of the solar zenith angle, R12 and the magnetic dip latitude. *Ducharme et al [1971]* established this IRI foF1 equation by making use of the worldwide ionosonde data that was available at that time. Very little reliable Southern African data was included in this development and, therefore, the IRI prediction of foF1 in the South African region is poor.

Up until now there has been no documented evidence of any group attempting to model foF1 using NNs.

5.3.1.1 The Inputs

There is a known seasonal, diurnal and solar variation in foF1 (*McNamara and Reinisch [1995]*). As for the other ionospheric characteristics, the seasonal and diurnal variations will be represented by the quadrature components of DN and HR, which are defined in equations (3-1) to (3-4).

As in section 5.2.2.1, the solar activity index was determined by training seven NNs to predict foF1 with differing time lengths of daily SSN. At this point it was also felt that reaffirmation of the use of SSN in preference to the 10.7 cm Solar Radio Flux (SF) was required. Therefore, a further seven NNs were trained to predict foF1 using differing time lengths of the daily SF value. Using the rms criterion, the solar activity index that proved to be optimum for predicting foF1 was found to be R2, as in the case of foF2 and hmF2. Figure 5-3 illustrates graphically the rms errors between the measured and predicted foF1 values obtained for each of the 14 NNs. RX is the SSN index and SFX is the Solar Flux index with X being the time length over which the running mean was taken. The X values are labeled on the graph.

The addition of a magnetic activity input further improved the rms error between the measured and predicted foF1 values. As with hmF2, four NNs were trained, each with the inputs DNS, DNC, HS, HC, R2 and AX, where AX is the magnetic activity input. The AX value corresponds to the running mean of the hourly a_k index over the preceding 12, 24, 48 and 96 hours; X = 4, 8, 16 and 32 respectively. From the rms errors of these four NNs, A8 was found to be the optimal input to represent the level of magnetic activity when predicting foF1.

5.3.1.2 Training the foF1 NN

Figure 5-4 shows the inputs and output to the foF1 NN. A NN was trained to predict foF1 for Grahamstown. There were 50310 vectors available in the foF1 dataset, 70% of which was used for training and 30% for testing the NN. The dataset spanned the period January 1973 to December 2000 inclusive.

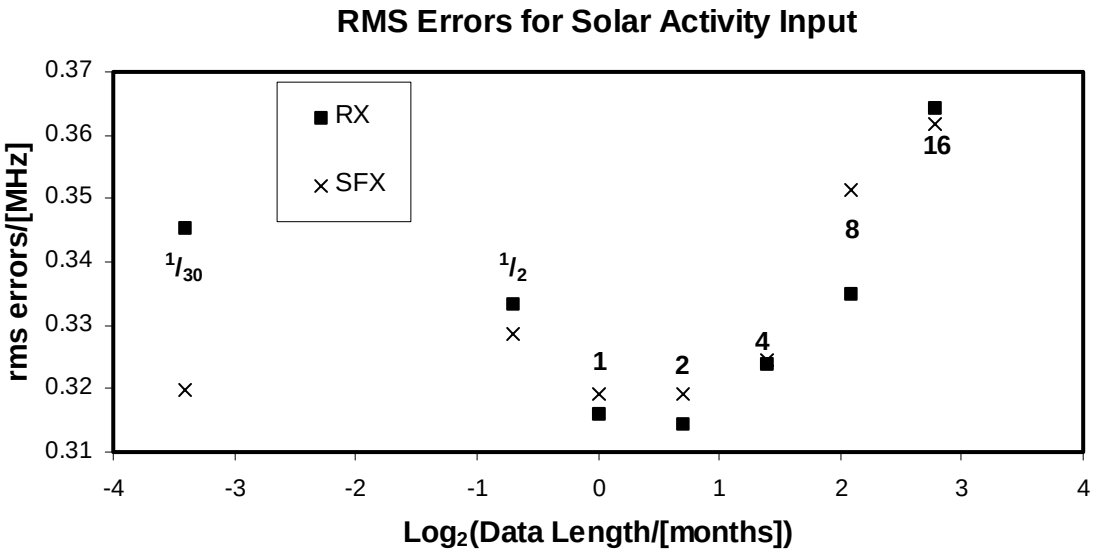

Figure 5-3: The rms errors between the measured and predicted foF1 values are shown. Different data lengths of SSN and SF were used as the solar activity input. The optimum input appears to be near R2.

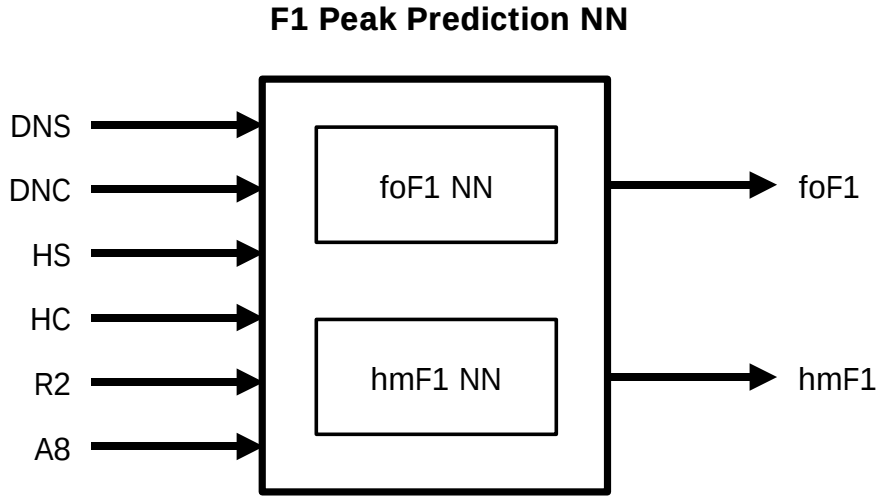

Figure 5-4: The F1 peak prediction NNs, showing the inputs and outputs to the foF1 NN and the hmF1 NN.

5.3.2 hmF1

The IRI (*Bilitza [1990])* does not provide an expression for determining the hmF1 value, but determines hmF1 as the height at which the IRI bottomside profile reaches the F1 peak electron density. This IRI profile is described by a parameter referred to as the thickness parameter, B0 (*Bilitza et al [2000])*. This B0 parameter is based on ionosonde measurements and will affect the value of hmF1 in the IRI.

Various groups (*McNamara and Reinisch [1995]*, *Radicella and Mosert de Gonzalez [1991])* have developed empirical relationships between hmF1 and the F1 peak electron density. No South African data was utilized in the development of these relationships, although *Radicella and Mosert de Gonzalez [1991]* did use Brazilian data from similar latitudes when developing their equation.

5.3.2.1 The Inputs

The optimal inputs for predicting hmF1 were determined by investigating the response of hmF1 to seasonal, diurnal, solar and magnetic variations. These investigations were carried out in an identical manner to those for determining the inputs required for predicting foF1 (section 5.3.1.1).

The optimal inputs were again found to be DNS, DNC, HS, HC, R2, and A8. To confirm the dependence of the hmF1 prediction on A8, this parameter was removed from the input space and the NN re-trained. The rms error between the measured and predicted hmF1 values increased by 5%, which proved that the A8 input should be included.

5.3.2.2 Training the hmF1 NN

A NN was trained to predict hmF1 (in km) given the inputs, DNS, DNC, HS, HC, R2 and A8. The block diagram of the inputs and output to the NN is shown in figure 5-4. For this NN, data was only available from April 1996 to December 2000 inclusive. This amounted to 10965 input vectors, of which 70% were used for training the NN and 30% for testing.

5.4 F1 Occurrence Probability

One of the problems in modelling the ionospheric F1 layer is that the F1 layer is not always present. Apart from the fact that the F1 layer is definitely not present at night, it is also absent during the day under certain conditions. The critical frequency of the F1 layer, foF1, is scaled when a definite cusp is apparent on the ionogram. In this case an F1 layer is definitely present. However, there are instances where a ledge appears on the ionogram instead of a cusp. In this case numerical values for foF1 are difficult to obtain from the ionogram, and the F1 layer is then scaled as “L-condition”. Any reliable ionospheric electron density model requires a mechanism for identifying the occurrence of an F1 layer and predicting the shape of the profile around that layer.

The IRI (*Bilitza [1990])* makes use of the *Ducharme et al [1971]* formula for determining the foF1 value, which also provides a formula for determining a critical solar zenith angle for the occurrence probability of the F1 layer. An F1 layer only exists when the zenith angle is less than this critical angle. In addition to the restriction imposed by this formula, the IRI also omits the F1 layer at night and in winter.

More recently, *Scotto et al [1997]* have proposed that the IRI use a probability function, which has a dependence on the solar zenith angle, R12 and geomagnetic latitude, as a means for determining the presence of an F1 layer. In developing this probability *Scotto et al [1997]* have included L-condition hours in their data base.

This section discusses pioneering attempts at using NNs to develop a mechanism for determining the probability of occurrence of the F1 layer, which can be incorporated into the LAM model.

5.4.1 Initial Attempts

Initially, a similar procedure to that used in chapter 4, section 4.4, for establishing the E limits NN was followed. Using the foF1 values data base, the start and end hour of each F1 day was extracted. Therefore, for each input set there existed two hours between which an F1 layer was measurable.

A NN was then trained to predict the start and end hours of a measurable F1 layer, given DNS, DNC and R2. Although this NN trained well it did not take into account those periods when there was no F1 layer during the day. Even though there was no training data for those periods, the NN still provided seemingly reasonable outputs when presented with the appropriate input set. However, a closer look at the input space revealed that there are large gaps in the areas where no F1 was measurable during the daytime. The NN is, therefore, being interrogated with input data with which it has not been trained. Also, this NN does not provide a good solution to all the aspects of the F1 occurrence problem since no provision has been made for L-condition times. This attempt was then abandoned in favour of a new method that provided an elegant solution to these problems.

5.4.2 F1 Probability NN

The occurrence of an F1 layer can be classified into three categories as follows:

- F: The F1 layer exists and can be measured
- L: The F1 layer exists in a L-condition state
- N: The F1 layer does not exist

In the case of category F, the peak layer characteristics as well as a description of the F1 profile would be predicted and smoothly inserted between the E layer and the F2 layer. With category N, no F1 layer is present and, therefore, no F1 predictions are required. However, in the event of category L, an algorithm needs to be developed for predicting a realistic description of the F1 layer part of the profile under this condition.

The data that has been measured with the DPS sounder and scaled with the Artist software does not include L-condition information. Fortunately, examples of all three categories can be found in the data base of Verti data from Grahamstown, which spans the period January 1973 to April 1996 inclusive. This dataset was manually scaled and instances of L-condition were recorded.

For every input datum (DN, HR, R2) in the data base, a category (F, L, N) was assigned according to the above criteria. Three outputs, defined as P(F), P(L) and P(N), were then attached to each input set. For a particular input set a value of 0 or 1 was assigned to each output as shown in table 5-1.

A NN was trained with the inputs DNS, DNC, HS, HC and R2 to predict the three outputs, P(N), P(L) and P(F). Using the rms criterion, the magnetic activity input was found to have no effect on the predicted outputs and therefore was not included in the input space for this NN. When interrogated the NN will produce a value for each of the outputs that falls between 0 and 1. Each of these output values can be viewed as the probability of the occurrence of the particular category represented by the output. This NN will be referred to as the "F1 Probability NN". Figure 5-5 is a block diagram of this NN's inputs and outputs.

Category	P(N)	P(L)	P(F)
F	0	0	1
L	0	1	0
N	1	0	0

Table 5-1: This table shows the values of each output for the three different categories.

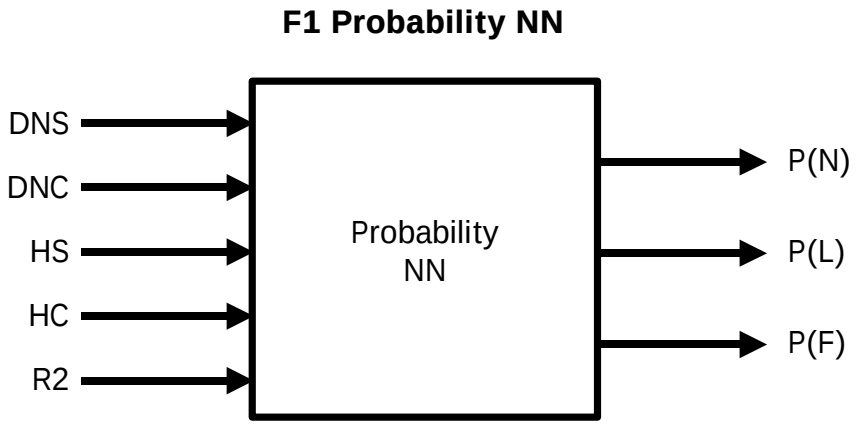

Figure 5-5: The inputs and outputs to the F1 Probability NN. The outputs represent the probability of occurrence of the three different F1 existence categories.

Conditions need to be applied to the three outputs that are predicted by this NN in order to determine which category has the highest probability. For every input set the sum of P(F), P(N) and P(L) is equal to 1. If P(N) is greater than 0.5 the category is N and no F1 layer exists, while if P(F) is greater than 0.5 the category is F. If both P(N) and P(F) are less than 0.5, the category is L and the L algorithm (described later in section 5.5.4) will be applied.

5.5 The F Layer Profile

A method for predicting the F layer profile from foE to foF2 that will produce valid predictions under any condition, and for all outcomes of the F1 Probability NN, is required.

As part of its SAO format output, the Artist scaling software of the DPS provides a description of the F1 layer profile, when present, and a description of the F2 layer profile. These descriptions take the form of a set of five Chebyshev coefficients for each layer. As the cheby method (chapter 4) is the preferred

method for profile prediction for the LAM model, the Chebyshev coefficient descriptions are of interest here.

The Grahamstown Verti data provides no profile information at all and so only the Grahamstown DPS data were used for profile prediction. This means that the dataset that was available for the development of the F layer profile contribution to the LAM model was limited to the period April 1996 to December 2000 inclusive, covering approximately 22% of a 22-year sunspot cycle.

5.5.1 Initial Attempts

This section describes an initial attempt at modelling the profile description of the F layer. Although this attempt was subsequently abandoned, it is described here for completeness.

The F layer profile consists of the F1 layer, when present, and the F2 layer. Each of these layers is described in the DPS output in terms of five Chebyshev coefficients and the ionospheric peak layer characteristics. In this initial attempt, the two layers are dealt with individually and therefore two NNs were trained, one to predict the F1 layer description (F1NN) and one to predict the F2 layer description (F2NN).

F1NN was trained to predict the five Chebyshev coefficients that describe the F1 layer (F1A0, F1A1, F1A2, F1A3 and F1A4), using the same input space that was found to be optimal for F1 peak prediction (DNS, DNC, HS, HC, R2, A8). The training and testing data for the F1NN contained only F1 layer information that came from the DPS F1 layer descriptions.

F2NN was trained to predict the five Chebyshev coefficients that describe the F2 layer. The same input space used for predicting the F2 peak characteristics (DNS, DNC, HS, HC, R2 and A16) was used for training F2NN. All F2 layer information, irrespective of the presence of an F1 layer, was used in the training and testing of F2NN.

These two NNs, F1NN and F2NN, were trained completely independently, although there was some overlap in the input space where both F1 and F2 layers were present for the same input set. After F1NN and F2NN have predicted the coefficients they are used together with the values for the layer peak in the analytical equation for determining the height given the frequency (*Huang and Reinisch [1996])*, which appears in chapter 4, equation (4-1).

Although F1NN and F2NN trained well, and the predicted coefficients resulted in realistic profiles for each layer, there was no continuity in the profile at the F1-F2 boundary. Additional information was required to ensure a smooth continuous profile at the F1-F2 boundary. When an F1 layer is present, the starting height of the F2 layer, hsF2, should equal the peak height of the F1 layer, hmF1. The two NNs, F1NN and F2NN, had learned the relationship between the input parameters and the output vectors that were the coefficients, as well as the dependence of the coefficients on each other. As was the case in chapter 4 with the E layer, the profile NNs required more information in the training stage than was originally planned for in this initial attempt. In order to determine the profile from equation (4-1) the peak layer information is required as well as the coefficients that describe the shape of the profile. Therefore, this approach was abandoned and a more satisfactory method was adopted.

The original datasets that were used to train the F1NN and F2NN were combined and then re-divided into two subsets. One subset consisted of all vectors where only F2 information was available (i.e. no F1 layer was measurable), while the second subset contained all vectors where both F1 and F2 layer information was available for the same input vector. The first subset will be referred to as the “F2 set” and the second as the “F1F2 set”.

5.5.2 The F2 Set

The F2 set contained all information required to predict the F2 layer profile description in the absence of an F1 layer. A NN was trained to predict the profile

description parameters, with six inputs and seven outputs. The inputs were DNS, DNC, HS, HC, R2 and A16 while the outputs were foF2, hmF2, F2A0, F2A1, F2A2, F2A3 and F2A4. F2AX, X = 0, 1, 2, 3, 4, refers to the five coefficients that describe the F2 layer. The dataset was made up of all ionograms for which no F1 layer was reported and covered the period April 1996 to December 2000 inclusive. Before training each output was plotted in chronological order against an index value and all outliers were eliminated. This was done in order to ensure that the prediction results from the NN were not skewed by incorrect data. In particular, there are instances where the ionograms have been inaccurately scaled. After eliminating outliers 20070 input vectors were available, 70% of which were used for training and 30% for testing. Figure 5-6 shows a visual representation of this NN's inputs and outputs. This NN will be referred to as the F2NN, and replace the earlier F2NN of the initial attempts section (section 5.5.1).

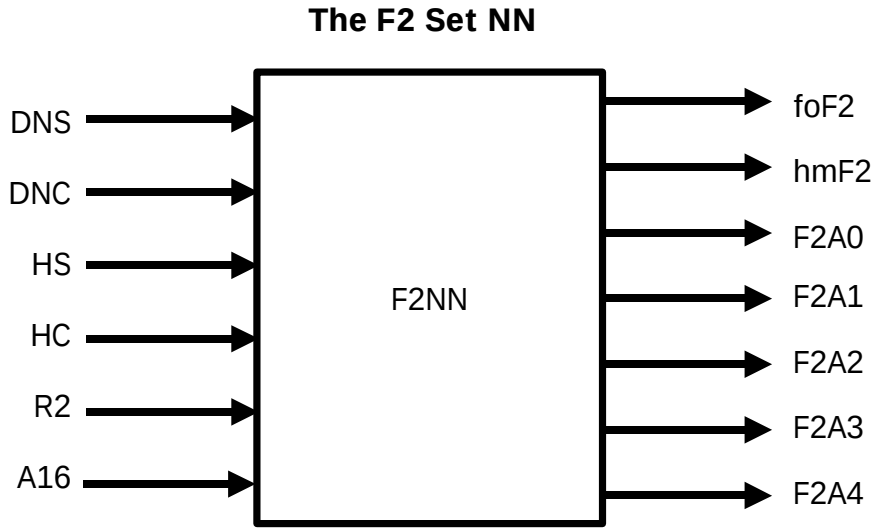

Figure 5-6: A block diagram of the inputs and outputs to the F2NN. This NN is trained to predict the parameters required for F2 profile description in the absence of an F1 layer.

5.5.3 The F1F2 Set

When an F1 layer is present, as determined by the F1 probability NN, all characteristics and coefficients required to determine a description of the shape of the F layer profile from foE to foF2, via foF1, are predicted. In this case fifteen parameters are required and, therefore, the NN trained to predict this description had fifteen outputs, namely foE, foF1, hmF1, foF2, hmF2, F1A0, F1A1, F1A2, F1A3, F1A4, F2A0, F2A1, F2A2, F2A3 and F2A4. F1AX and F2AX, X = 0, 1, 2, 3, 4, refers to the five coefficients that describe the F1 and F2 layers respectively. The inputs, DNS, DNC, HS, HC, R2 and A16, were the same as for F2NN.

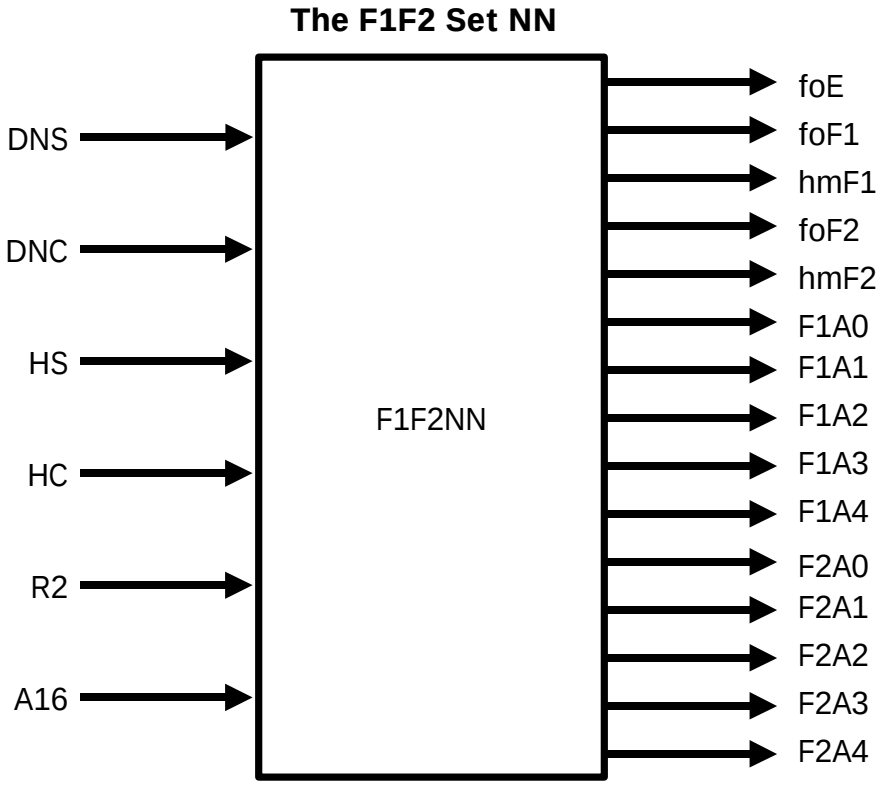

Figure 5-7: The inputs and outputs to the F1F2NN are shown in this diagram. There are 15 outputs that represent the characteristics and coefficients required to construct the profile from foE to foF2 when an F1 layer is present.

All Grahamstown data from April 1996 to December 2000, inclusive, that contained F1 layer information were used for training and testing this NN. After eliminating outliers, a total of 9979 input vectors were available and, again, 70% were used for training and 30% for testing the NN. This NN will be referred to as the F1F2NN. A block diagram of the inputs and outputs appears in figure 5-7.

5.5.3.1 The F1-F2 Boundary

Given that an F1 layer is present, as determined by the F1 probability NN, the F1F2NN predicts the fifteen parameters that are required by equation (4-1) to determine the F layer profile from foE to foF2. The F1F2NN produces an average output to the best of its ability for each one of these fifteen parameters. In order for the profile to be continuous at the F1-F2 boundary, the peak height of the F1 layer, hmF1, must be equal to the starting height of the F2 layer, hsF2. The predicted value of hsF2 is determined by the coefficients and peak characteristics of the F2 layer as predicted by the F1F2NN, while hmF1 is predicted directly.

The difference between hmF1 and hsF2 is a value that can be either positive or negative and appears to always be smaller than the estimated uncertainty in hmF1.

Following a similar procedure to that discussed in chapter 4 section 4.7.5, an estimate of the uncertainty in hmF1 was predicted. The difference between the measured and predicted hmF1 values for each input set was calculated and a NN was trained to predict the square of this difference. The uncertainty in hmF1, hmF1(error), is the square root of the output of the squared differences NN.

If hmF1(error) is greater than (hmF1-hsF2), then the entire F2 profile can be shifted by an amount equal to (hmF1-hsF2) to ensure a continuous profile through the F1-F2 boundary. Provided the hmF1(error) condition is met, this height domain shift is well within the statistical variation of the predicted profile.

5.5.4 The L-Condition Algorithm

If the F1 probability NN reports an L-condition as being most likely to occur, then an F1 layer does exist and should be predicted. However, in reality no measurements would have been possible for that layer. For the LAM model, an algorithm is required that will produce an F layer profile, which, once converted into its equivalent ionogram, will show evidence of the L-condition on the ionogram. In addition, the L-condition F layer profile must provide a smooth transition from the F layer profile before L-condition, to the F layer profile after L-condition.

Values for the F1 layer peak (foF1, hmF1) can be predicted for the L-condition input set using the F1 peak NNs. These NNs will interpolate through the input space to produce these values, and they will be accurate enough to use here.

L-conditions can be reported either for a few hours around sunrise and sunset, or over the whole day from sunrise to sunset, therefore the algorithm must take into account both of these situations.

The LAM model is presented with a particular input set (DN, HR, R2 and A16), for which it is required to determine the F layer profile. If the F1 probability NN reports an L-condition as probable for that input set, then the period of time over which an L-condition is most probable for that given DN is determined.

Working backwards and forwards from the input set hour, HR, in steps of 0.1 hour, a time is reached on either side where L-condition occurrence is not probable. A weighting function, wf, is then calculated, which determines whether HR is close to a time of N category (no F1 present) or close to a time of F category (F1 definitely present). The value for wf will be a number between 0 and 1, with 0 for the HR nearest to N category (min), and 1 for the HR nearest to F category (max).

In the special case where an L-condition is reported for all hours in an F1 day, the L occurrence period is divided into two, and each half is dealt with separately. For this case, wf is calculated with the middle point as the maximum value, and either end the minimum value.

The weighting function, wf, is calculated as follows:

$$Y = \frac{P(L)}{P(L) + P(F)} \tag{5-1}$$

$$wf = \frac{Y_x - Y_{min}}{Y_{max} - Y_{min}} \tag{5-2}$$

P(L) and P(F) are outputs from the F1 probability NN, and Y is calculated for each of the three hours, min, max and x, where min and max are the start and end hours of L-condition occurrence, as discussed above, and x is the hour of interest.

For the L-condition hour, two F layer profiles are predicted using F1F2NN and F2NN, and a foF1 value is predicted using the foF1 NN. At each frequency between foE and foF2 two heights exist as determined from predictions made by the two F layer profile NNs. These heights will be referred to as h_N (no F1 layer) and h_F (definite F1 layer) respectively. The height for the L-condition hour, h_x, is calculated as follows:

$$h_x = h_N + (h_F - h_N) \times wf \tag{5-3}$$

5.6 Results

The results presented in this chapter are those related to the F layer contribution to the LAM model. As in chapter 4, some results will be presented as comparisons with actual DPS data and the IRI 2001, while other results will illustrate the response of the output vector to the variation of the input parameters.

For illustration purposes, typical high and low values were chosen for each input parameter using the same procedure as described in chapter 4. For the F layer model the inputs were DN, HR, and R2, with additional inputs being A16 for the F2 peak and F profile models, and A8 for the F1 peak model. Typical values of DN were arbitrarily chosen as 20 for the summer months and 180 for the winter months.

For the critical frequency models, foF2 and foF1, a larger dataset (28 years) was available for training the NNs than for the other model contributions (5 years). The 28-year dataset (Verti plus DPS data) covered the time period January 1973 to December 2000 inclusive, while the 5-year dataset (DPS data only) began in April 1996 and ended in December 2000.

For the R2 variable, the typical low and high values were chosen such that approximately 70% of the data lay symmetrically between the chosen values. This was applied to both the 28-year and 5-year datasets, resulting in a typical low value of 15 for both datasets, and high values of 140 and 120 representing the 28-year and 5-year datasets, respectively.

The distribution of R2 for the smaller dataset (April 1996 to December 2000) is shown in figure 5-8, with the selected low and high values indicated.

As typical indicators of low and high levels of magnetic activity, the values of 3 and 15 respectively were chosen. These values were selected such that approximately 70% of the data lay between the low and high values with approximately 18% on the high end and 12% on the low end. The A16 distribution was used to select these values and is shown for the smaller dataset (April 1996 to December 2000) in figure 5-9. The A8 distribution produced the same low and high values as A16 for typical indicators of the A8 input. There was only a small difference between the 28-year and 5-year datasets for the A16 and A8 distributions and, therefore, these selected values will be used throughout.

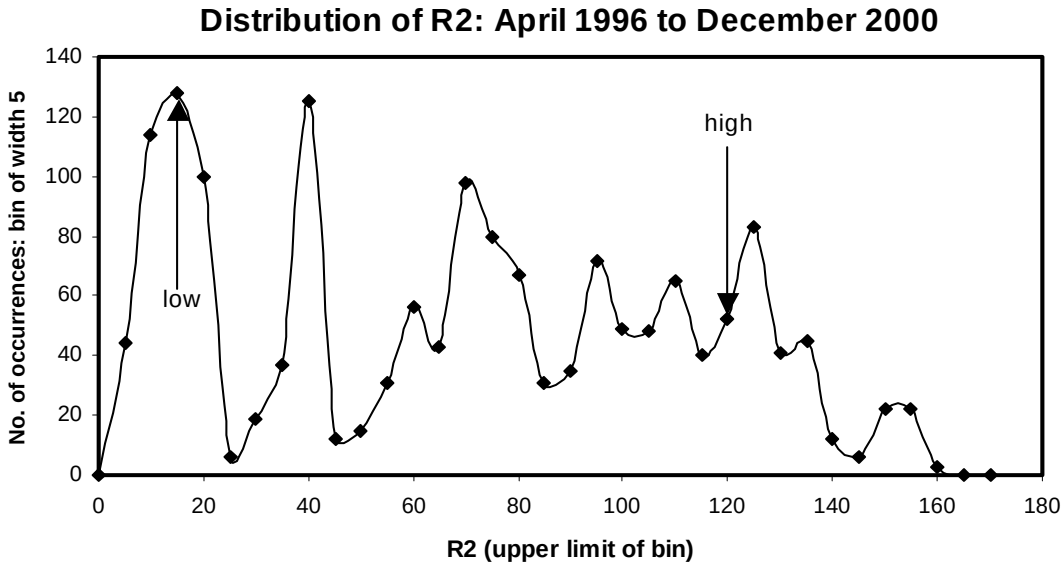

Figure 5-8: The distribution of R2 values, for the period April 1996 to December 2000 inclusive, that was used to determine typical low and high values of R2.

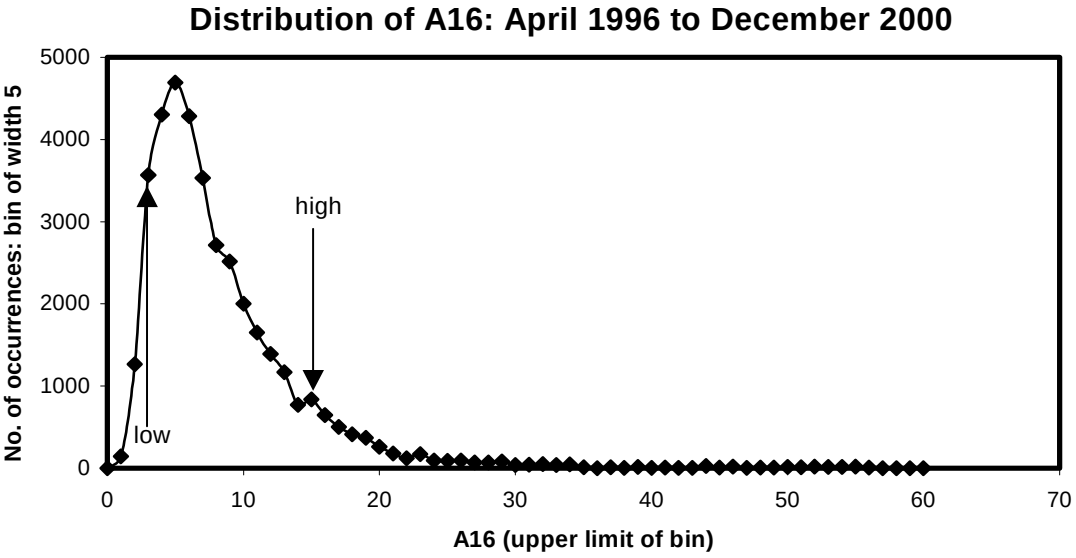

Figure 5-9: The distribution of A16 values, for the period April 1996 to December 2000 inclusive, that was used to determine typical low (A16=3) and high (A16=15) indicators of magnetic activity. The same values were used for the A8 input.

5.6.1 F2 Peak

Williscroft and Poole [1996], *McKinnell [1996]* and *Poole and McKinnell [2000]* all show results from the NN based model for predicting foF2, the maximum electron density in the ionosphere, for Grahamstown. In particular *McKinnell [1996]* shows the variation of the 12h00 SAST foF2 value with changes in solar and magnetic activity. These results will not be repeated here but new results from the updated foF2 model will be shown.

Figure 5-10 shows the measured and predicted 12h00 SAST foF2 values for the year 2001. This is unseen data for the NN since it was trained and tested with data from 1973 to 2000 inclusive. However, the input data for the year 2001 is covered by the training input space and, therefore, the NN can be interrogated with this data. The rms error between the measured and predicted 12h00 SAST foF2 values for 2001 was 0.93 MHz.

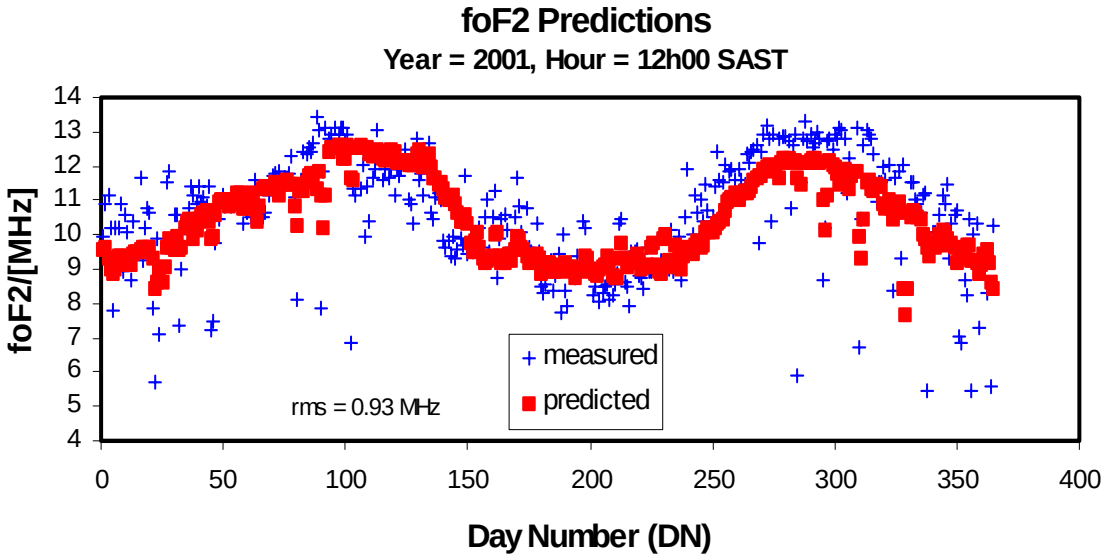

Figure 5-10: The measured and predicted 12h00 SAST foF2 values for 2001.

The diurnal variation is investigated in figure 5-11, which shows four graphs of foF2 versus hour. Each graph illustrates the variation of foF2 over three days, a day in summer, winter and spring, at the four different combinations of low and high levels of solar and magnetic activity. These results confirm those of *McKinnell [1996]*, where only the 12h00 SAST values were dealt with.

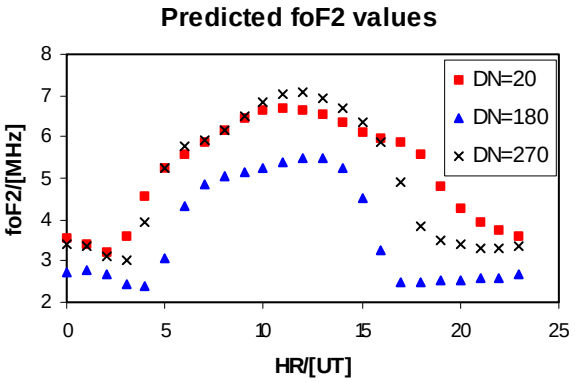

(a) R2 = low, A16 = low

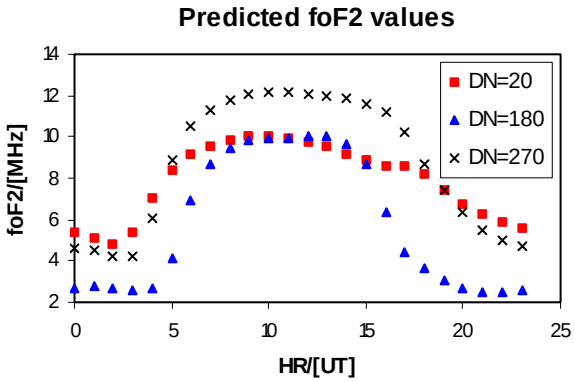

(b) R2 = high, A16 = low

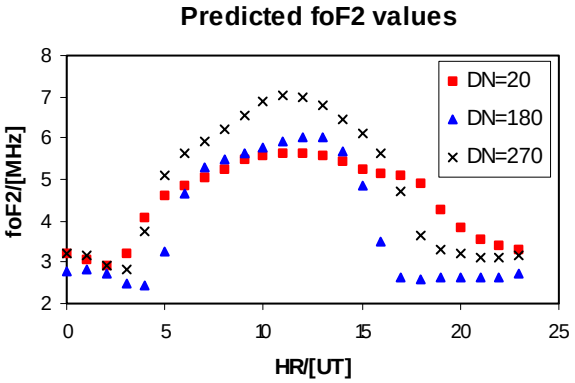

(c) R2 = low, A16 = high

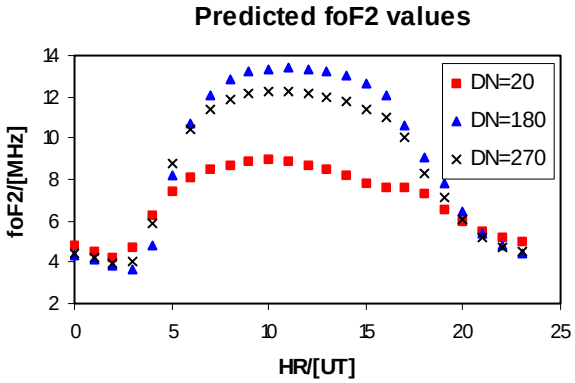

(d) R2 = high, A16 = high

Figure 5-11: Four graphs are shown illustrating the diurnal variation of the predicted foF2 value for three days of the year. These graphs are shown for different levels of solar and magnetic activity.

The inputs required for predicting the peak height, hmF2, from the LAM model are DN, HR, R2 and A16. Just over five years of Grahamstown hmF2 data (April 1996 to December 2000) were used for training a NN to predict hmF2. Figure 5-12 shows the measured hmF2 values over this period for one hour, 12h00 SAST, along with the predicted values. The NN has produced an average hmF2 value for each input set.

The relationship between hmF2 and the input parameters is investigated in figures 5-13 and 5-14. In figure 5-13, the HR has been fixed at 12h00 SAST and the DN varied from 1 to 365. Four subsets of hmF2 values were then predicted using the four combinations of the low and high values of R2 and A16.

From these graphs it can be seen that high magnetic activity decreases the hmF2 value during the summer but increases it during the winter. At high solar activity in the winter months the effect of the magnetic activity input is stronger than in the summer.

Figure 5-14 illustrates the diurnal variation of hmF2 by varying the HR input from 0 to 23. Four graphs that illustrate the hmF2 values for low and high R2 are shown. Figures 5-14(a) and 5-14(b) are the predicted hmF2 values for a summer day at low and high A16 respectively. Figures 5-14(c) and 5-14(d) are the predicted values for a winter day at low and high A16 respectively.

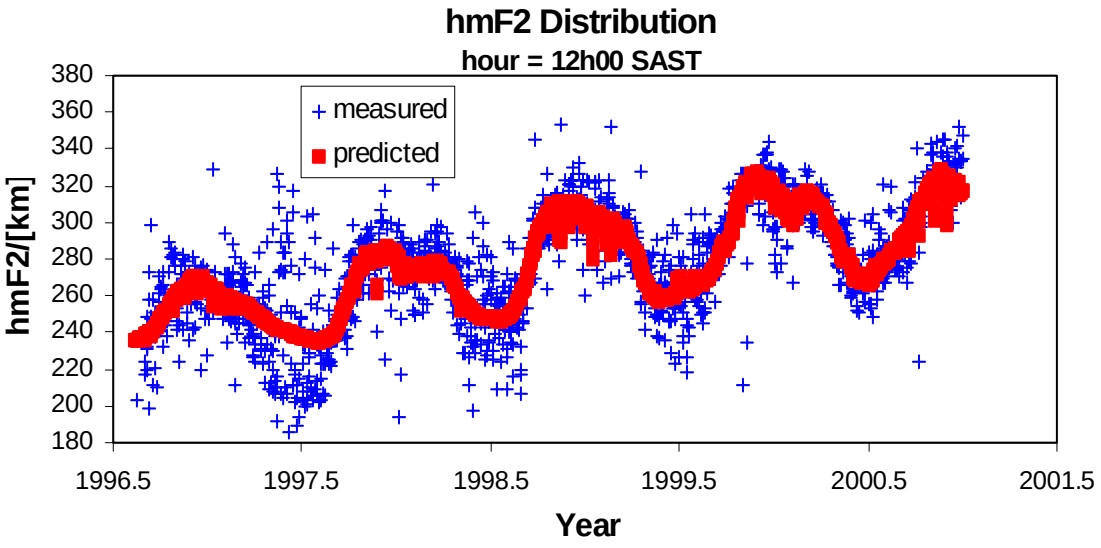

Figure 5-12: The measured and predicted hmF2 values for April 1996 to December 2000. These are the 12h00 SAST values only.

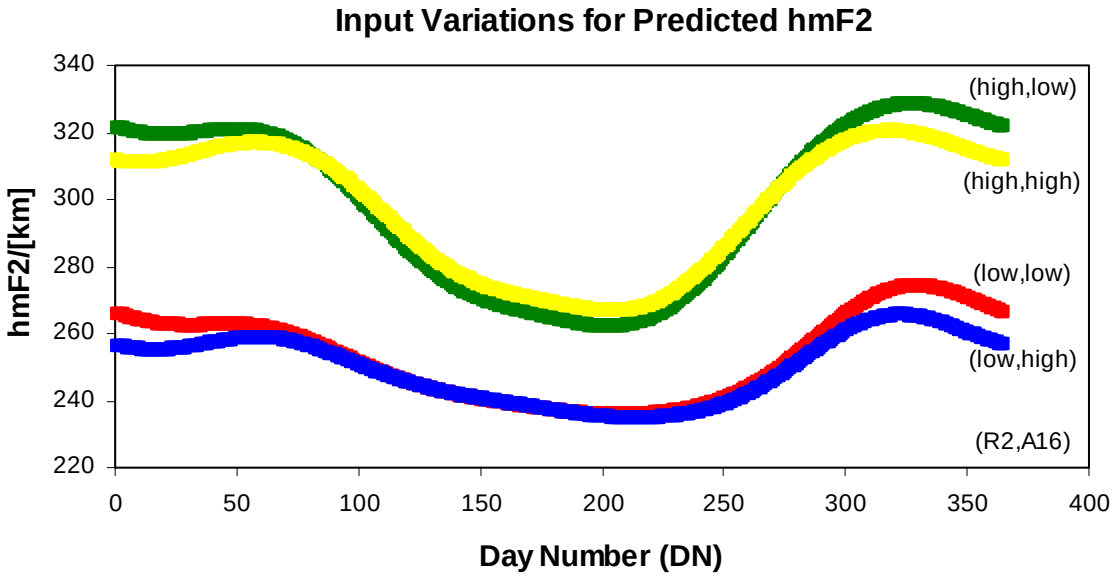

Figure 5-13: An illustration of the relationship between hmF2 and the input parameters. The high and low labels refer to the high and low levels of R2 and A16.

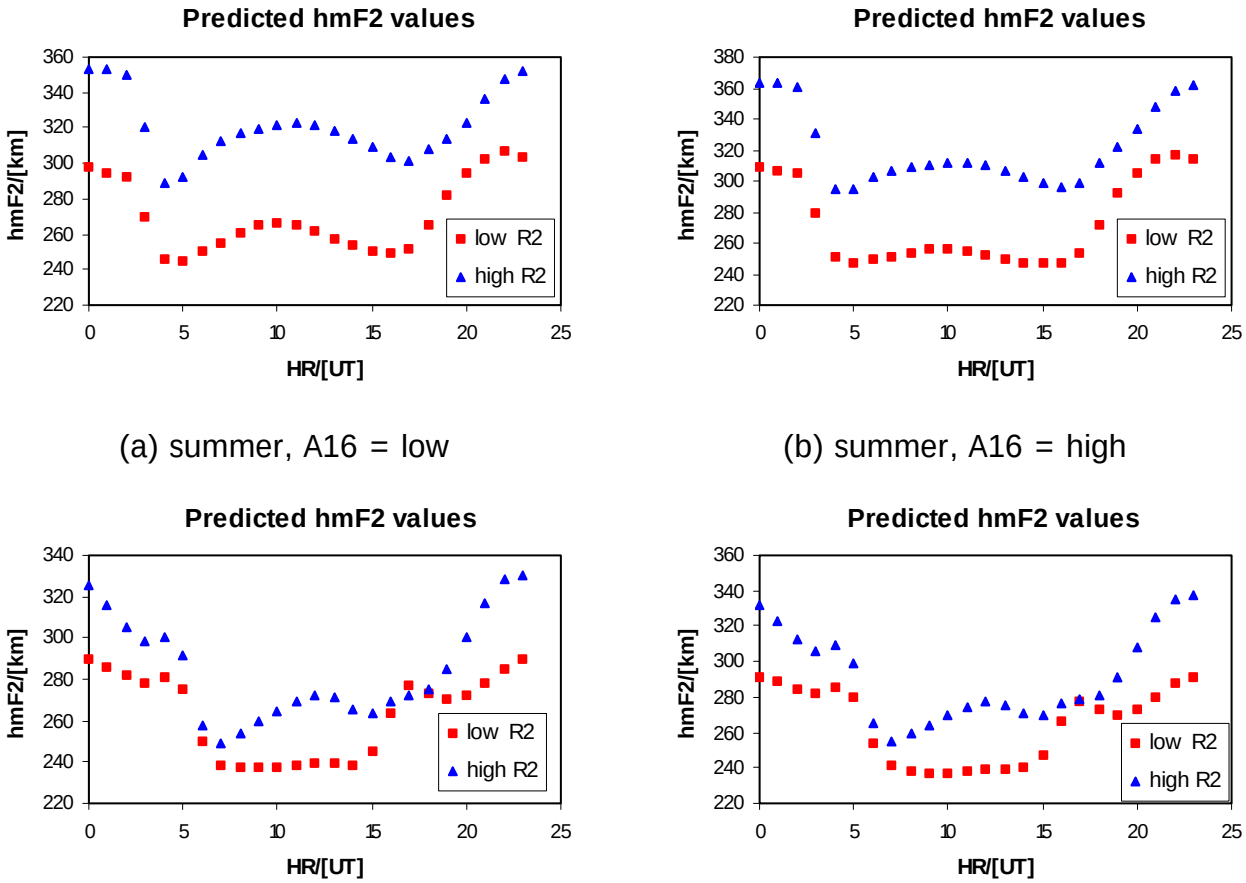

(a) summer, A16 = low

(b) summer, A16 = high

(c) winter, A16 = low

(d) winter, A16 = high

Figure 5-14: Four graphs illustrating the diurnal variation of the hmF2 value for low and high R2 are shown. Graphs (a) and (b) show a summer day while graphs (c) and (d) show a winter day at low and high A16 respectively.

5.6.2 F1 Probability

The F1 Probability NN predicts three outputs that describe the probability of an F1 occurrence given the inputs DN, HR, and R2. These outputs are defined as P(N), P(L) and P(F), where N, L, and F are the three categories of F1 existence as described in section 5.4.2. That section also describes the procedure followed in using these outputs to determine the state of the F1 layer.

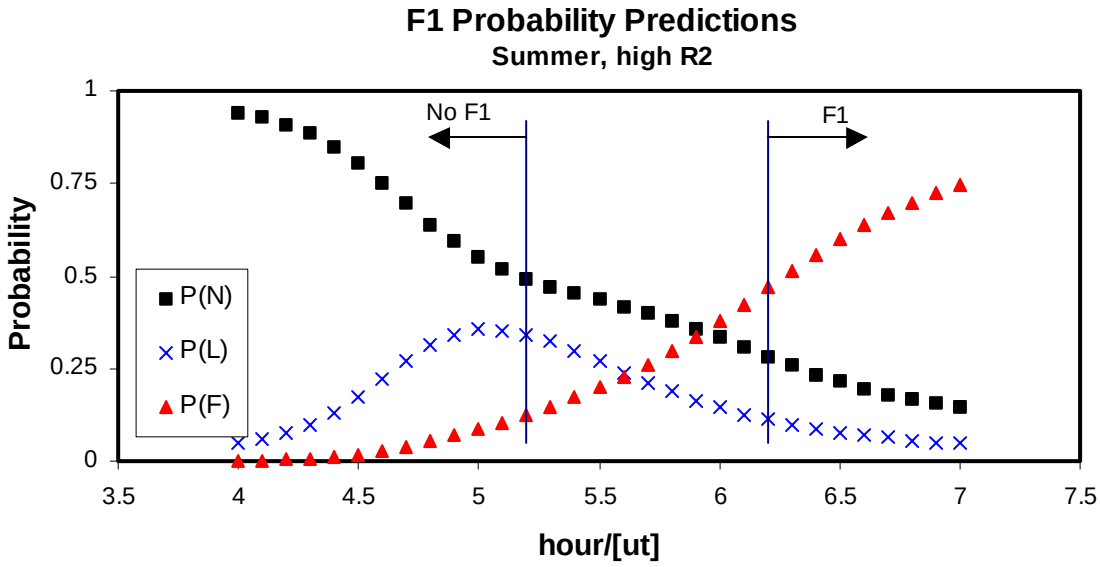

(a)

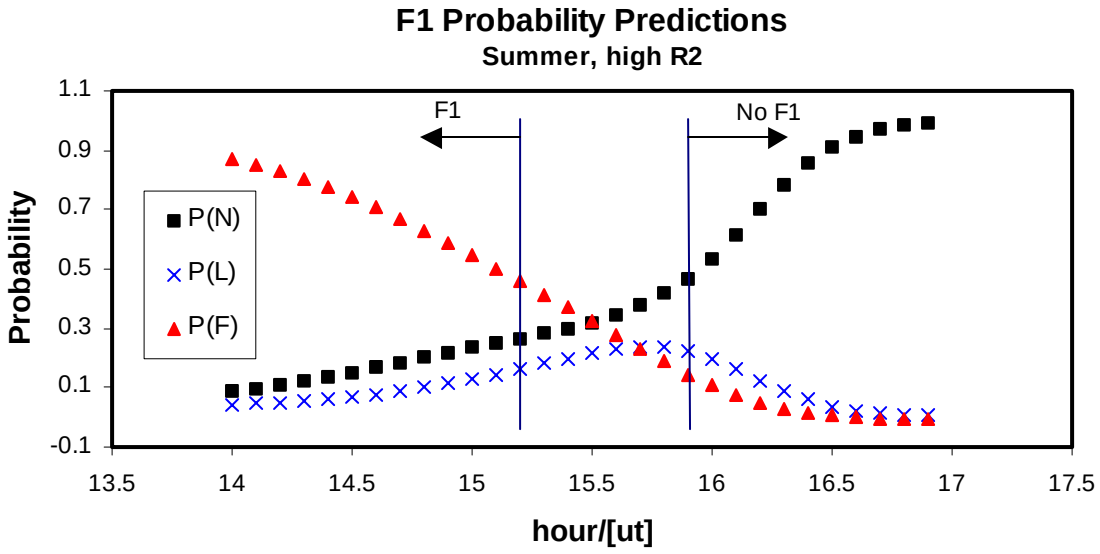

(b)

Figure 5-15: These two graphs illustrate graphically the outputs from the F1 Probability NN. The occurrence probability of an F1 layer for a summer day at high R2 at (a) the start and (b) the end of an F1 day is shown. On the graphs the vertical black lines indicate the boundaries between which the L-condition algorithm is applied.

High solar activity is a time when all three of the states of F1 occurrence are most likely to occur in any one day. Figure 5-15 shows the three outputs from the F1 probability NN for a summer day at high R2. Two graphs are shown to illustrate the start and end of an F1 day, where it can be seen that the NN has learnt the average progression from a state of no F1 (category N) to a state of definite F1 (category F). On these graphs the two vertical solid lines represent the boundaries between which the L-condition algorithm (section 5.5.4) is applied.

Another example of the predictions made by the F1 probability NN is shown in figure 5-16. This example is for an autumn day (DN=90) at high R2, which is an area of the input space that is most likely to have L-condition status over the entire day. This is an example of the special case referred to in section 5.5.4.

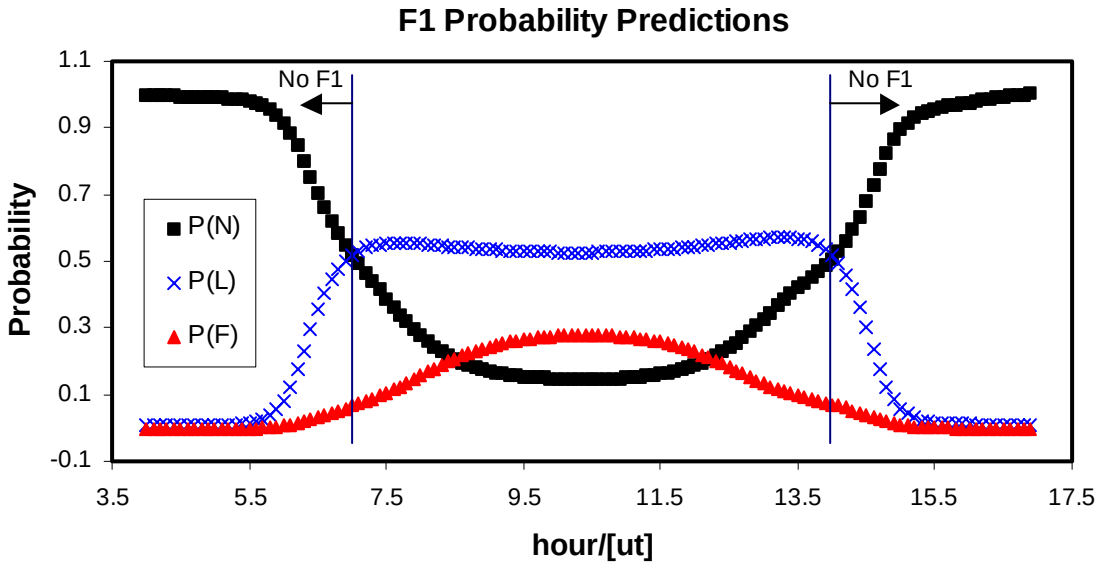

Figure 5-16: The three outputs from the F1 probability NN are shown to illustrate an example where L-condition status is most probable over an entire F1 day. In this case the L-condition algorithm will be applied to all hours that fall inside the boundaries indicated by the vertical solid lines.

5.6.3 F1 Peak

Two NNs were trained to predict the critical frequency of the F1 layer, foF1, and the peak height, hmF1, given the inputs, DN, HR, R2 and A8. In the LAM model, these NNs are only interrogated at times when the existence of an F1 layer is probable, as determined by the F1 probability NN.

The dataset used for training the foF1 NN spanned the years 1973 to 2000 inclusive. Figure 5-17 shows the 12h00 SAST measured and predicted foF1 values for two years taken from this dataset, a year at low R2 (1976) and a year at high R2 (1980). The NN provided predicted foF1 values for input vectors that produced a P(N) output from the F1 probability NN of less than 0.5. Since a value of foF1 is provided by the NN for use in the L-condition algorithm, foF1 predictions for the incidences of L-condition have been included for all of the results presented in this section. The F1 probability NN has learnt that during autumn and winter of a high solar activity year the F1 layer does not exist in any state. This explains the gaps in the predicted foF1 values for 1980 shown in figure 5-17.

There are measured foF1 values available for Grahamstown for the year 2001 which the NN has never seen before. Figure 5-18 shows the 2001 measured and predicted foF1 values for 12h00 SAST. The rms error between these measured and predicted values was 0.47 MHz.

To investigate the relationship between foF1 and the inputs, HR, R2 and A8, each input was varied in turn while the others remained fixed at the typical low and high values. The diurnal variation is shown in the four graphs of figure 5-19. Each graph represents a season, summer (DN=20), autumn (DN=90), winter (DN=180), and spring (DN=270). Only hours for which the F1 probability NN determined the probable existence of an F1 layer are shown. For each season, the predicted foF1 values at the four combinations of low and high R2 and A8 are shown. These graphs reveal that the magnetic activity input, A8, has a very small effect on the value of foF1, which is seen mostly in summer and at high R2.

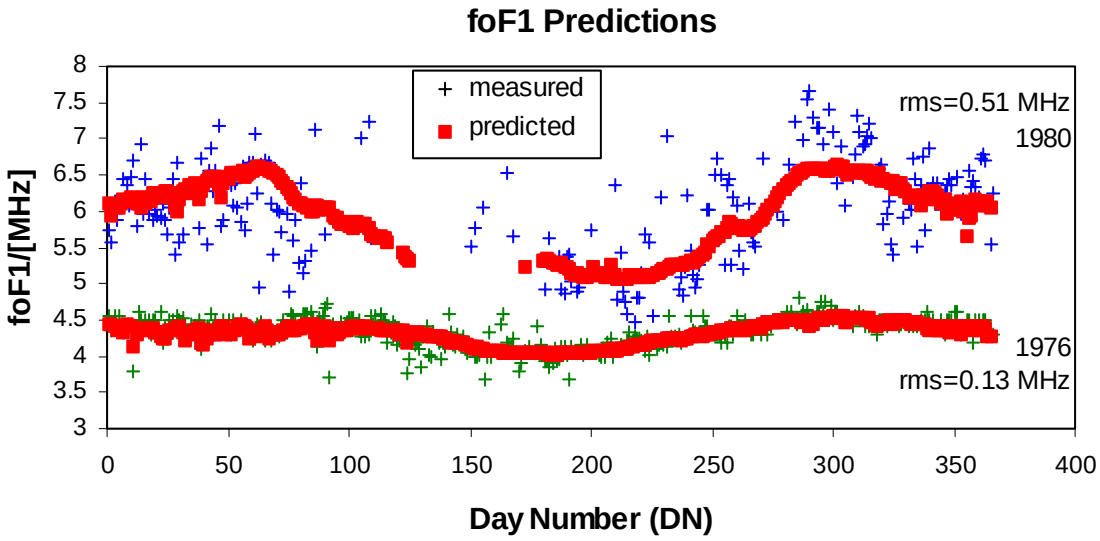

Figure 5-17: The measured and predicted 12h00 SAST foF1 values for 1976 (low R2) and 1980 (high R2). The rms errors were 0.13 MHz and 0.51 MHz respectively.

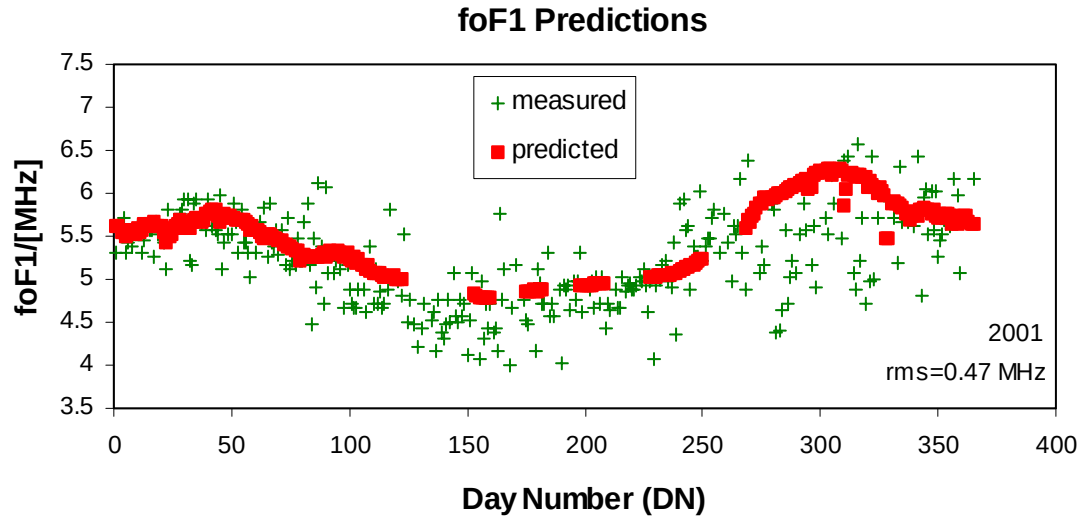

Figure 5-18: This figure shows the measured and predicted 12h00 SAST foF1 values for 2001, a year of high R2. The rms error was 0.47 MHz.

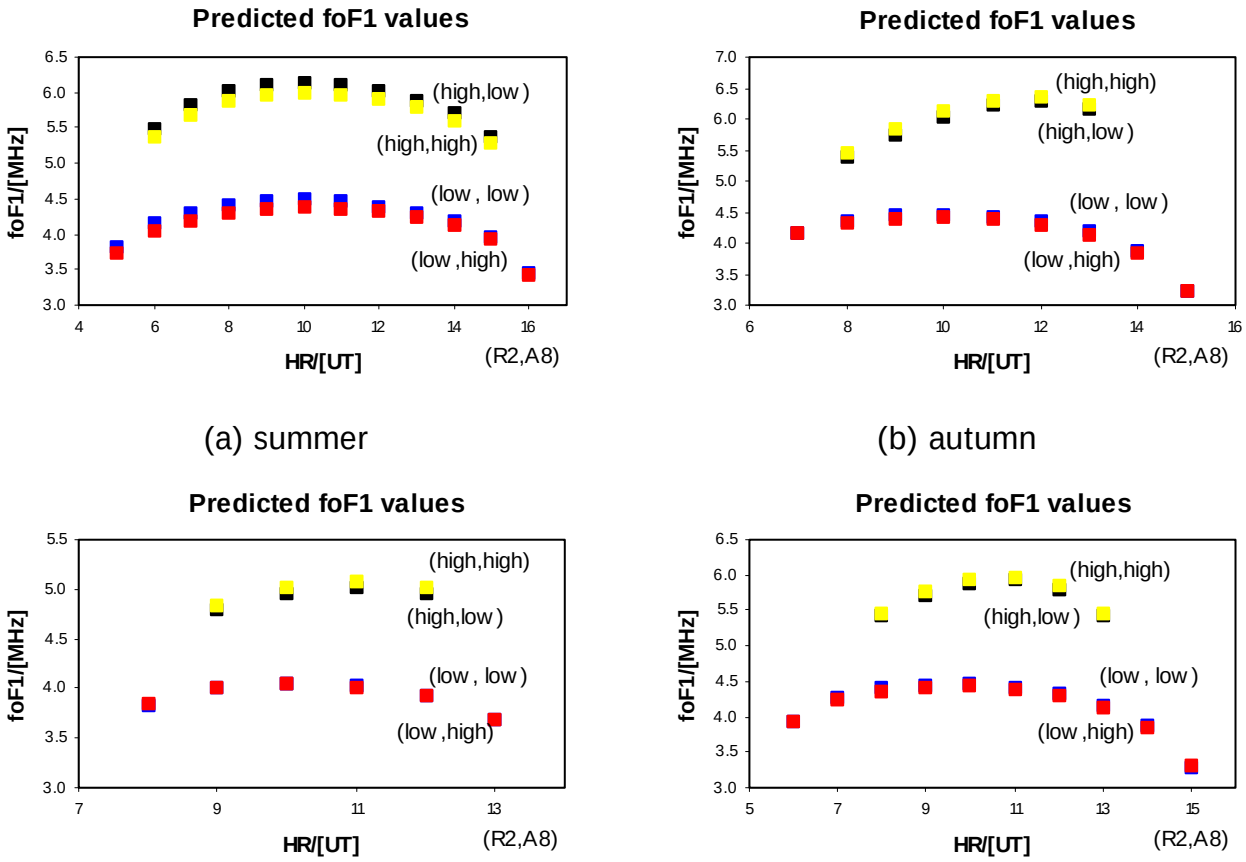

Figure 5-19: These four graphs show the predicted foF1 values for test input sets that were used to investigate the relationship between the input parameters and foF1. The low and high labels refer to the typical low and high values of R2 and A8.

Figures 5-20 and 5-21 confirm the findings of figure 5-19, while investigating the solar and magnetic variations further. In figure 5-20, R2 was allowed to vary while the other inputs were fixed. The 12h00 SAST foF1 values were predicted for a summer and winter day at low and high A8. Figure 5-21 illustrates the seasonal and solar response of foF1 to increases in magnetic activity.

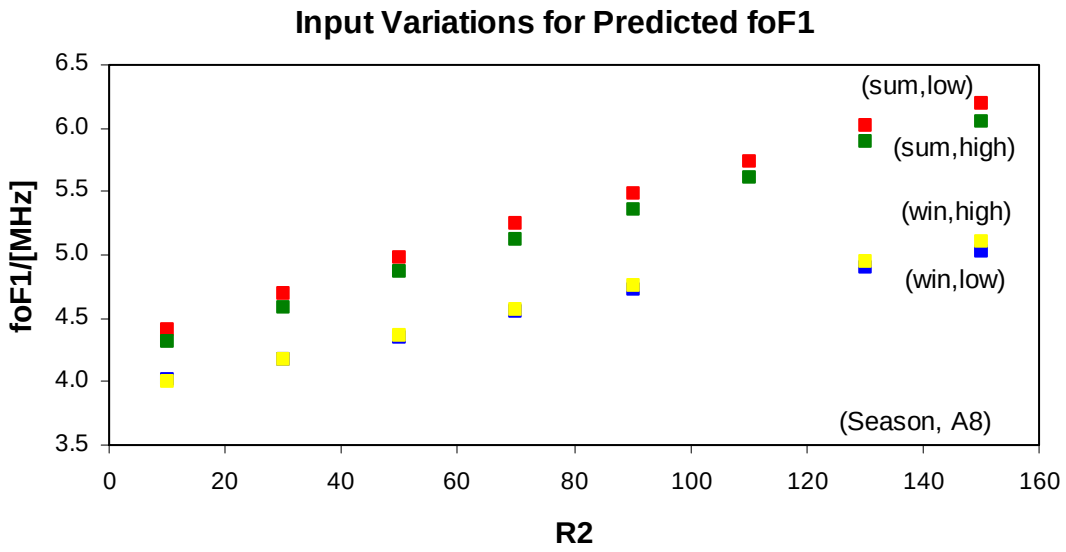

Figure 5-20: This graph represents the seasonal response of foF1 to increased solar activity at high and low levels of magnetic activity. The break in the winter graphs at a R2 of 110 is due to that area being where the probability of no F1 layer presence is high.

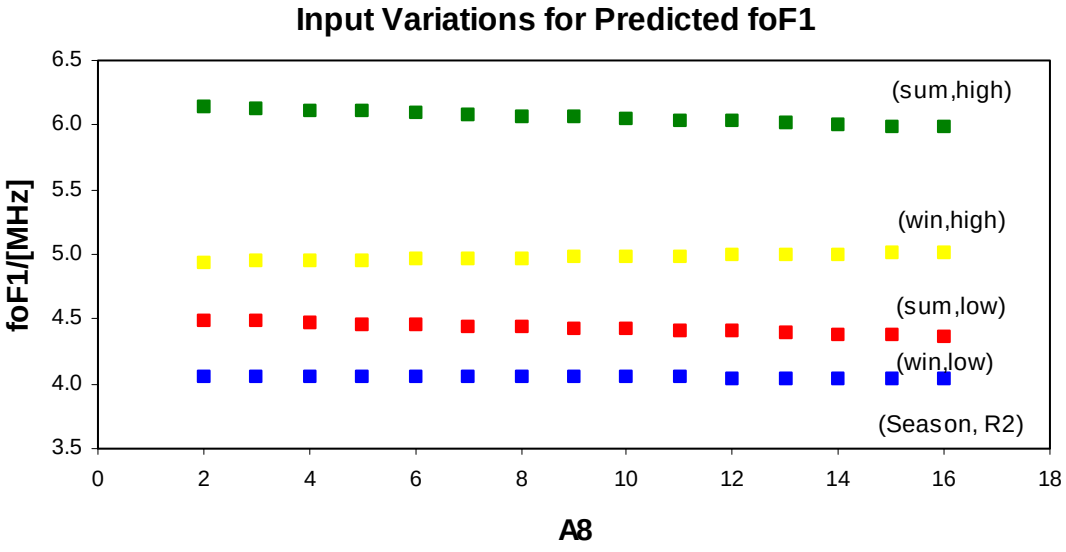

Figure 5-21: This graph illustrates the small influence that the magnetic activity input, A8, has on the prediction of foF1. The most notable effect on the value of foF1 is at high R2.

Figures 5-20 and 5-21 verify that there is almost no response from the foF1 value to a change in the level of magnetic activity in the winter months at low solar activity. It is also apparent that the foF1 value increases in winter at high R2 and decreases in summer at all levels of R2 for increasing A8.

The Grahamstown data available for training the hmF1 NN spanned the period April 1996 to December 2000 inclusive. Figure 5-22 shows the measured and predicted 12h00 SAST hmF1 values for this period. From this graph it can be seen that the NN is producing an average hmF1 value for each input set.

Figures 5-23 and 5-24 illustrate the relationship between hmF1 and the input parameters, DN, HR, R2 and A8. The seasonal variation of hmF1 at 12h00 SAST is demonstrated in figure 5-23, where the DN has been varied from 1 to 365 and the other parameters fixed. The four graphs represent the four combinations of the typical low and high values of R2 and A8. A value for hmF1 was only predicted for those input sets that yielded a probable F1 layer outcome from the F1 probability NN ($P(N) < 0.5$).

The diurnal variation of hmF1 is shown in the four graphs of figure 5-24. The graphs show predicted hmF1 values for the four combinations of low and high R2 and A8 in summer and winter.

From these graphs it can be seen that the hmF1 value increases in summer and decreases in winter with increasing solar activity. Also, the effect of magnetic activity on the hmF1 value is considerably greater than its effect on the foF1 value. In summer an increase in magnetic activity results in a large increase in hmF1, while in winter the increase is less.

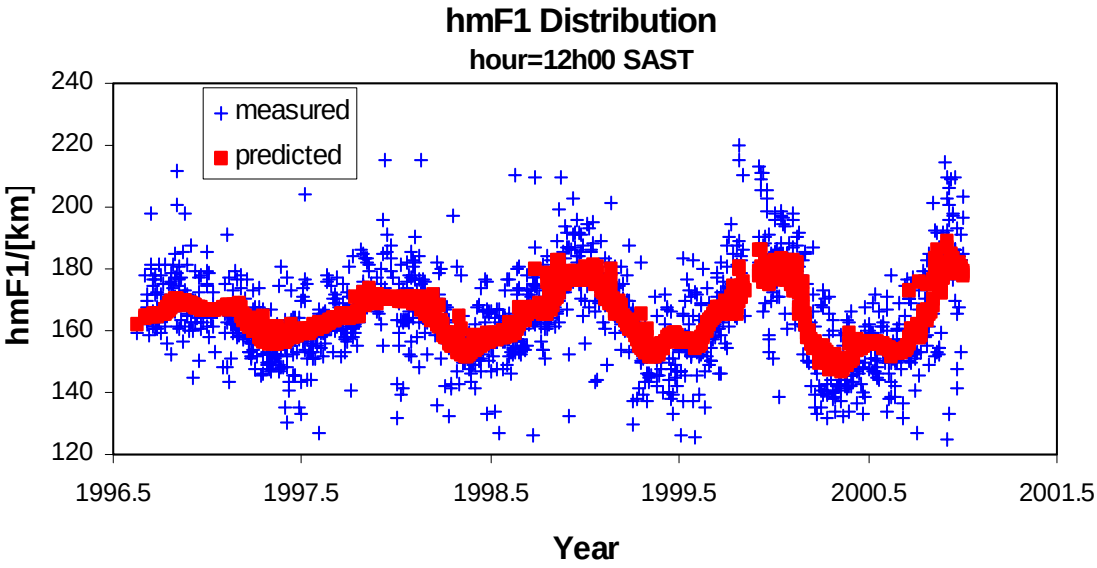

Figure 5-22: All 12h00 SAST measured and predicted hmF1 values are shown in this graph. The measured values are those that were used to train and test the hmF1 NN.

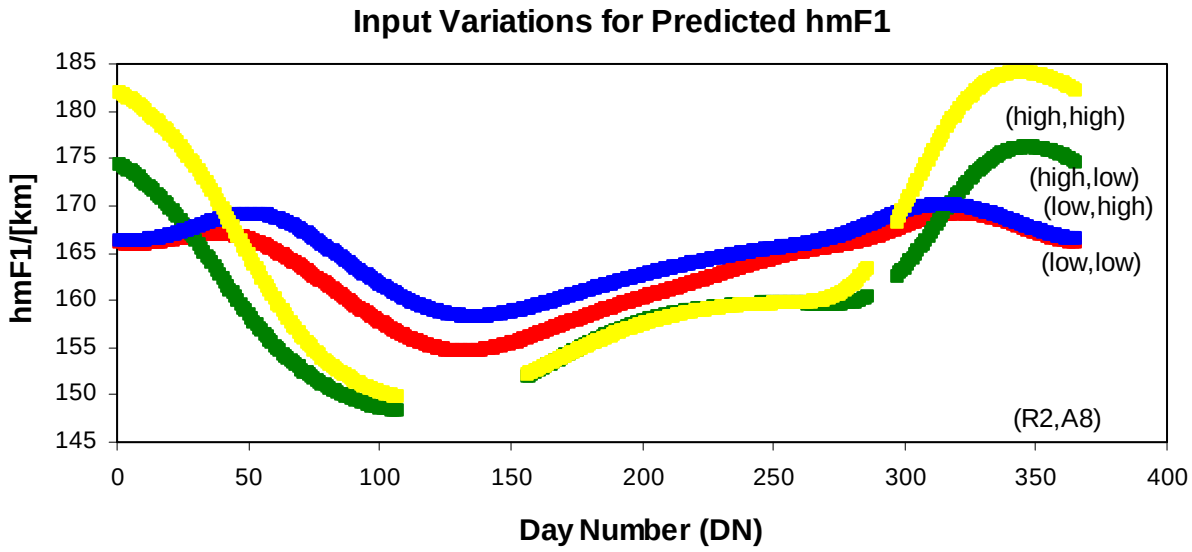

Figure 5-23: Predicted hmF1 values were obtained for each DN from 1 to 365 at four combinations of the low and high R2 and A8 values.

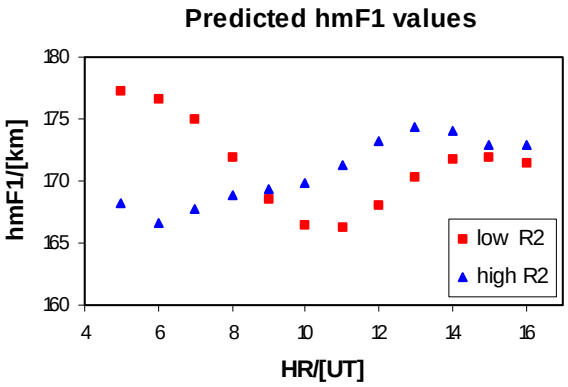

(a) summer, A8 = low

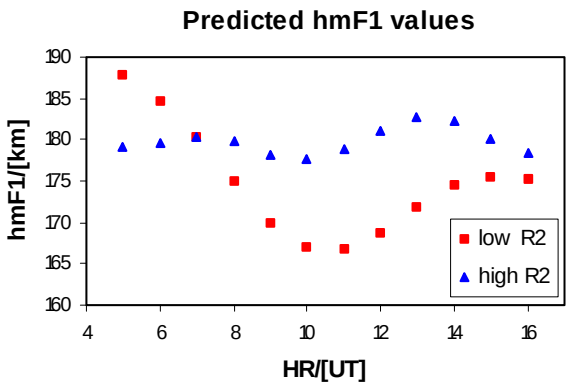

(b) summer, A8 = high

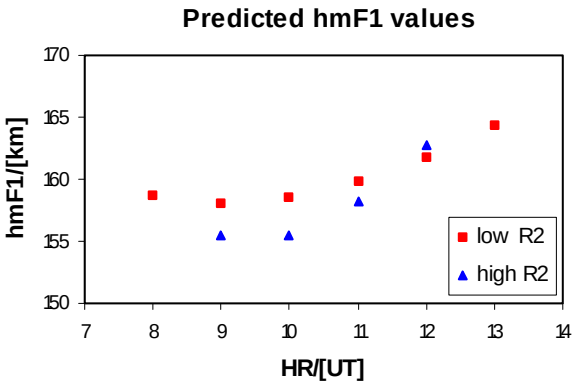

(c) winter, A8 = low

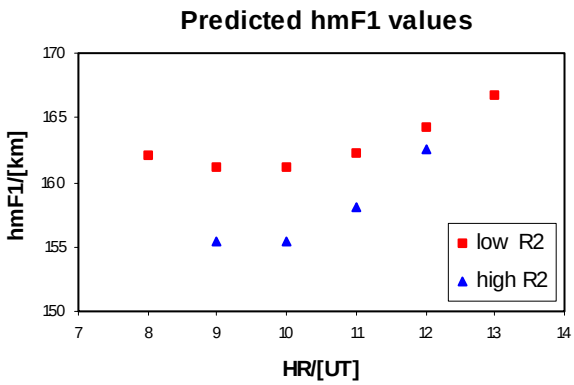

(d) winter, A8 = high

Figure 5-24: The diurnal variation of the hmF1 values for a summer and winter day at low and high R2 are shown in this figure. Graphs (a) and (c) are at low magnetic activity and graphs (b) and (d) are at high magnetic activity.

5.6.4 F Layer Profile Results

The F layer profile contribution to the LAM model describes the electron density distribution from foE to foF2. First results show that the NN has learnt the relationship between the shape and location of the profile and the input variables.

Two NNs, F1F2NN and F2NN, were trained with the input set, DN, HR, R2 and A16, to predict the profile description under certain conditions. A program was written which takes a given input set, and the F1 probability NN, to determine which NN (F1F2NN or F2NN) is required. The outputs from the NNs are then used in conjunction with equation (4-1) to determine the electron density profile for that input set. Therefore, the output from the F layer profile model is a complete bottomside F layer profile, and the results in this section will be shown as such.

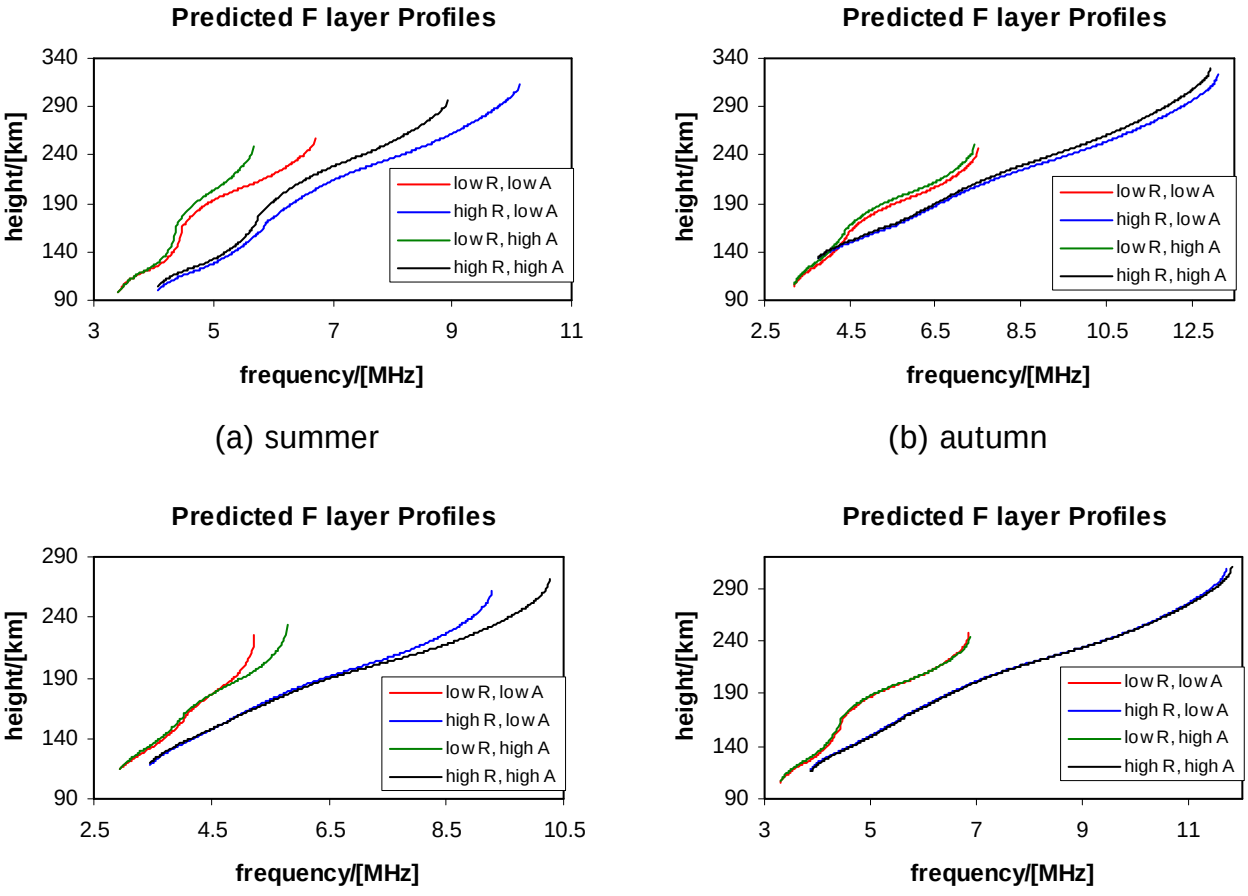

Figure 5-25: Predicted F layer profiles for different combinations of the input variables are shown. R refers to solar activity and A refers to magnetic activity.

Figure 5-25 shows four graphs that represent the response of the profile to changes in the input variables. The hour input was fixed at 12h00 SAST and the other three input parameters were varied. The profiles for the four combinations of low and high solar (R2) and magnetic (A16 or A8) activity are illustrated for each of the four seasons, summer, autumn, winter and spring.

These results confirm the findings of *McKinnell [1996]* for foF2. It can be seen from the graphs of figure 5-25 that, at high solar activity, a well-defined F1 layer is only present in the summer. Also, the effect of the magnetic activity on the F layer profile is greatest in the summer and smallest in the spring; while in the winter and autumn months, increasing the magnetic activity input had very little effect on the F1 layer but a noticeable effect on the F2 layer.

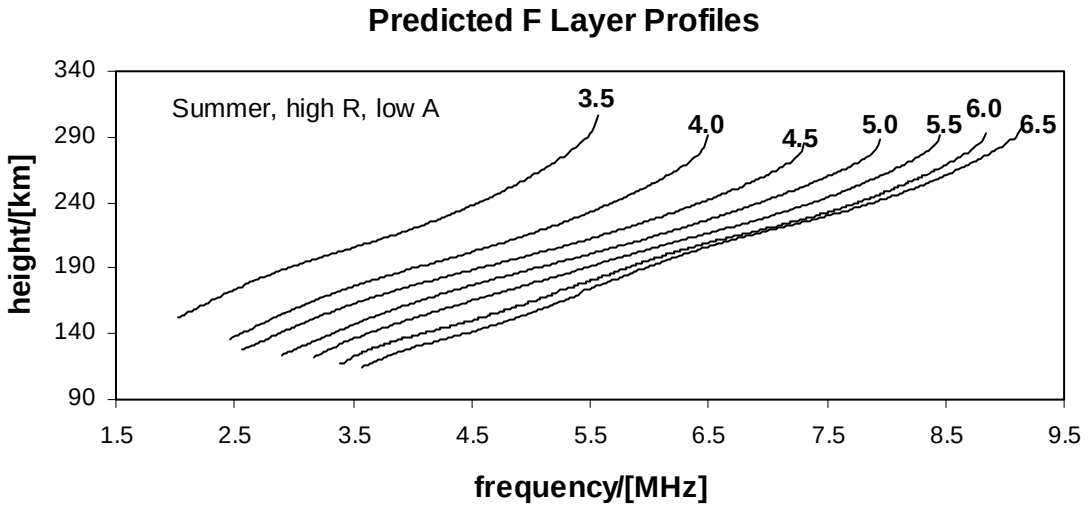

Figure 5-26: An example of the diurnal variation of the F layer profile for a summer day at high solar and low magnetic activity. The profiles are labeled according to the hour input in terms of hour, e.g. 3.5 = 03h30 UT.

To illustrate the diurnal variation of the F layer profile during a period where the F1 layer is developing, the HR input was varied from 03h30 UT to 06h30 UT in steps of 0.5 hour for a summer day at high solar and low magnetic activity. An L-condition profile was reported as probable for the hour 05h30 UT with a weighting function of 0.53. The L-condition algorithm (section 5.5.4) was applied here and figure 5-26 shows the variation in the predicted profiles as the hour moves through the start of the F1 day.

Six examples of actual 12h00 SAST F layer profiles from DPS ionograms are shown in figure 5-27. The input variables from these profiles were used as inputs to the LAM model and the IRI 2001. Figure 5-27 includes the LAM model and IRI 2001 predicted F layer profiles, for comparison.

It is clear from these graphs that once again the LAM model is a better predictor of Grahamstown profiles than the IRI. In some of the examples the LAM model fits the actual data very well (e.g. figure 5-27(c)) while in other examples the LAM model deviates from the actual data. This deviation usually falls within the estimated uncertainty limits for the predicted profile.

Figure 5-28 shows comparisons of actual 23h00 SAST F layer DPS profiles with the LAM model and IRI 2001 predicted profiles. At this hour there is only an F2 layer present and, therefore, the F2NN was used for predicting the characteristics and coefficients required for describing the LAM model profile.

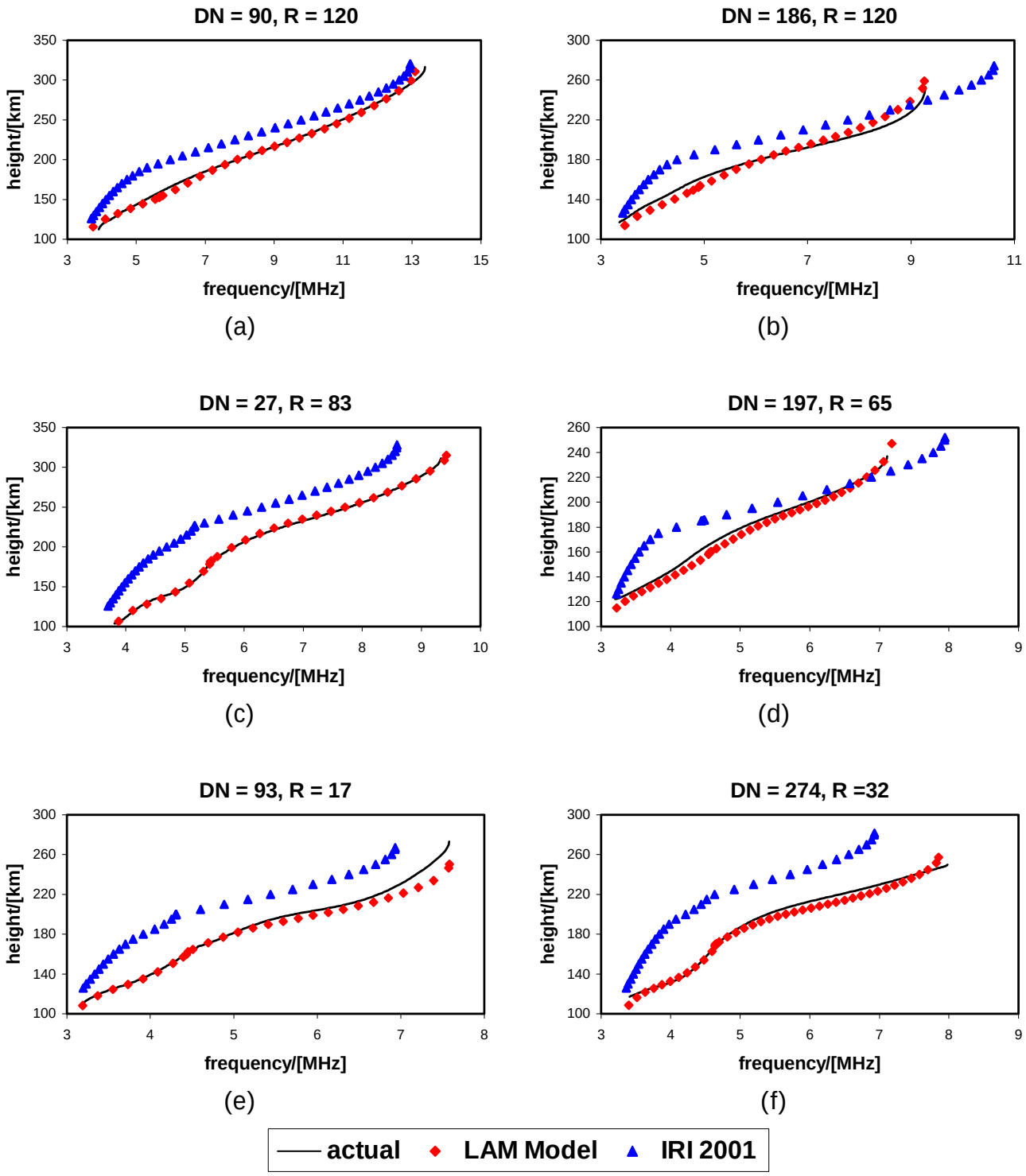

Figure 5-27: Comparisons of the LAM model F layer profile with actual DPS and IRI 2001 profiles. All of these profiles are 12h00 SAST profiles.

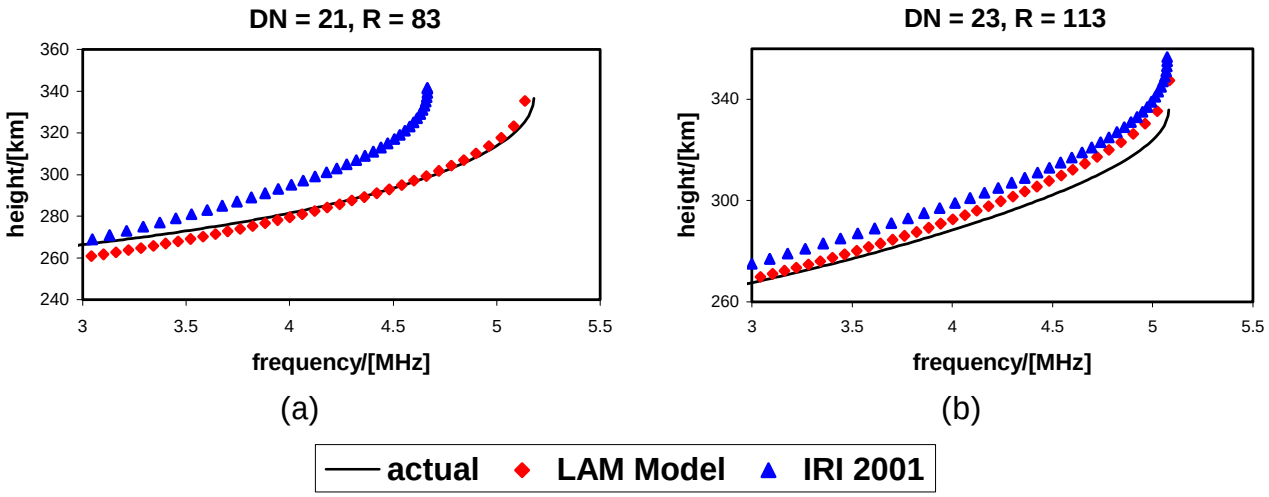

Figure 5-28: Comparisons of actual DPS F layer profiles with LAM model and IRI 2001 profiles at 23h00 SAST.

5.6.5 Estimating the Uncertainty

To estimate the uncertainty profiles for the F layer contribution to the LAM model, the same technique that was applied to finding the uncertainty estimate for the E layer contribution was used. A procedure for determining a statistical measure of the uncertainty in the output of a NN was introduced and discussed in *Poole and McKinnell [2000]*. Applying this procedure to finding uncertainty estimates for profile models that are NN based, is discussed with reference to the E layer in section 4.7.5 of this thesis.

For each NN trained to predict a parameter required for the F layer profile prediction model, the squared differences between the measured and predicted outputs were determined. Additional NNs were then trained, with the same input sets, to predict the squared differences.

To determine an estimate of the uncertainty profiles for the F layer, the variation in each of the heights that contribute to the predicted profile, from hsF to hsF2, is required. The predicted Chebyshev coefficients and peak characteristics were applied to equation (4-1) to determine these heights. Determining the

uncertainty would be simple if these Chebyshev coefficients were independent, but they appear to be related to each other by an unknown function. These relationships are illustrated in figure 5-29 where F1A1 and F1A2 have been plotted against F1A0, and F2A1 and F2A2 have been plotted against F2A0. All available Grahamstown data were used for plotting these graphs and the relationships between the first three coefficients of each layer (F1 and F2) are shown. It is possible that each coefficient depends on more than one of the other coefficients. Since these relationships are unknown and appear to be too complicated to be approximated, a simpler procedure for determining the uncertainty at each height was required.

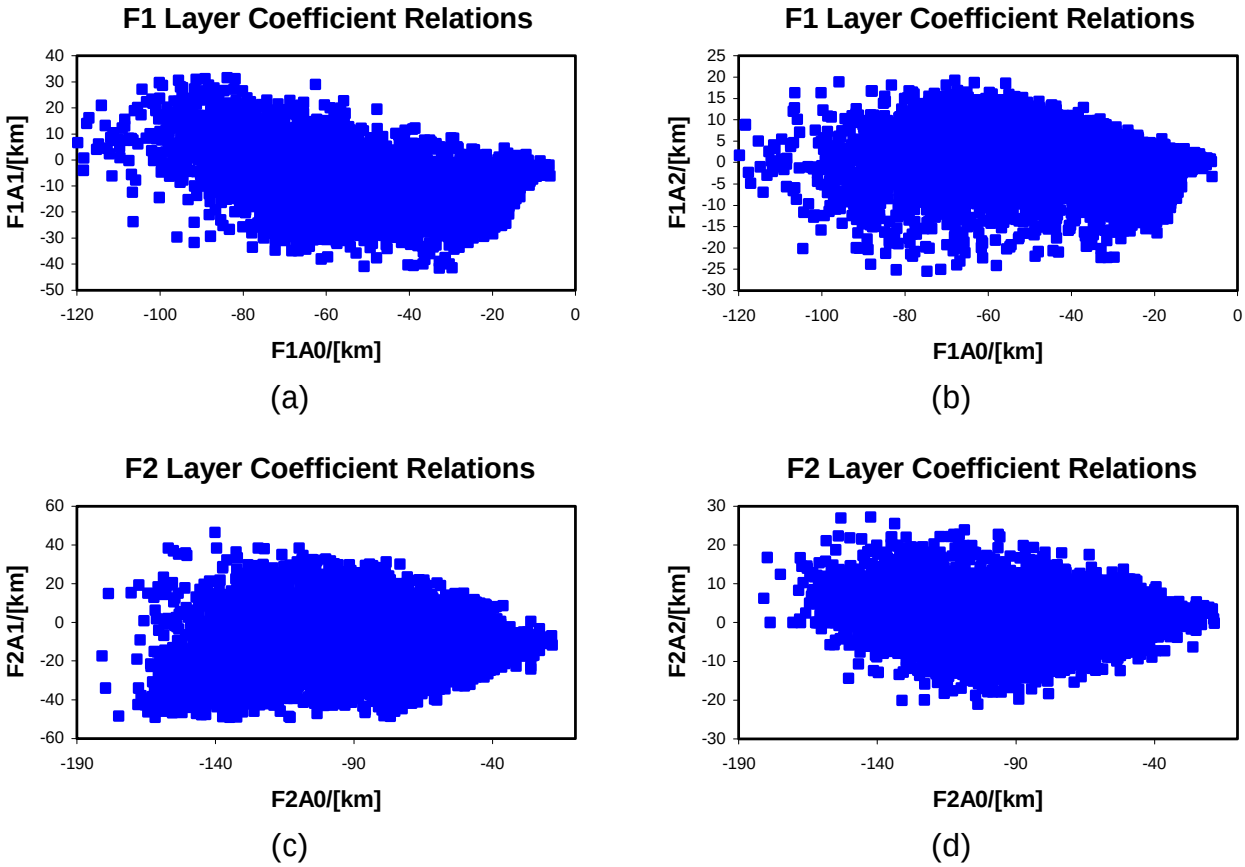

Figure 5-29: The relationship between the coefficients within each layer was investigated by plotting these graphs. They showed that the relationship is not a simple one and cannot be easily approximated.

For the predicted peak height of each layer, the square root of the output from the corresponding squared differences NN provided the uncertainty in the peak height directly. Therefore, the variation in the peak height of each layer can be predicted with confidence. Since the profile shape of each layer is described by a Chebyshev polynomial that is forced to pass through the peak of the previous layer, the estimated uncertainty in the peak height can be used as the uncertainty in the start height of the next layer. When an E layer is predicted by the E layer NNs (chapter 4), the estimated uncertainty in hsF (start height of the F layer) is determined by a combination of the uncertainties on hmE (E layer peak height) and W (valley width). In the case of a JET model prediction for hmE, an uncertainty of 0.5 km is used for hsF (*Titheridge [2000]*). The estimated start and peak heights of each layer is, therefore, known.

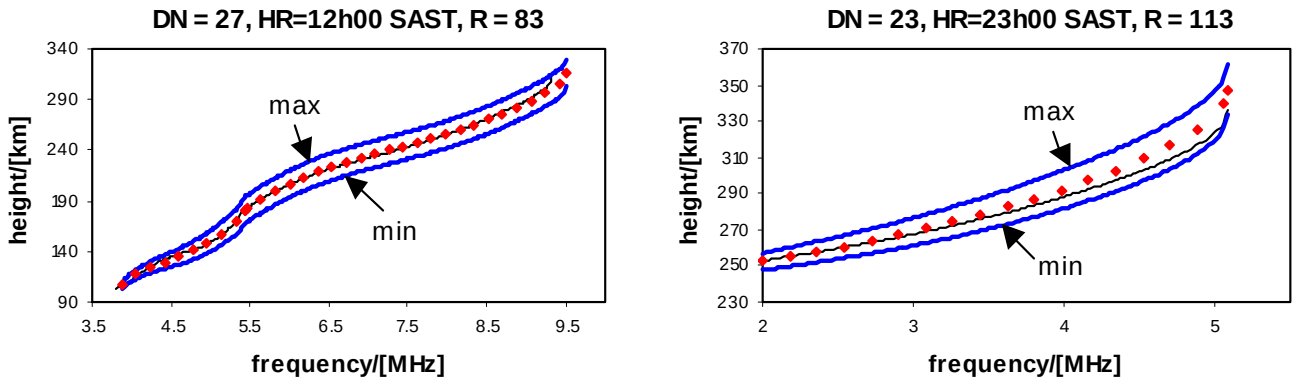

Figure 5-30: A daytime and nighttime profile are shown with their uncertainty profiles. The solid black line is the actual DPS profile; the red diamond shape points are the LAM model predicted profile and the solid blue lines are the uncertainty profiles.

Using these uncertainties, the start and peak heights of each layer were adjusted by adding and subtracting the uncertainty from the predicted value, to determine the maximum and minimum values respectively. At heights between the two end heights, the uncertainty was determined by interpolating between the adjusted start and peak heights while retaining the shape of the predicted profile. In this way maximum and minimum uncertainty profiles were obtained for the F layer.

Figure 5-30 illustrates the uncertainty profiles for two examples. The first example shows a 12h00 SAST profile for a summer day for which an F1 layer has been reported. In the second example, a nighttime profile is shown for a summer day at high solar activity.

These uncertainty profiles represent the maximum possible statistical variation of the average predicted profile for a given input set.

5.7 Discussion and Conclusion

This chapter has discussed the development of the F layer contribution to the LAM model for predicting the bottomside profile. NNs have been used for the first time as a tool for providing predictions of the electron density profile description. Also, NNs have provided an effective mechanism for determining the probability of existence of an F1 layer.

The nature of a NN is to provide an average output for a given input set to the best of its ability. The ability of a NN is affected by the quantity and quality of the data with which it is trained. The dataset used to train most of the components required for predicting the F layer profile was limited to data derived from DPS measurements for the period April 1996 to December 2000. This time frame only contains one quarter of the solar activity information ideally required for predicting ionospheric characteristics. In addition, the data from the DPS is scaled with the Artist scaling software, which on occasion inaccurately scales the F1 region and makes no allowance for the L-condition category. Equation (4-1), developed by UMLCAR for use in Artist and adopted by the LAM model, produces

a profile from knowledge of the Chebyshev coefficients. The disadvantage of this approach is that the slope of the height with respect to the frequency, dh/df, tends to infinity at the critical frequency of the layer. Although this works well at foE and foF2, whenever a value for foF1 is recorded, an F1 profile is inserted and an irregular F1-F2 boundary is observed on the profile. In the next chapter it is shown that profiles that have dh/df equal to infinity at foF1, do not convert into realistic ionograms. Also, the electron density profiles do not have a smooth transition from the F1 layer to the F2 layer. A smoothing technique will be introduced into the LAM model to ensure that the predicted profiles are smooth, and that they convert into realistic ionograms.

However, in spite of the limitations imposed on the model by the available data, it has been shown that the LAM model is capable of predicting accurate descriptions of the shape and location of the average profile for a given input set. In particular, when predicting the F1 region the LAM model is a better solution than the IRI for Grahamstown.

In chapter 6, the E and F layer contributions to the LAM model are combined to form a model that will predict a smooth electron density profile for Grahamstown under any condition.

Chapter 6

LAM MODEL: FINAL PROFILE

6.1 Introduction

The previous two chapters discussed the development of the E and F layer contributions to the LAM model. In this chapter, these two layers are joined to produce a smooth bottomside electron density profile that provides a realistic description of the average behaviour of the ionosphere under given conditions.

There are two boundaries that require careful consideration, the E-F boundary and the F1-F2 boundary. Both of these have been discussed briefly in the previous chapters, but will be revisited in this chapter.

As a means of determining the ability of the LAM model to produce realistic results, the predicted profiles have been converted to their equivalent ionograms. The procedure for converting profiles into ionograms is included in this chapter.

The LAM model's "smoothing technique" is introduced as an attempt to find an elegant solution to the problem of discontinuity at the F1-F2 boundary in both the predicted profiles and the ionograms.

6.2 E-F Boundary

As discussed in chapter 4, section 4.6, there exists an ionization valley between the E and F layers.

Although there are a few different approaches to developing the profile in the E-F transition region (*Bilitza [1998]*, *Chasovitin et al. [1996])*, the LAM model adopts the UMLCAR E-F valley model (*Huang and Reinisch [1996])*. All of the available profile data for Grahamstown is derived from measurements taken by the DPS sounder and scaled with the UMLCAR Artist software. Since the ionograms do not provide enough information to determine the shape of the valley region, a mathematical construction technique is required. For both of these reasons, the best approach for the LAM model is to use the E-F valley from the UMLCAR model.

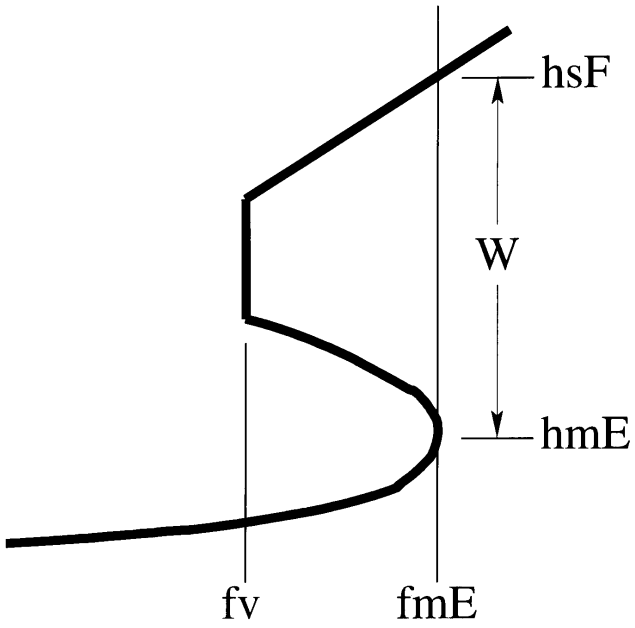

Figure 6-1: The shape of the valley model that forms the transition from the E to F layer. For a smooth transition, hsF must equal hmE+W.

To ensure a smooth transition from the E layer to the F layer via the valley, the starting height of the F layer, hsF, must be equal to the peak height of the E layer plus the valley width, hmE+W. These points are indicated on the diagram shown in figure 6-1, which is a replica of the valley shape shown in figure 4-8, with the addition of annotation relevant to this discussion.

The E limits NN determines the hours between which the E layer NNs can be interrogated to predict the E layer. Between these hours, the E layer NNs predict average values for hmE and W, while the F layer NNs predict an average value for hsF. Each of these predicted values has a corresponding estimated uncertainty. These uncertainties are a measure of the statistical variation that can be expected from the prediction. Since the valley model, for which W is the only required parameter, is a mathematical construction, and provided that the difference between hsF and hmE+W does not exceed the estimated uncertainty of either, the predicted F layer in the LAM model is shifted by an amount equal to the difference between hsF and hmE+W. Thus a smooth E-F boundary is ensured for LAM model predictions.

Outside of the hours predicted by the E limits NN, the UMLCAR (*Huang and Reinisch [1996])* and JET (*Titheridge [2000])* models are used. In this case, there is no problem with the E-F boundary, as the valley width, W, is determined by taking the difference between hmE and hsF. The JET model determines the predicted value of hmE, while the F layer contribution to the LAM model determines the predicted value of hsF.

6.3 Converting to Ionograms

In order to determine the ability of the LAM model to predict profiles that realistically describe ionospheric behaviour, a procedure for converting the profiles into their equivalent ionograms was required. This conversion procedure was especially required in the case where the L algorithm was implemented in the prediction, as an L-condition can only really be visualized on an ionogram.

Since this conversion procedure is not the emphasis of this thesis, the formulae are not reproduced here but can be found in *Paul [1967]*. As well as the f(h) profile points, an analytical expression for the slope, dh/df, is required. Initially, the derivative of equation (4-1) was taken since this equation is used to determine the real height at a particular frequency, given the Chebyshev coefficients. A simpler method is to assume linear segments between the real height points and calculate dh/df by determining the slope of each segment. Experimentation showed that this linear segment method did not reduce the accuracy of the conversion significantly. By using the real height points instead of equation (4-1), the benefit of additional techniques implemented in the LAM model (e.g. the L algorithm) will be apparent in the ionogram after conversion.

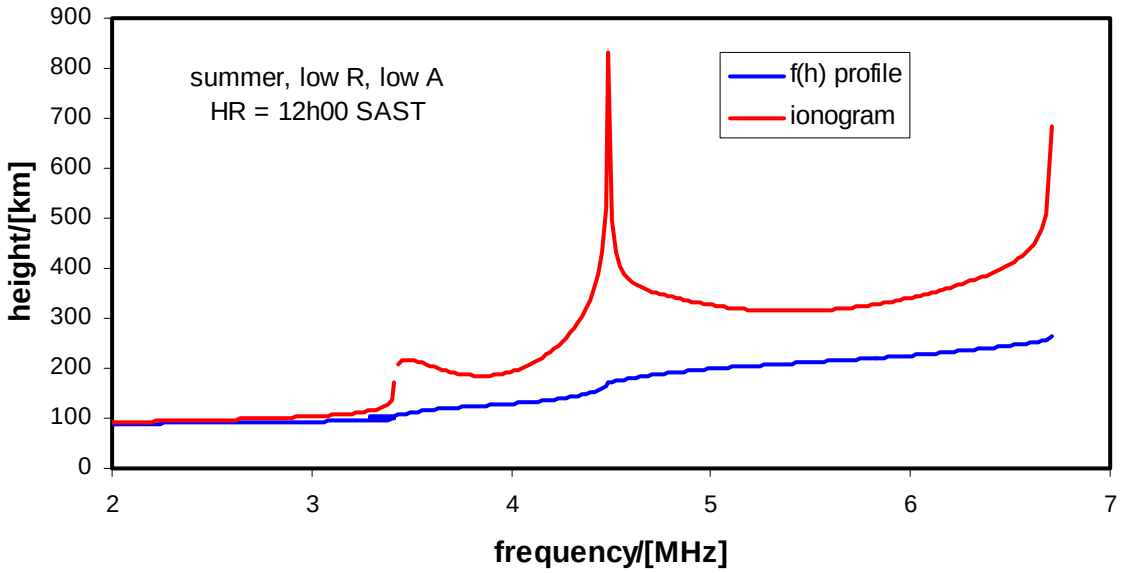

Figure 6-2: An example of a frequency vs. height profile and its equivalent ionogram. The input set for this example is such that a sharp cusp at foF1 would be expected on the ionogram.

Using equations from *Paul [1967]* and the programming code from *Poole [1985]*, a program was developed that took the profile as a listing of real height versus frequency points and produced the equivalent ionogram, in the form of virtual heights at each frequency. This program shall be referred to as “NHTOVI”.

Although the programming code of *Poole [1985]* converted ionograms into electron density profiles, which is the opposite of what was required here, it proved useful as a starting point for creating NHTOVI.

To illustrate results from NHTOVI, an example of a profile and its equivalent ionogram is shown in figure 6-2. The input set chosen for this illustration is a summer day (DN=20) at 12h00 SAST for low solar and magnetic activity, which is an area of the input space where a sharp cusp at foF1 would be expected on the ionogram.

6.4 F1-F2 Boundary

The F1-F2 boundary was discussed in chapter 5, section 5.5.3.1, but will be revisited here since there is still a problem outstanding.

Any profile that is determined by using Chebyshev polynomials will exhibit an unnatural step at the F1-F2 boundary. Although this Chebyshev polynomial method ensures that the peak height of the F1 layer, hmF1, is equal to the starting height of the F2 layer, hsF2, the slope of the profile, dh/df, tends to infinity at the critical frequency of the F1 layer, foF1. Two examples of the F1-F2 boundary are shown in figure 6-3; one is a profile derived from actual DPS measurements and the other is a profile predicted by the LAM model. The profiles have been enlarged to show only the area surrounding the F1-F2 boundary, and the vertical line identifies the location of the foF1 value.

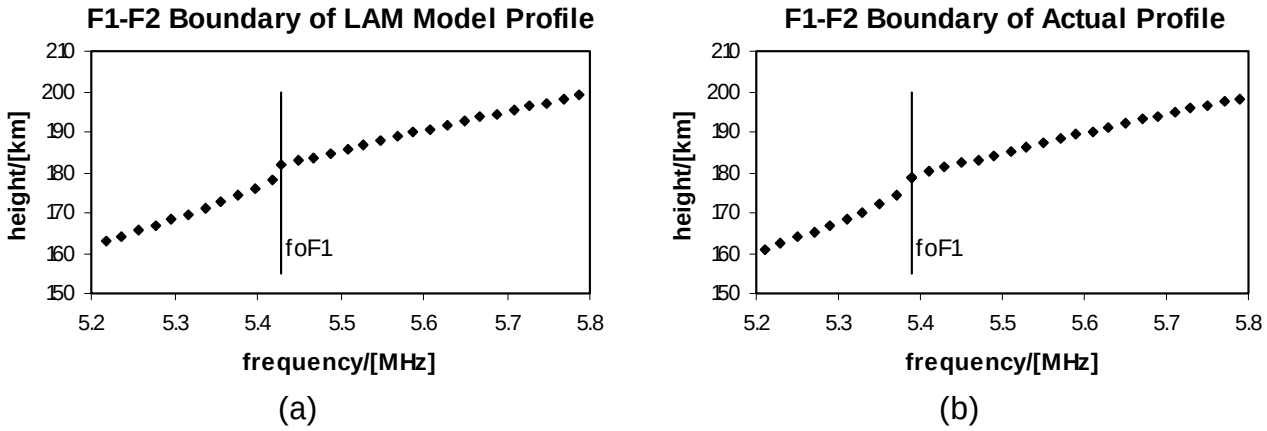

Figure 6-3: The area surrounding the F1-F2 boundary of a profile is shown for (a) LAM model predicted profile and (b) an actual DPS profile. At foF1 the slope of the profile tends to infinity, which explains the unnatural step in the profile at foF1.

Ionograms resulting from profiles that have this step at the F1-F2 boundary show a sharp cusp at foF1. All profiles derived from the Chebyshev coefficient method that have an F1 layer will, therefore, convert to ionograms with a sharp cusp at foF1. A small area of the input space exists where a sharp cusp at foF1 is expected. Examples of the output from three input sets are shown in figures 6-4, 6-5 and 6-6. Figures 6-4 and 6-5 illustrate predicted LAM model profiles with their corresponding ionograms for an input set where a probable L-condition was predicted (figure 6-4), and where a sharp cusp would be expected on the ionogram (figure 6-5). Figure 6-6(a) is an example of an actual DPS ionogram, while figure 6-6(b) shows the profile, determined by using Chebyshev coefficients provided by the Artist scaling software, and the equivalent ionogram, as determined by converting the profile. This figure illustrates a case where a sharp cusp should not appear on the ionogram at foF1, but an F1 layer still exists. In order to solve these problems, a mechanism is required for smoothing out the F1-F2 boundary in such a way that the slope of the profile at foF1 never approaches infinity and that a more realistic profile is predicted for all input sets.

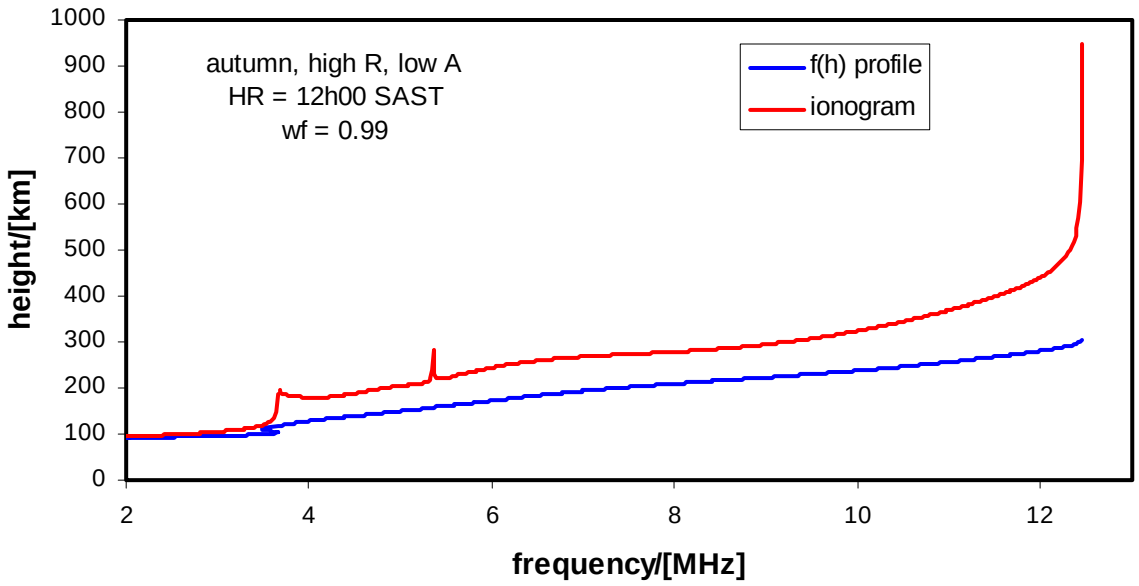

Figure 6-4: A LAM model predicted profile with its equivalent ionogram is shown for 12h00 SAST on an autumn day at high solar activity and low magnetic activity. The cusp on the ionogram at foF1 should not be present for this input set.

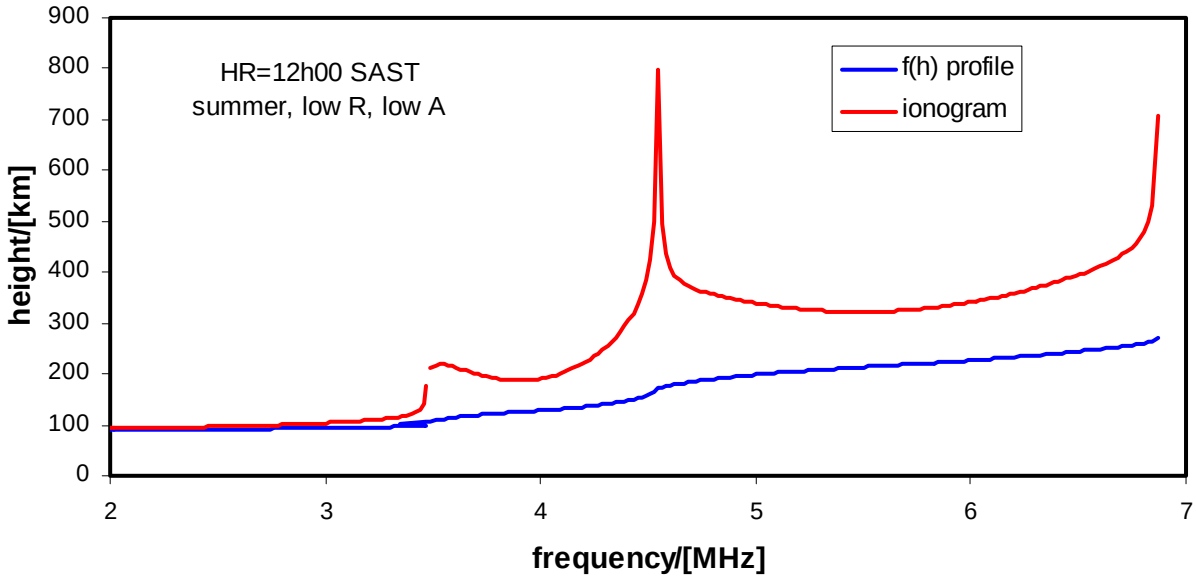

Figure 6-5: A LAM model predicted profile and ionogram are shown for 12h00 SAST on a summer day, at low solar and magnetic activity.

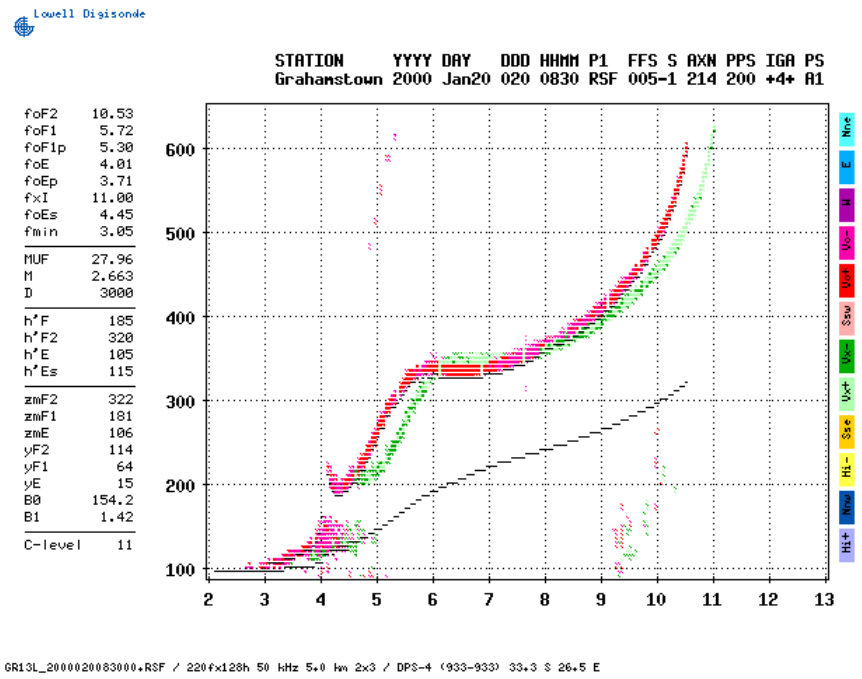

(a)

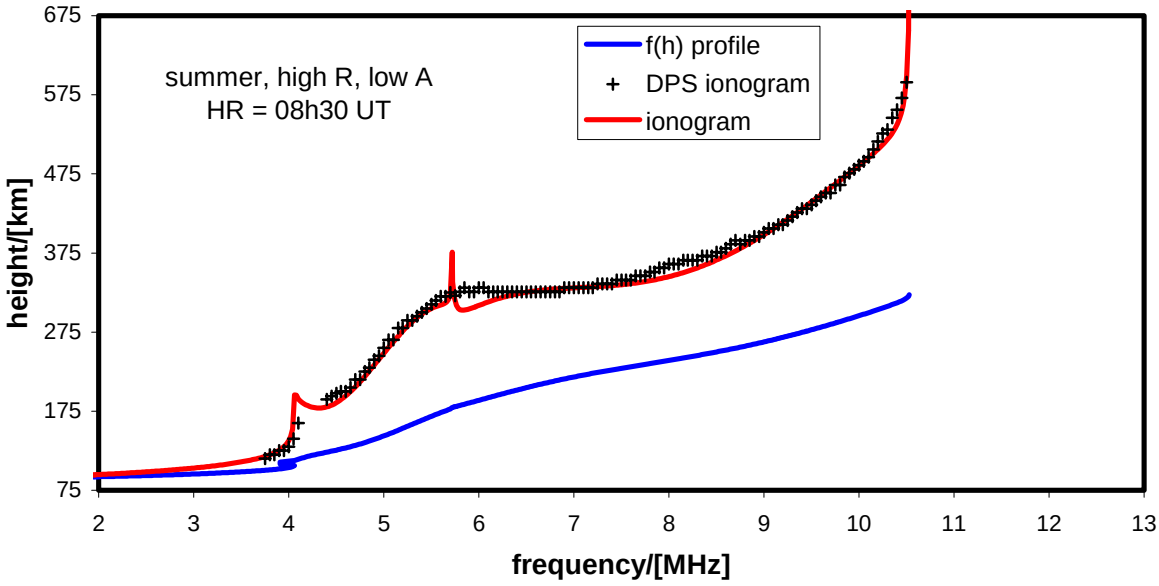

(b)

Figure 6-6: An actual DPS ionogram is shown at the top with the Artist determined profile, and converted ionogram below. The Artist virtual height points are superimposed on the converted ionogram in (b) to illustrate the differences in the F1 region.

6.5 The Smoothing Technique

A technique was developed that could be applied to any profile, actual or predicted, determined by using the Chebyshev coefficient method. This technique, called the “smoothing technique”, was implemented in order to smooth out the F1-F2 boundary on the profile and ensure that the resulting profiles reflected realistic ionospheric behaviour. The smoothing technique will be applied whenever an F1 layer is present, whether or not the F1 layer was recorded as an L-condition. The development of this technique is discussed in this section with the assumption that the profile has already been determined for a given input set.

Two points, f1 and f2, on the profile are selected such that they lie on either side of the critical frequency of the F1 layer, foF1. The method by which f1 and f2 are selected is described later. The real height is then constrained to vary from f1 to f2 in a manner that does not allow the height to go asymptotic at foF1. The constraints were as follows:

- the heights, h1 and h2, corresponding to points, f1 and f2, were fixed
- the slope of the profile, dh/df, was fixed at f1 and f2

After extensive experimentation, the best results were found when a 3rd order polynomial was fitted between f1 and f2, while adhering to the above constraints.

A criterion is required that allows for distinction between three different types of input set;

(i) one where a sharp cusp is expected on the ionogram,

(ii) one where an L-condition is probable,

(iii) one where an F1 layer is definitely present but no sharp cusp is expected.

The third case would typically occur in the few hours after and before an L-condition event. It is unrealistic to expect a sharp cusp on the ionogram that occurs immediately after or before an L-condition ionogram.

The probability of the existence of an F1 layer is predicted by the F1 probability NN, chapter 5 section 5.6.2. Archived Grahamstown chirp-sounder (Verti) data from the twenty-five years prior to 1998 were used in developing this F1 probability NN. In addition to the probability of occurrence of the F1 layer, as a definite layer or in an L-condition state, this NN can provide information regarding the hours between which a definite F1 layer can be expected.

After examining many ionograms, an hour limit to determine the hours in a particular day between which a type (i) input set could be expected, was decided upon. This hour limit was set at three hours; which means that a sharp cusp can be expected on the ionogram from three hours after the definite F1 start hour, to three hours before the definite F1 end hour. The definite F1 start and end hours are determined by the F1 probability NN. Although this hour limit criterion proved adequate for use here, a detailed investigation is required in order to find a more stringent criterion. This detailed investigation would require manually rescaling all available Grahamstown DPS ionograms and time constraints did not allow for that at this stage.

Type	**n**	**m**
(i)	6	3
(ii)	10	50
(iii)	3	50

Table 6-1: The points, f1 and f2, are located at n points before, and m points after foF1, where the points are spaced at frequency intervals of 0.02 MHz. This table lists values for n and m, which depend on the type of input set.

The selection process for the points, f1 and f2 is dependent on which type (i, ii, iii, as described on page 112) of input set the profile has been determined for. Each real height in the profile is determined at discrete frequencies that are spaced at 0.02 MHz intervals. The location of the frequency points, f1 and f2, is determined by starting at the foF1 value and moving n frequency points in the decreasing direction and m frequency points in the increasing direction. Table 6-1 lists the values of the integers n and m corresponding to each type of input set.

Figure 6-7 illustrates an enlarged view of the F1-F2 boundary of a profile before and after the smoothing technique has been applied. This smoothing technique has been implemented in the LAM model.

The criteria for determining whether an input set is type (i) or not, and the selection process for f1 and f2, were decided upon after extensive experimentation with many f(h) profiles and their corresponding ionograms. Although these decisions work well in this smoothing technique, a new and more rigorous investigation is required on this topic. NNs could possibly be employed to determine more stringent criteria.

Examples of predicted profiles with the smoothing technique applied, and their corresponding ionograms are shown in figures 6-8 to 6-10.

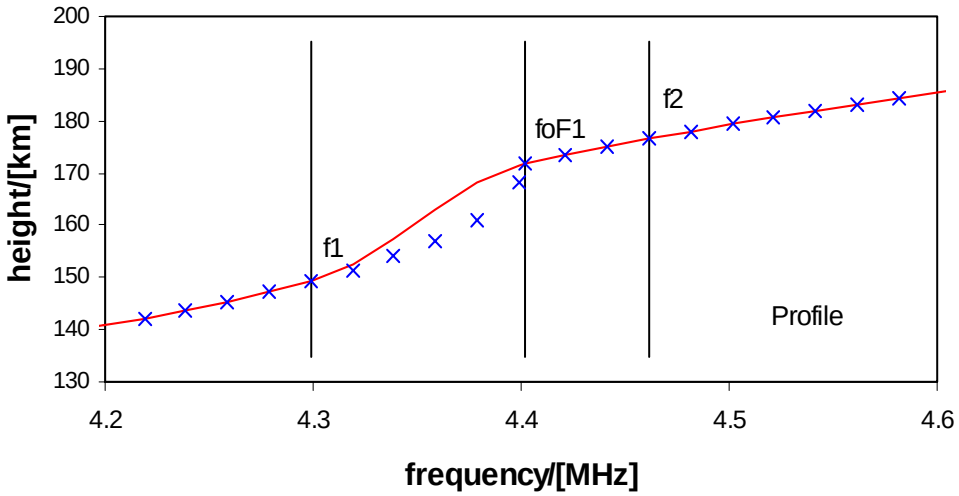

Figure 6-7: An illustration of an enlarged view of the F1-F2 boundary of the profile. The red line shows the shape of the profile after the smoothing technique has been applied. The vertical lines indicate the f1, foF1 and f2 points.

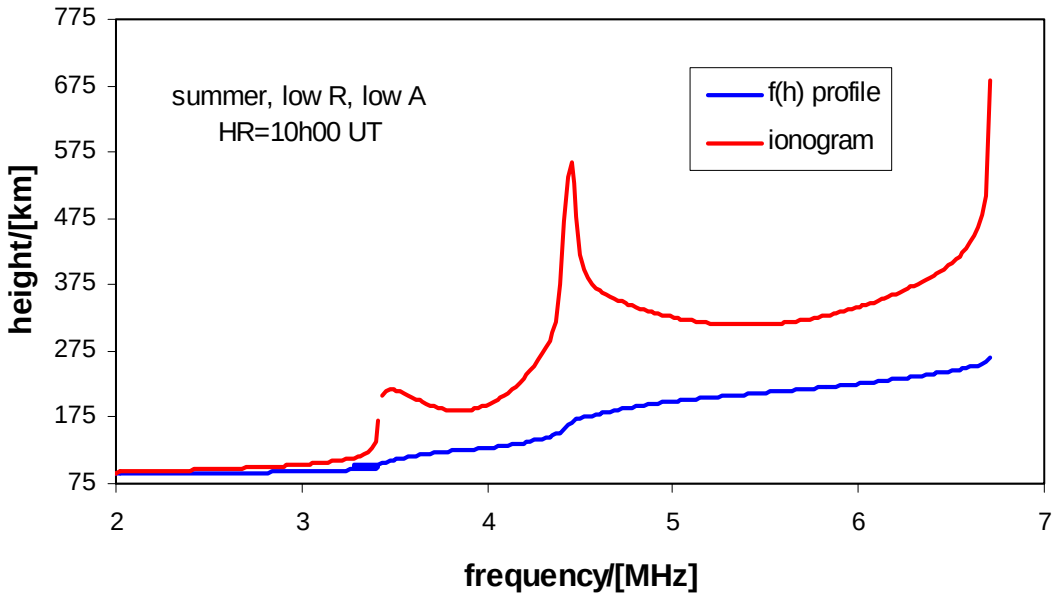

Figure 6-8: A LAM model predicted profile with its equivalent ionogram for 10h00 UT on a summer day at low solar and magnetic activity. This is a type (i) input set.

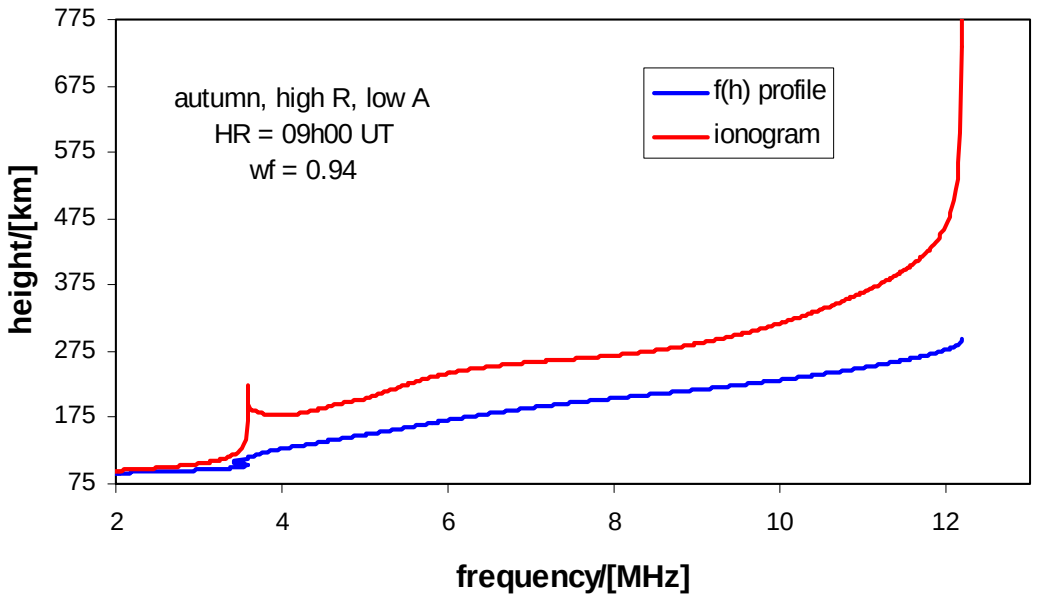

Figure 6-9: This LAM model predicted profile plus ionogram is for an input set where a L-condition was predicted as probable. The L-condition algorithm (with a weighting function of 0.94) has been used as well as the smoothing technique in predicting this profile.

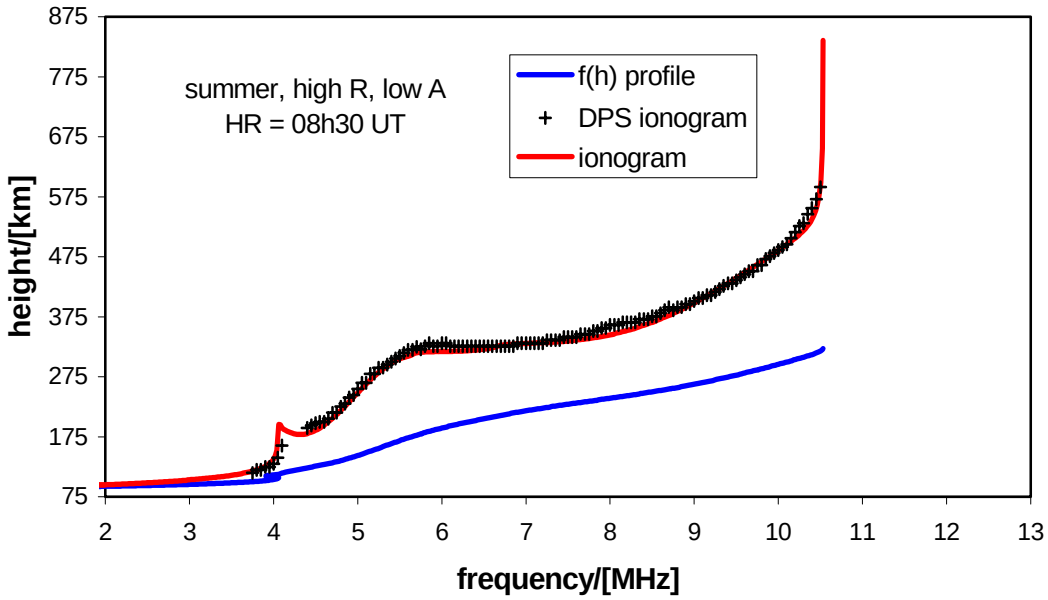

Figure 6-10: This is the same actual DPS profile shown in figure 6-6, but after the smoothing technique has been applied. The virtual height points from the original ionogram have again been superimposed.

6.6 Conclusion

The E and F layer contributions to the LAM model have been combined in this chapter to produce a model that has the ability to predict the entire bottomside electron density profile for Grahamstown. A valley layer has been inserted between the E and F layers and a smoothing technique has been developed to ensure a smooth transition from F1 to F2. Results from the LAM model will be presented in the next chapter.

Chapter 7

RESULTS

7.1 Introduction

The LAM model has been implemented using C++ programming code and designed to accept one of two different input sets; either year, day number and hour, or day number, hour, R and A, where R and A are indications of the level of solar and magnetic activity expected. When the first input set is given, the required R and A values are calculated using a given database of daily sunspot numbers and hourly magnetic a_k indices. The output from the LAM model is the predicted bottomside electron density profile for Grahamstown for the given input set. For the results presented in this chapter, the predicted output was given as a listing of frequency and height points that can be plotted to produce a smooth profile.

The first set of results illustrates the response of the bottomside electron density profile to changes in input variables, while the second set shows comparisons between the measured and predicted electron density profiles.

7.2 Input Space Variations

The results section of chapter 4 and chapter 5 illustrated the response of the individual ionospheric characteristics and coefficients to changes in the input variables. These characteristics and coefficients were then used to produce predicted profiles for the E layer (chapter 4) and the F layer (chapter 5).

This section illustrates the response of the entire bottomside profile, as predicted by the LAM model, to changes in the input variables. The input variables are day number (DN), hour (HR), solar activity (R) and magnetic activity (A). To represent the seasonal variation in the input space, typical values of DN were selected to coincide with the summer solstice (DN=356), winter solstice (DN=173), autumn equinox (DN=81), and spring equinox (DN=265). Typical values were chosen to indicate high and low levels of solar and magnetic activity. These values were selected, using the 5-year dataset, such that 70% of the data lay symmetrically between the chosen values. This procedure is similar to that followed in chapter 4, section 4.7 and chapter 5, section 5.6, where graphical illustrations showing how these values were chosen are presented. For the solar activity input, values of 15 and 120 were selected to be typical indicators of low and high solar activity respectively, while for the magnetic activity input values of 3 and 15 were selected to represent the low and high levels of magnetic activity respectively. It is important to realize that this “high” level of magnetic activity is based on the available dataset, which only spans 5 years. In true magnetic terms, an a_k value of 15 describes unsettled conditions rather than severe, which only occurs very rarely. When a fixed value for the diurnal variation (HR input) is required, 12h00 SAST is typically used.

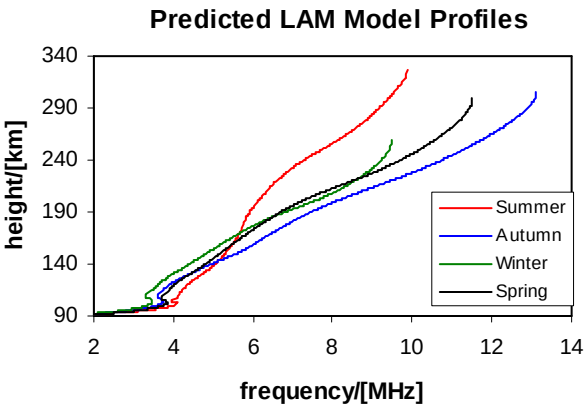

(a) R = high, A = low

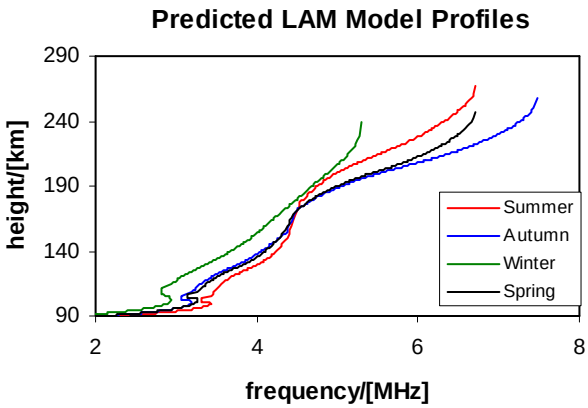

(b) R = low, A = low

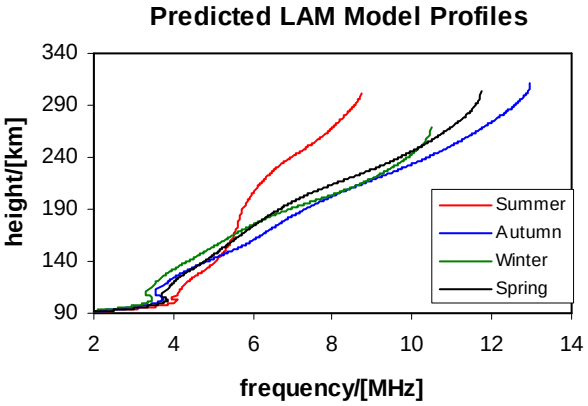

(c) R = high, A = high

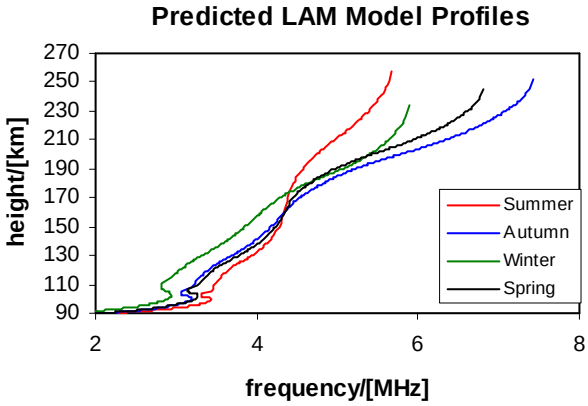

(d) R = low, A = high

Figure 7-1: An illustration of the profile's response to changes in the input variables. The seasonal variations for the four combinations of high and low solar and magnetic activity are shown.

Figure 7-1 illustrates the seasonal variation of the electron density profile for the four combinations of low and high solar and magnetic activity. These profiles were determined for 12h00 SAST at each of the four typical DN values mentioned above.

The solar and magnetic input variations are shown in figure 7-2 and 7-3 respectively. In figure 7-2 the solar input, R, has been varied from 10 to 130 in increments of 20 and the predicted profiles determined for low and high magnetic activity at 12h00 SAST on a summer and a winter day.

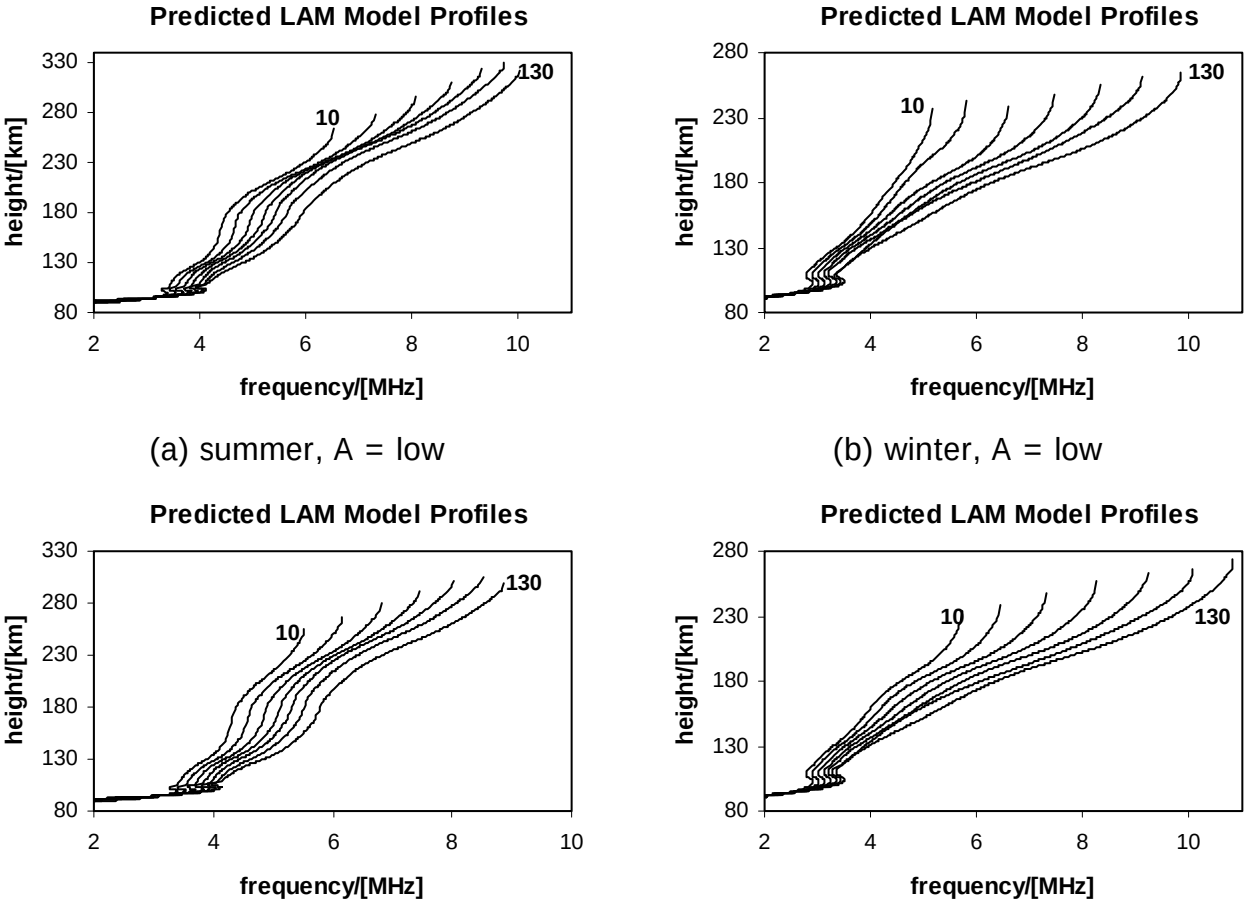

(a) summer, A = low

(b) winter, A = low

(c) summer, A = high

(d) winter, A = high

Figure 7-2: For these profiles the solar input variable has been varied from 10 to 130 in steps of 20 while the other inputs were kept fixed. These are the summer and winter 12h00 SAST profiles for low and high levels of magnetic activity.

The response of the electron density profile to changes in the magnetic activity, A, is illustrated in figure 7-3. For two days of the year at low and high solar activity, the 12h00 SAST electron density profiles have been predicted with the magnetic input, A, varying from 0 to 24 in steps of 2. These graphs clearly show that the magnetic activity input produces the most significant change in the F2 layer heights at high solar activity in the summer. As shown in chapter 5, the magnetic activity input has a very small effect on the F1 layer with almost no effect visible in the winter at high solar activity. There is no magnetic activity influence in the E layer prediction.

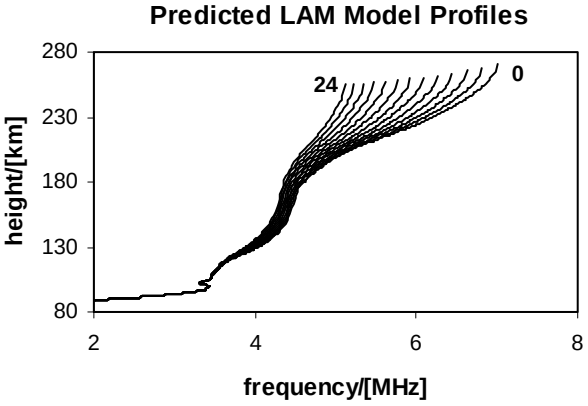

(a) summer, R = low

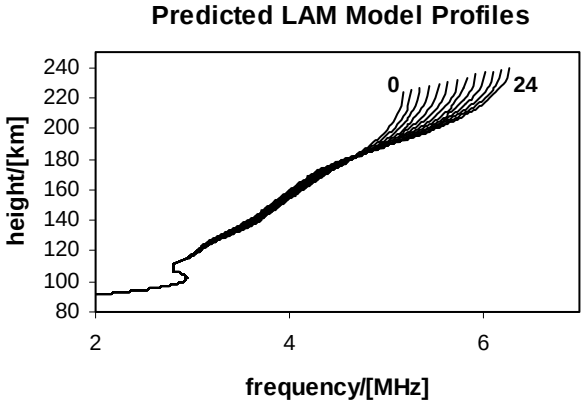

(b) winter, R = low

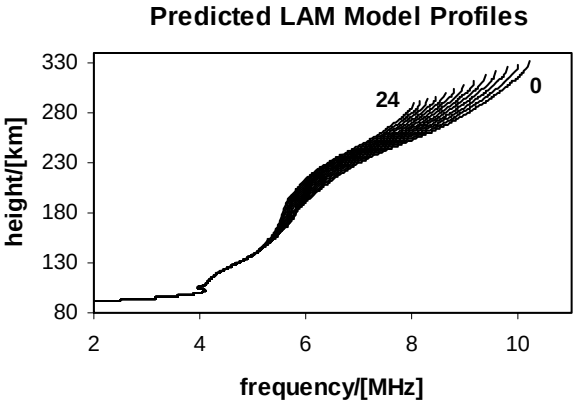

(c) summer, R = high

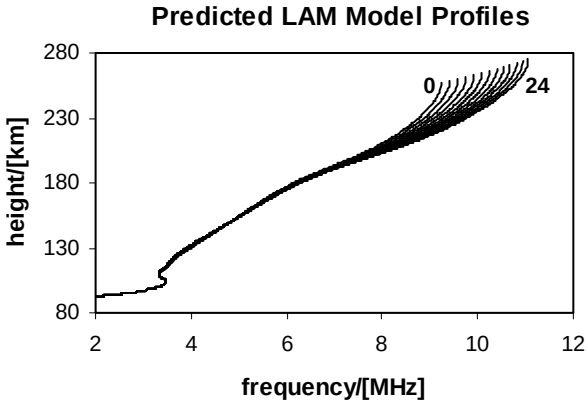

(d) winter, R = high

Figure 7-3: These graphs illustrate the response of the electron density profile to variations in the magnetic input, A, for a summer and winter day at low and high solar activity, R.

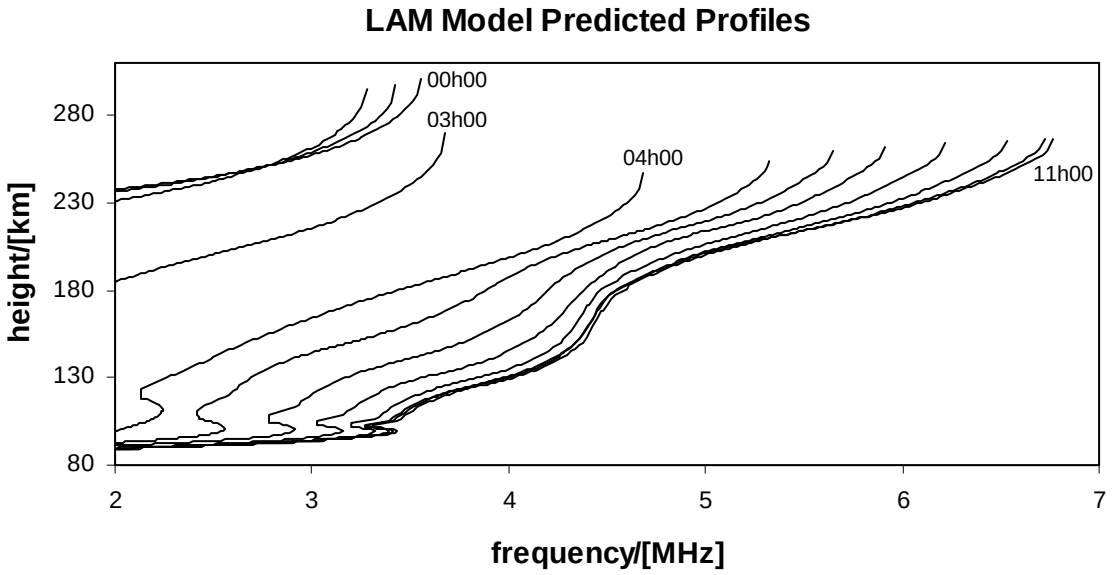

(a)

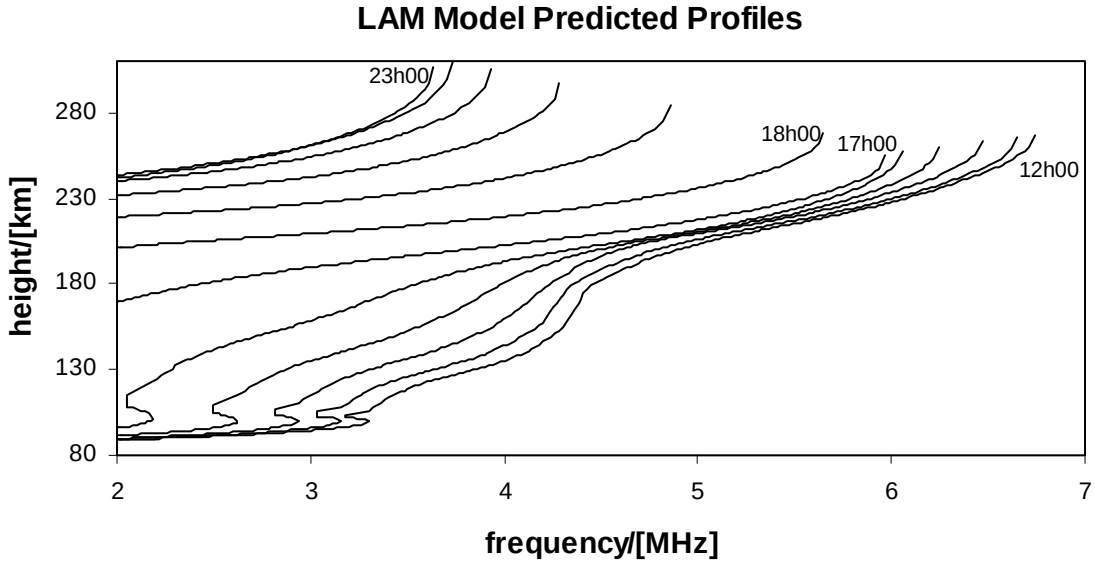

(b)

Figure 7-4: The LAM model predicted profiles for a summer day at low solar and low magnetic activity. The profiles are shown at hourly intervals for (a) the first 12 hours, and (b) the second 12 hours of the day. Labels on the graphs indicate the hours in UT.

The diurnal variation is demonstrated in figures 7-4 and 7-5, where the predicted LAM model profiles are shown for a summer and winter day at low solar and low magnetic activity. These profiles were determined at intervals of one hour and the hour is indicated on the graphs in universal time (UT).

From figure 7-4, it can be seen that the lowest maximum electron density (quantified by the foF2 value) occurs at about 02h00 UT and not at midnight. This is confirmed by the findings of *Poole and McKinnell [2000]*.

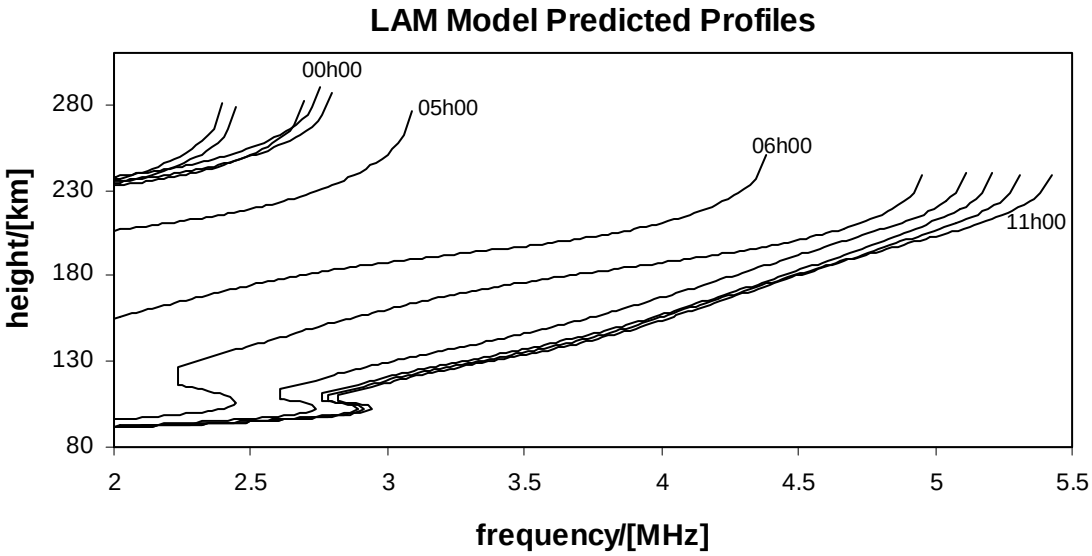

(a)

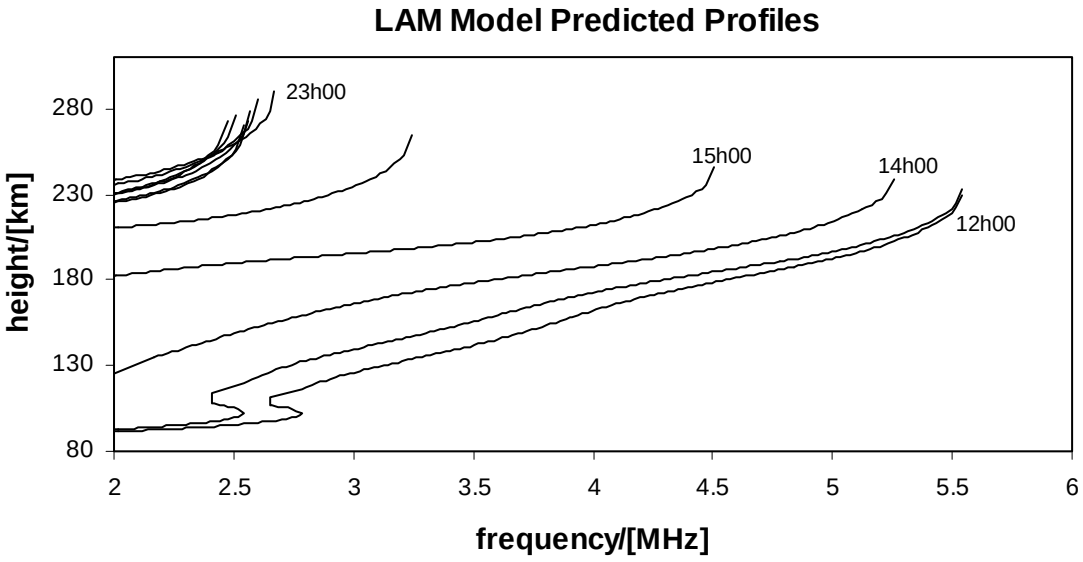

(b)

Figure 7-5: The LAM model predicted profiles for a winter day at low solar and low magnetic activity. The profiles are shown at hourly intervals for (a) the first 12 hours, and (b) the second 12 hours of the day. Labels on the graphs indicate the hours in UT.

In figure 7-6, an hour increment of 0.16 hour (10 minutes) has been used in order to show the change the profile undergoes during an L-condition period. For this example, no F1 layer is present at 04h10 UT and a definite F1 layer is present at 06h00 UT.

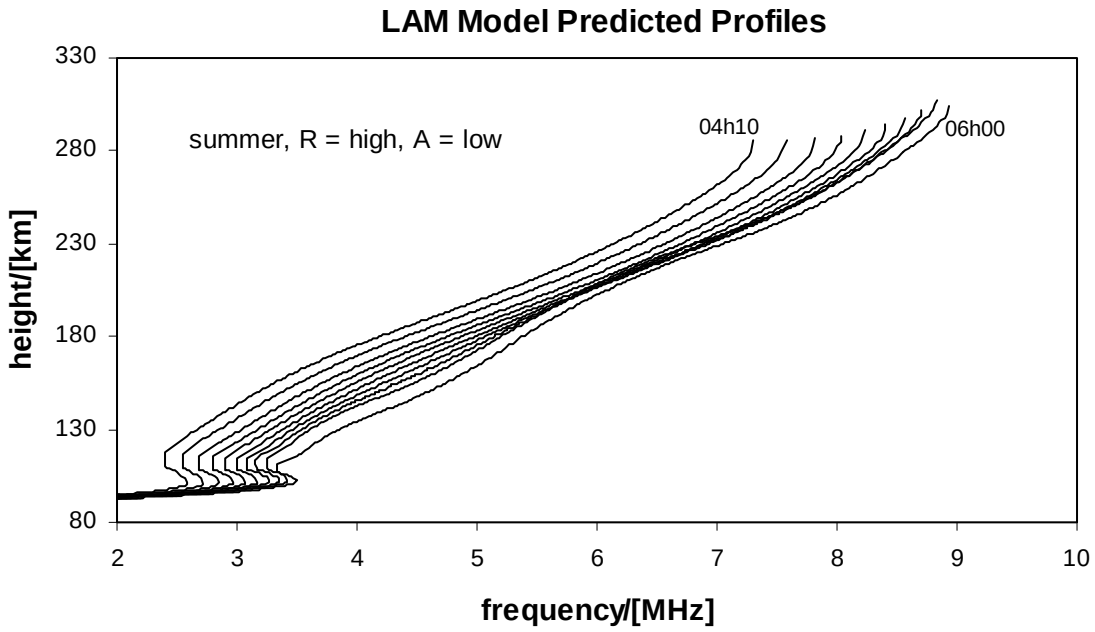

Figure 7-6: The LAM model predicted profiles are shown for the period 04h10 UT to 06h00 UT on a summer day at high solar and low magnetic activity. This graph illustrates the transition from a profile with no F1 layer to a profile with a definite F1 layer.

7.3 Profile Comparisons

In this section, several examples of actual DPS profiles have been selected and compared to profiles predicted by the LAM model and the IRI 2001. The predictions were made using the input sets from the actual DPS profiles. These examples have been deliberately selected to show both best and worst case scenarios.

In figure 7-7 six actual DPS profiles from 12h00 SAST are shown with the equivalent predicted LAM model and IRI 2001 profiles. These six input sets were selected such that three levels of solar activity and all seasons were covered.

In figures 7-8 and 7-9, further comparisons between actual DPS profiles and predicted profiles are shown. Both the LAM model and IRI 2001 predicted profiles for each actual DPS input set are shown. Each figure illustrates six examples, two examples at three different hours.

Although in some of these examples the LAM model predicted profile deviates from the actual DPS profile, the deviation is always well within the estimated uncertainty of the profile. It is also clear from these examples that the IRI 2001 is not providing accurate predictions of the electron density profile over Grahamstown, particularly in the F1 region.

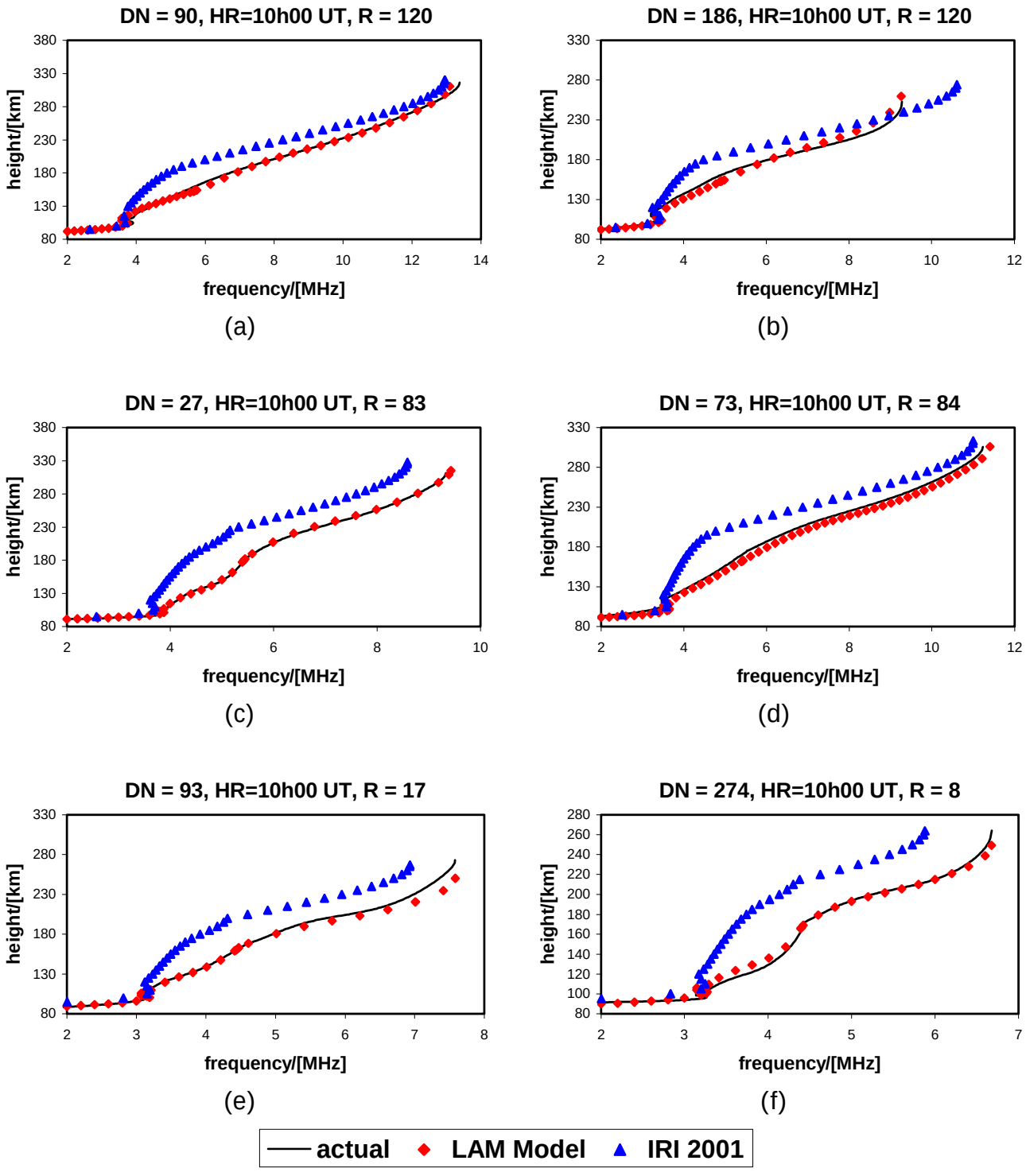

Figure 7-7: In this figure six examples of actual midday SAST DPS profiles are shown for three levels of solar activity. The equivalent LAM model and IRI 2001 profiles are also shown for comparison.

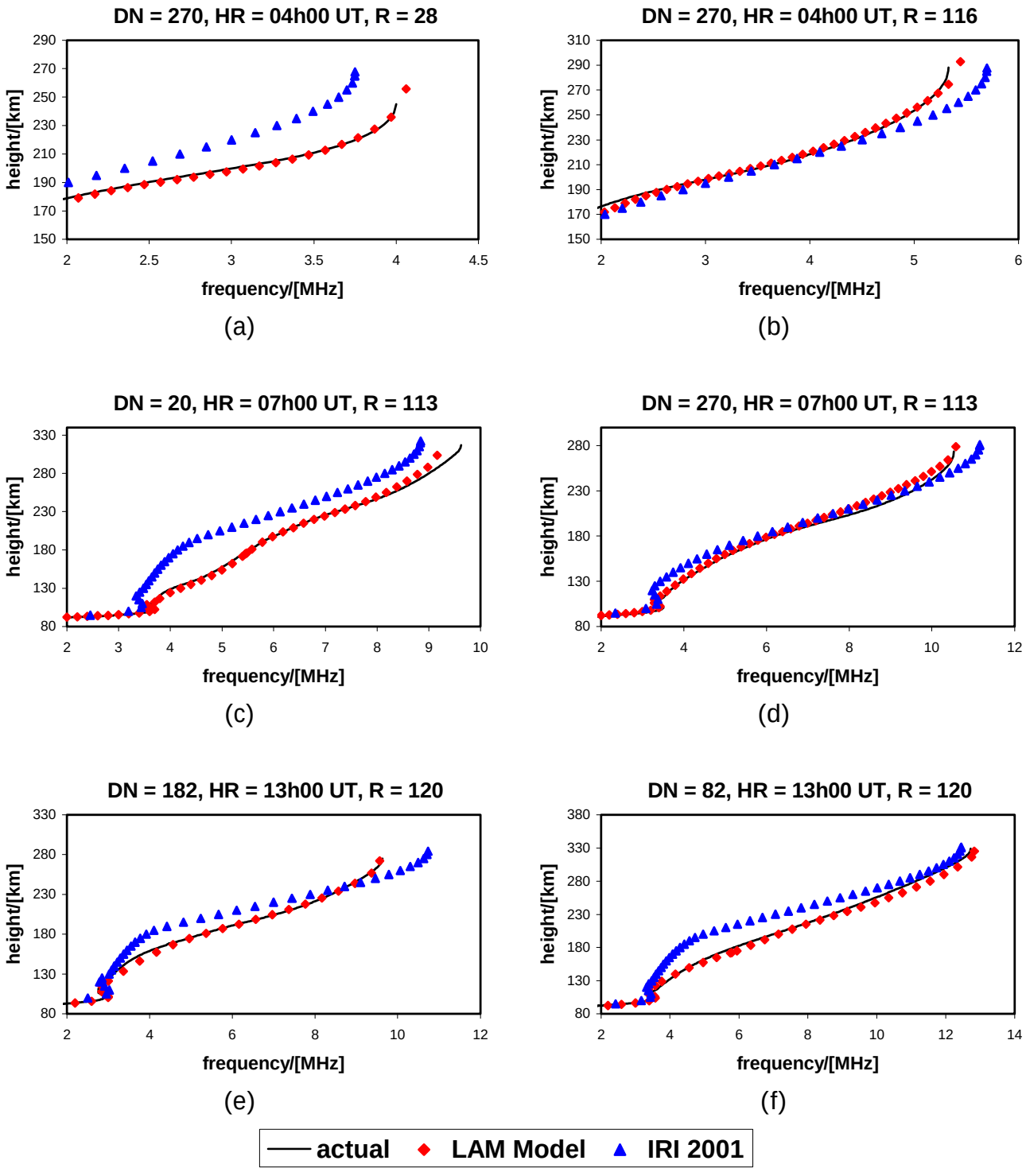

Figure 7-8: Two examples of actual DPS profiles for three different hours, 04h00 UT, 07h00 UT and 13h00 UT are shown. The equivalent LAM model and IRI 2001 profiles are also shown for comparison.

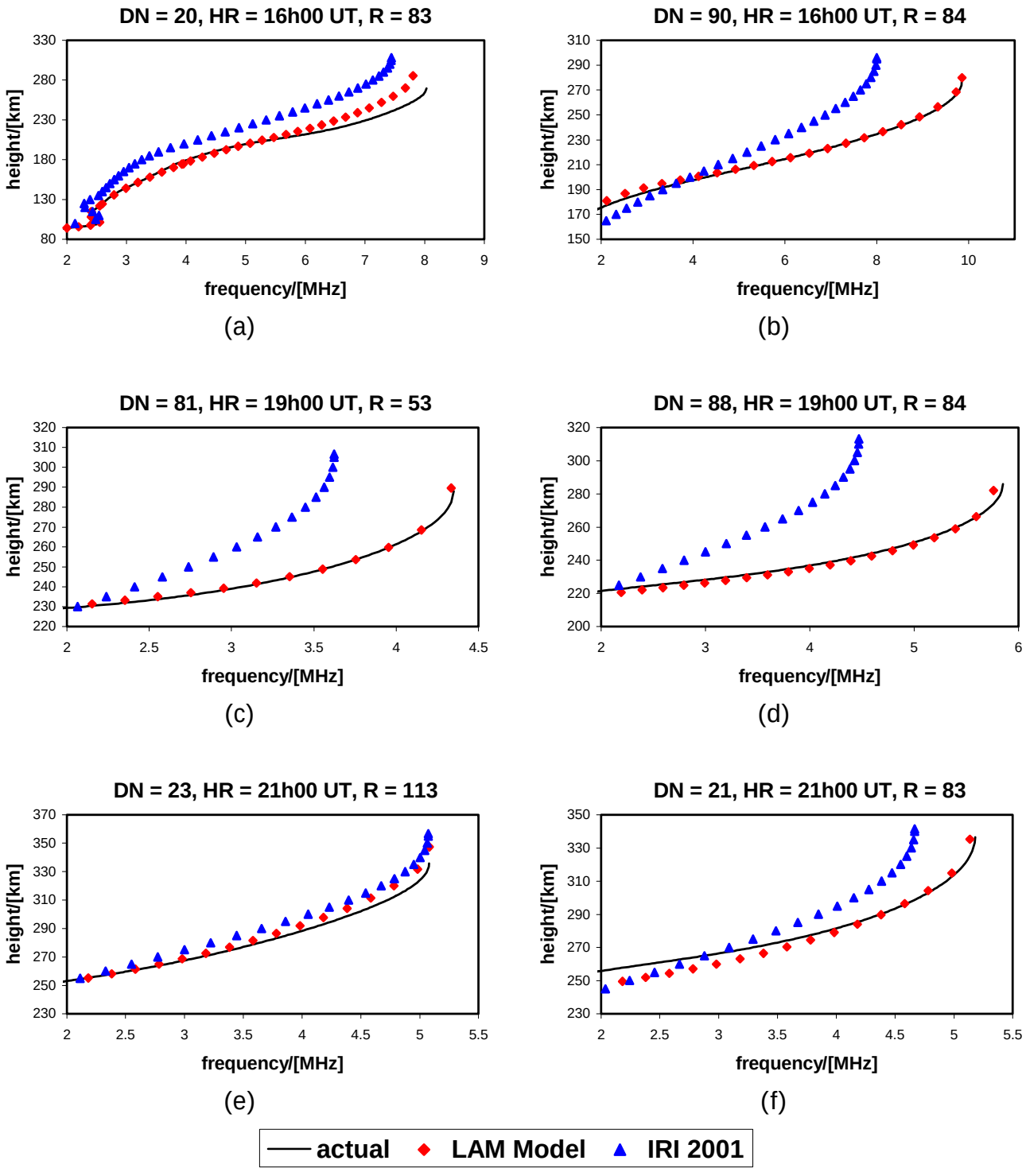

Figure 7-9: Two examples of actual DPS profiles for three different hours, 16h00 UT, 19h00 UT and 21h00 UT are shown. The equivalent LAM model and IRI 2001 profiles are also shown for comparison.

7.4 Uncertainty Profiles

The LAM model predicts an average electron density profile for a given input set. As an indication of the variability that can be expected on this prediction, uncertainty profiles have been estimated. The details of the procedure followed in determining these uncertainty profiles have been explained in chapters 4 and 5, with reference to the E and F layers respectively and, therefore, will not be repeated here.

Figures 7-10 and 7-11 shows two examples of predicted profiles with their estimated uncertainty profiles. In these examples the predicted profiles were determined for input sets where actual DPS profiles were available, and these actual profiles are also shown for comparison.

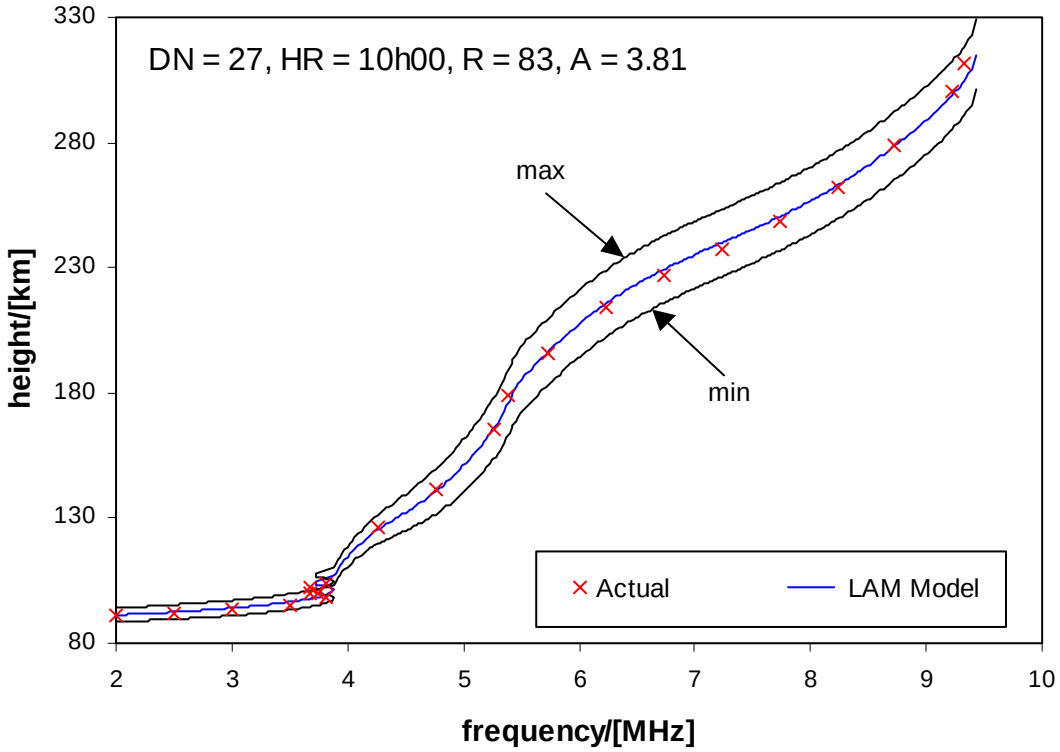

Figure 7-10: A predicted daytime LAM model profile with its uncertainty profile. The red crosses show the actual DPS profile corresponding to the input set given to the LAM model.

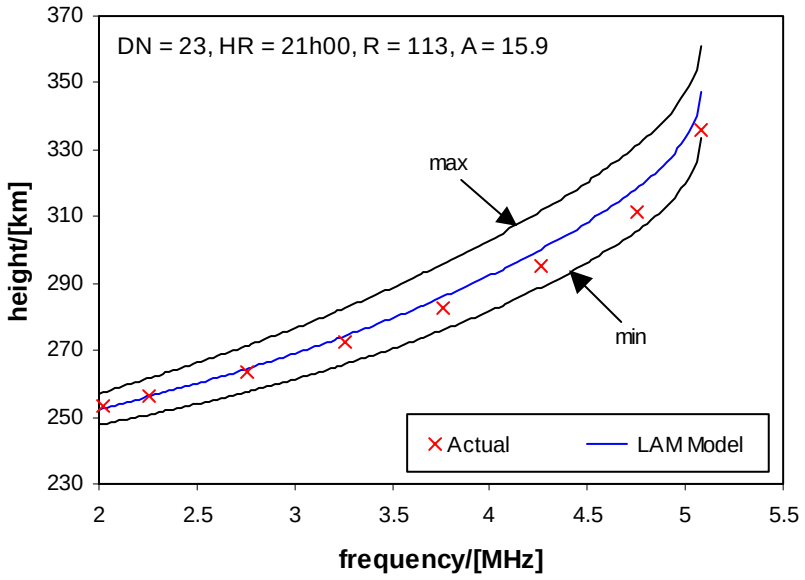

Figure 7-11: A predicted nighttime LAM model profile is shown with its uncertainty profiles. The red crosses show the actual DPS profile corresponding to the input set given to the LAM model.

Chapter 8

APPLICATION

8.1 Introduction

The traditional user of the ionosphere is the high-frequency (HF) communicator. In spite of current modern technologies, such as satellites, HF communication via the ionosphere is still popular. This is mainly due to the fact that the ionosphere is an inexpensive natural medium and, therefore, accessible in developing countries where the expensive infrastructure required for more modern technologies has not been built.

The main application for the LAM model ionosphere is in the field of direction finding (DF) systems. DF systems use a technique referred to as single station location (SSL) for determining the location of an HF transmitter by means of ray tracing. This technique is dependent on the radio waves being reflected by the ionosphere and, therefore, a reliable description of the ionosphere is required in order to obtain an accurate location. Reliable ionospheric models are essential, as real-time data are not always available.

Ray tracing is the technique used to determine the ground range between a transmitter and a receiver by following the path that the radio wave takes through the ionosphere from the transmitter to the receiver. SSL is ray tracing in reverse, since the path is followed from the receiver back to the transmitter.

To illustrate a basic application for the LAM model, a simple ray tracing algorithm is presented and demonstrated in this chapter.

8.2 Ray Tracing

With a knowledge of the elevation angle and radio frequency of the signal, as well as a suitable description of the ionosphere, which can take the form of an ionospheric profile for a particular input set, the path that the radio signal follows from the transmitter to the receiver, or vice versa, can be determined. A ray tracing algorithm was set up to determine and compare the paths of the signal through the LAM and IRI model ionospheres.

The curved earth-ionosphere geometry (*Davies [1990])* used in the algorithm is illustrated in figure 8-1. The elevation angle (E) is provided by the user and is the angle between the tangent to the ground at the transmitter location (T) and the ray path. The radio frequency, fr, is related to the plasma frequency, fv, at the height of reflection by the secant law (*Davies [1990])*, which takes the form:

$$fr \approx fv \times \sec A \tag{8-1}$$

A is the angle between the ray path and the radius vector at the point of entry into the bottom of the ionosphere. The distance from the center of the earth to the bottom of the ionosphere is the sum of the earth radius (a=6371.2 km) and ho, where ho is the first real height that occurs in the given electron density profile. The angle B is the angle subtended at the earth's center by the segment of the path from the transmitter (T) to the bottom of the ionosphere. Both of these angles, A and B, are determined geometrically.

To determine the path through the ionosphere, Snell's Law is applied in the form (*Davies [1990])*:

$$\mu_1 \sin A_m = \mu_2 \sin A2_{(m+1)} \tag{8-2}$$

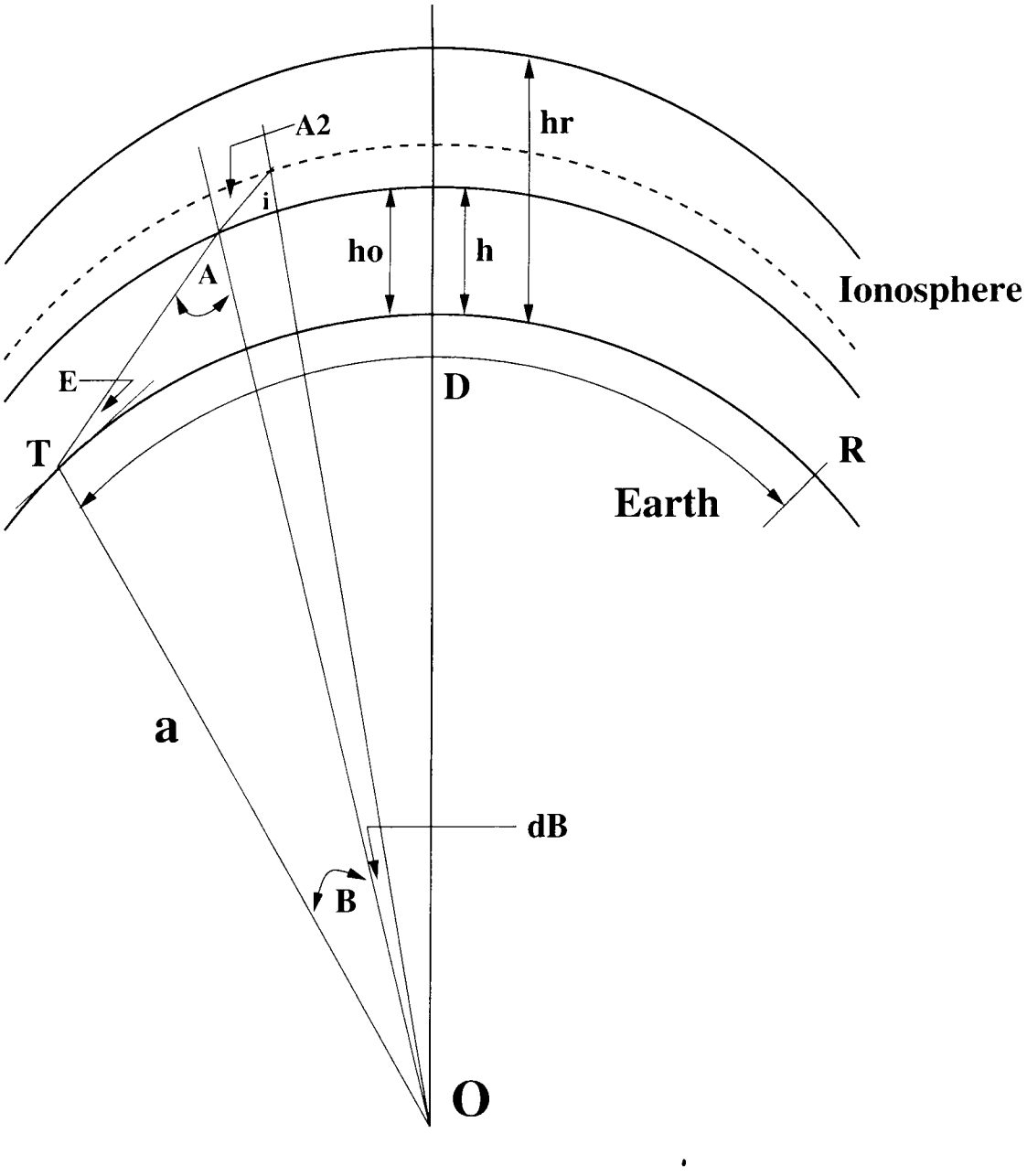

Figure 8-1: An illustration of the curved earth-ionosphere system used to determine the ray tracing algorithm. The ground range, D, is the distance from the transmitter to the receiver, which is the final output required from the algorithm.

The phase refractive index, μ, is dependent on the plasma frequency, fn, and is calculated, ignoring the effects of the magnetic field, (*McNamara [1991])* by

$$\mu^2 = 1 - \left(\frac{fn}{fr}\right)^2 \qquad (8\text{-}3)$$

From the bottom of the ionosphere, height=ho, to the height of reflection, hr, the ionosphere is divided into small height segments with a height increment, dh, of 0.02 km. For each segment, values for the angles, A2 and i, are determined using equation (8-2), where m is the current segment number, and geometry. Once these angles are known, the small angle, dB, which is subtended at the earth's center by the small segment, can be calculated. From the radian definition of the angle (*Ohanian [1985])*, the increase in ground range, dx, is determined as follows:

$$dx = a \times dB \qquad (8\text{-}4)$$

where a is the radius of the earth. This is repeated for each small segment until the height of reflection is reached, which is defined to be the height at which the value of sin A2 is greater than 1. The ray path is taken to be symmetrical about the height of reflection. A graph of altitude versus ground range is then plotted to illustrate the ray path, where altitude is the real height above the ground.

8.3 Ray Tracing Results

Chapter 7 demonstrated the differences between the IRI and LAM models. To further illustrate these differences, the ray tracing algorithm was applied to each of these model ionospheres. For a particular input set (DN, HR, R, A) each model predicted an electron density profile. The path of a radio wave through each of these model ionospheres, at a particular frequency and elevation angle, was then determined. It was found that there were significant differences in both the ground ranges and paths corresponding to the two different models.

Examples of the ray paths of a radio wave passing through the LAM and IRI model ionospheres are shown in figures 8-2, and 8-3. The paths are plotted as altitude versus ground range, where altitude is the height above ground level with the maximum altitude corresponding to the height of reflection. Ground range is the distance along the earth's surface from transmitter to receiver.

In figure 8-2, the input set is 12h00 SAST on a summer day at a medium level of solar activity. The elevation angle and radio frequency were chosen to be 20.0 degrees and 19.1 MHz respectively, which corresponded to reflection within the F2 layer. The difference in ground range between the LAM and IRI model ionospheres, expressed as a percentage of the LAM model ground range, was 33.6%.

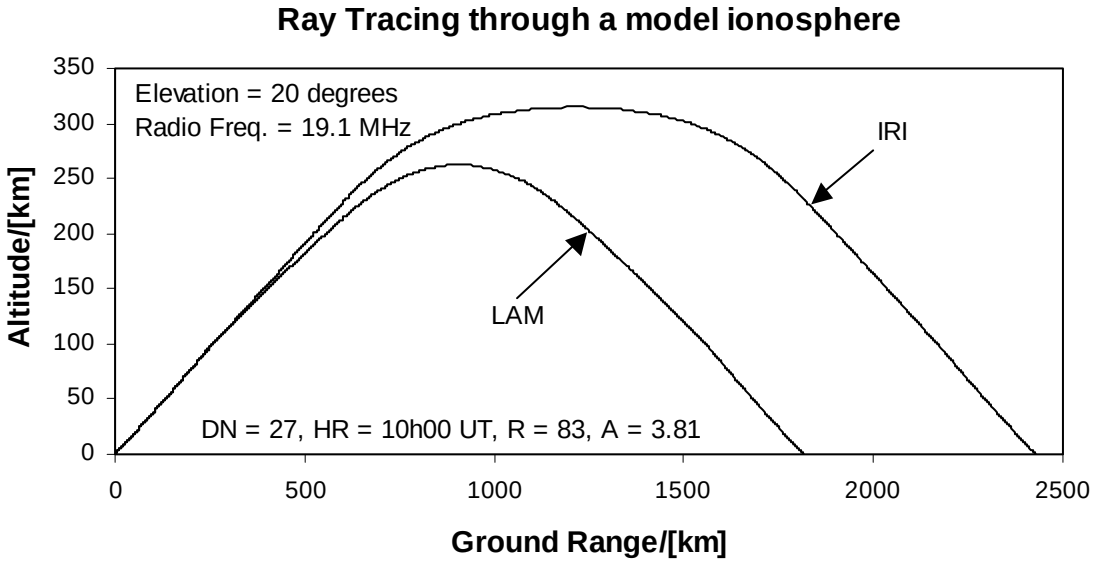

Figure 8-2: Ray tracing through the LAM and IRI model ionospheres, at a radio frequency that corresponded to a height of reflection within the F2 region. Identical input parameters produced different ground range values.

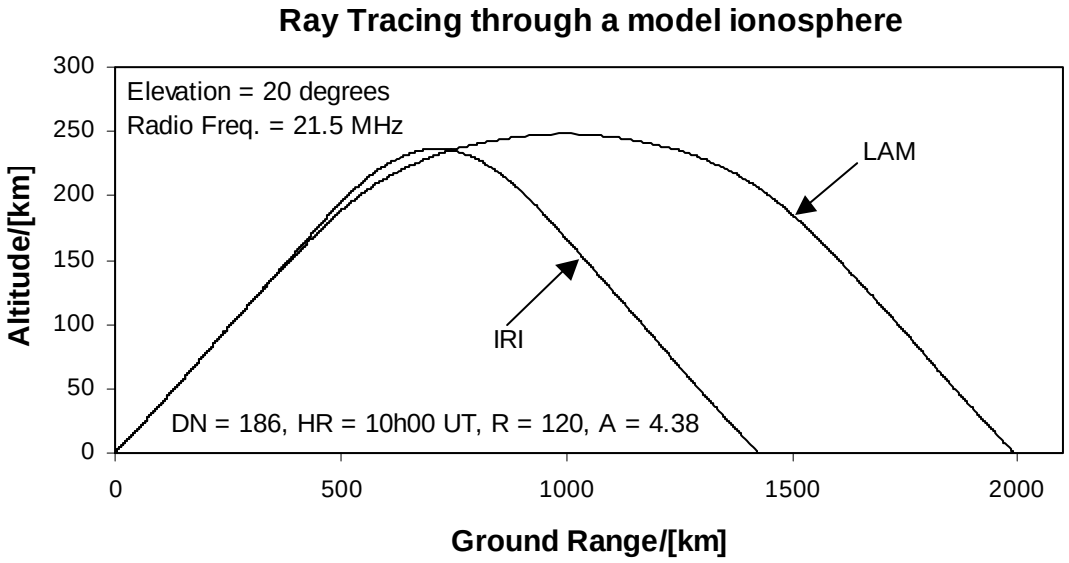

Figure 8-3: Another example of the difference between the LAM and IRI model ionospheres. Again identical input parameters produced a significant difference in ground range.

A second example is shown in figure 8-3, where the input set is 12h00 SAST on a winter day at high solar activity. The elevation angle and radio frequency were chosen to be 20.0 degrees and 21.5 MHz respectively. For this example, the difference in ground range between the LAM and IRI model ionospheres, again expressed as a percentage of the LAM model ground range, was 28.5%.

The LAM and IRI model profiles corresponding to the input sets used in figures 8-2 and 8-3 are illustrated with their corresponding actual DPS profiles in chapter 7, figure 7-7.

The LAM and IRI model ionospheres that were used in the figure 8-2 example are used again in figure 8-4, but this time the elevation angle and radio frequency were selected such that the height of reflection occurred within the F1 layer close to the critical frequency foF1. The difference in ground ranges corresponded to 26.7% of the LAM model ground range.

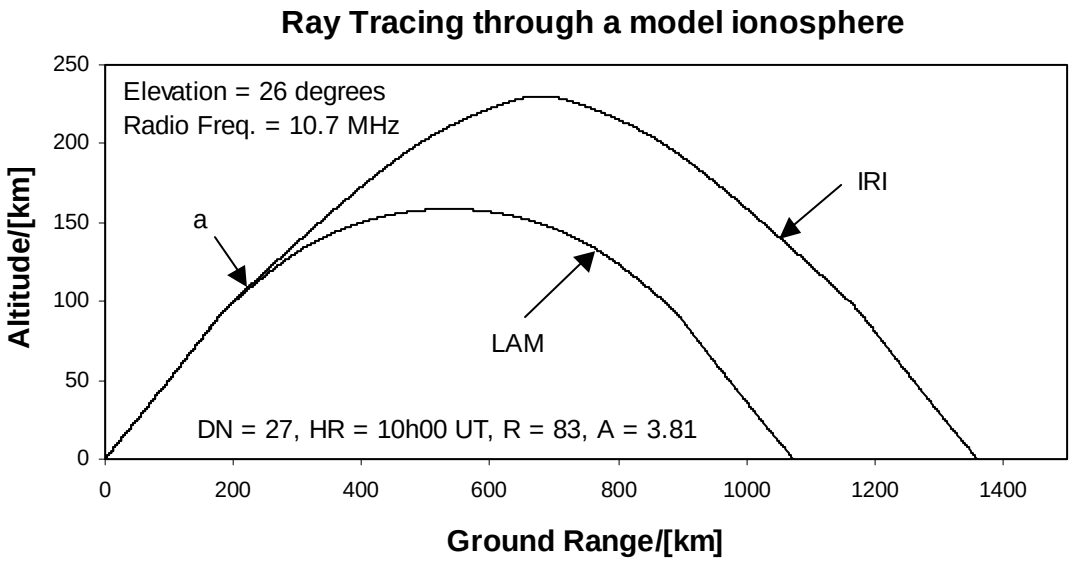

Figure 8-4: Ray paths through the LAM and IRI model ionospheres at an elevation angle and radio frequency that resulted in a height of reflection within the F1 region, close to foF1.

A radio wave traveling through the ionosphere is continuously refracted or bent towards the ground. The amount of refraction is controlled by the phase refractive index, μ, which depends on the radio frequency, fr, and the plasma frequency, fn (equation 8-3). In the case where fn is near in value to fr the index μ becomes significantly less than 1, which results in a noticeable bend in the ray path at a height lower than the height of reflection. This effect on the ray path is evident in figure 8-4 (the point is marked a on the graph), where fr was chosen to be 10.7 MHz and the plasma frequency at the height of reflection was 5.1 MHz. In figures 8-2, and 8-3, the values of fr chosen were significantly greater than the plasma frequencies at which reflection occurred, therefore, the ray paths in those cases were smooth at all heights.

Evidence of the effect that the LAM model smoothing technique (chapter 6, section 6-5) has on the model profile, is also visible when ray tracing. The smoothing technique was implemented in order to ensure a smooth continuous transition from the F1 layer to the F2 layer. Figure 8-5 illustrates the difference in ground range and ray path before and after the smoothing technique was applied. The difference in ground range in figure 8-5, expressed as a percentage of the ground range after smoothing, is 8.45%.

It seems reasonable in the light of the results presented in chapter 7 to deduce that the range determination using the LAM model is more accurate than that using the IRI.

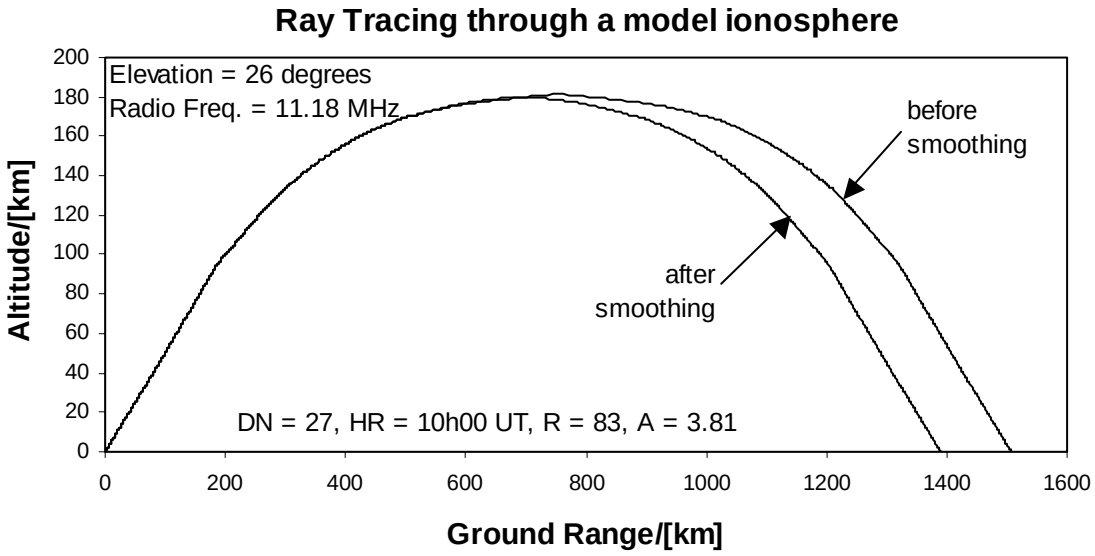

Figure 8-5: Ray paths through the LAM model ionosphere before and after the smoothing technique had been applied. The height of reflection is close to foF1.

The difference in ground range between the LAM and IRI model ionospheres is dependent on the two variables, elevation angle and radio frequency. To illustrate the extent of these differences, the ground ranges resulting from ray tracing through the LAM and IRI model ionospheres were determined for different combinations of these two variables. The difference in ground range, dD, was expressed as a percentage of the LAM model ground range, D(LAM), and calculated as follows:

$$\%dD = 100 \times \frac{D(IRI) - D(LAM)}{D(LAM)} \qquad (8\text{-}5)$$

where D(IRI) is the ground range determined by ray tracing through the IRI model ionosphere.

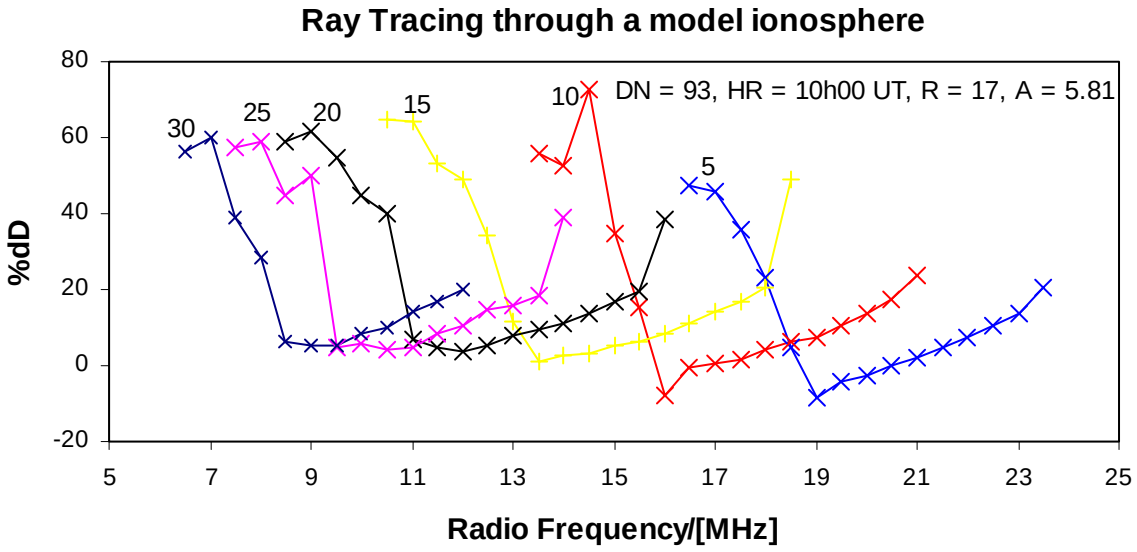

Figure 8-6: A graph of the percentage difference (%dD) in ground range between the LAM and IRI model ionospheres for various radio frequencies and elevation angles. The elevation angles, in degrees, are indicated on the graph as labels next to the relevant curves.

A graph of %dD versus radio frequency, fr, is shown in figure 8-6. The input set used for this illustration was 12h00 SAST on an autumn day at low R and A. The corresponding profiles for this input set are plotted in chapter 7, figure 7-7. For elevation angles from 5.0 degrees to 30.0 degrees in steps of 5.0 degrees, %dD was calculated for values of fr that ranged from f_b to f_e in steps of 0.5 MHz. The value of f_b is defined to be the first radio frequency at which the height of reflection occurs within the F region of the LAM model, and the value of f_e is defined to be the maximum possible radio frequency for which reflection will occur in either model ionosphere. The values of f_b and f_e depend on the elevation angle. Only reflection heights that occur within the F region of the LAM model have been considered for this illustration. The results from each elevation angle are shown in figure 8-6, where the values of the elevation angles are indicated as labels on the graph.

This graph illustrates the extent to which the LAM and IRI model ionospheres differ. In particular, the greatest %dD occurs in the F1 region, where the IRI model is known to be inadequate. For every elevation angle, the maximum radio frequency, f_e, occurred within the IRI model ionosphere, which indicates that reflection would have continued to occur at higher radio frequencies in the LAM model.

8.4 Direction Finding Systems

GrinTek Ewation (GEW) is a company that designs and builds direction-finding (DF) systems. These DF systems use the SSL technique to determine the location of remote transmitters. The success of this technique relies on the availability of accurate ionospheric data, with which to perform the ray tracing required for identifying the transmitter location.

In the first instance, the DF system makes use of the real-time data that is available from the three South African ionospheric stations, which are located in such a way as to optimize the coverage of the available data over the whole

country. However, this data is frequently unavailable, due to hardware and manpower problems and, therefore, the availability of a reliable ionospheric model is of particular importance.

At present the GEW DF systems make use of the IRI model ionosphere in the event that real-time data is unavailable. To test the DF systems, attempts are made to determine the location of known transmitters. During these tests, operators of these systems are reporting that the ground range determined when the IRI model ionosphere is used, misses the mark by approximately 30%. Since this is clearly not adequate, it is of extreme importance that a more accurate replacement is found for the IRI. This difference is in the right direction and is consistent with the differences between the IRI and the LAM model.

It has been shown in the previous chapters of this thesis that the LAM model is a better predictor of the Grahamstown ionosphere than the IRI. Therefore, the LAM model is a better candidate for replacing the IRI in the GEW DF systems.

It was hoped that results from implementing the LAM model into the GEW DF systems would be available for presentation in this thesis. Unfortunately due to software problems on the DF system side and time constraints, the implementation by GEW has not been completed yet. However, it is a future plan that the LAM model will replace the IRI in the GEW DF systems, thereby improving the accuracy of these systems for the South African region.

Chapter 9

CONCLUSION

9.1 The LAM Model – Version 2002

This thesis has described the development of the first version of the LAM model, a single station ionospheric model for the bottomside electron density profile. In addition to predicting the ionospheric behaviour over Grahamstown more accurately than the IRI, the LAM model has also provided elegant solutions to a few of the more troublesome problems that arise in ionospheric modelling. In particular, the probability of occurrence of an F1 layer can be predicted very easily.

The LAM model is available as a C++ program that requires as input the year, day number and hour in universal time (UT), e.g. year=2002, DN=180, HR=10h00 UT. The user has the option to enter the sunspot number (R) and magnetic index (A) as inputs instead of the year. Where the year has been given as an input, the required solar and magnetic indices are calculated using data that is provided in additional files.

The output from the LAM model program is available as a listing of frequency and height points, as used in the previous chapter, or as a description of the profile in terms of Chebyshev coefficients.

A block diagram of all the components that contribute to the LAM model, version 2002, is shown in figure 9-1.

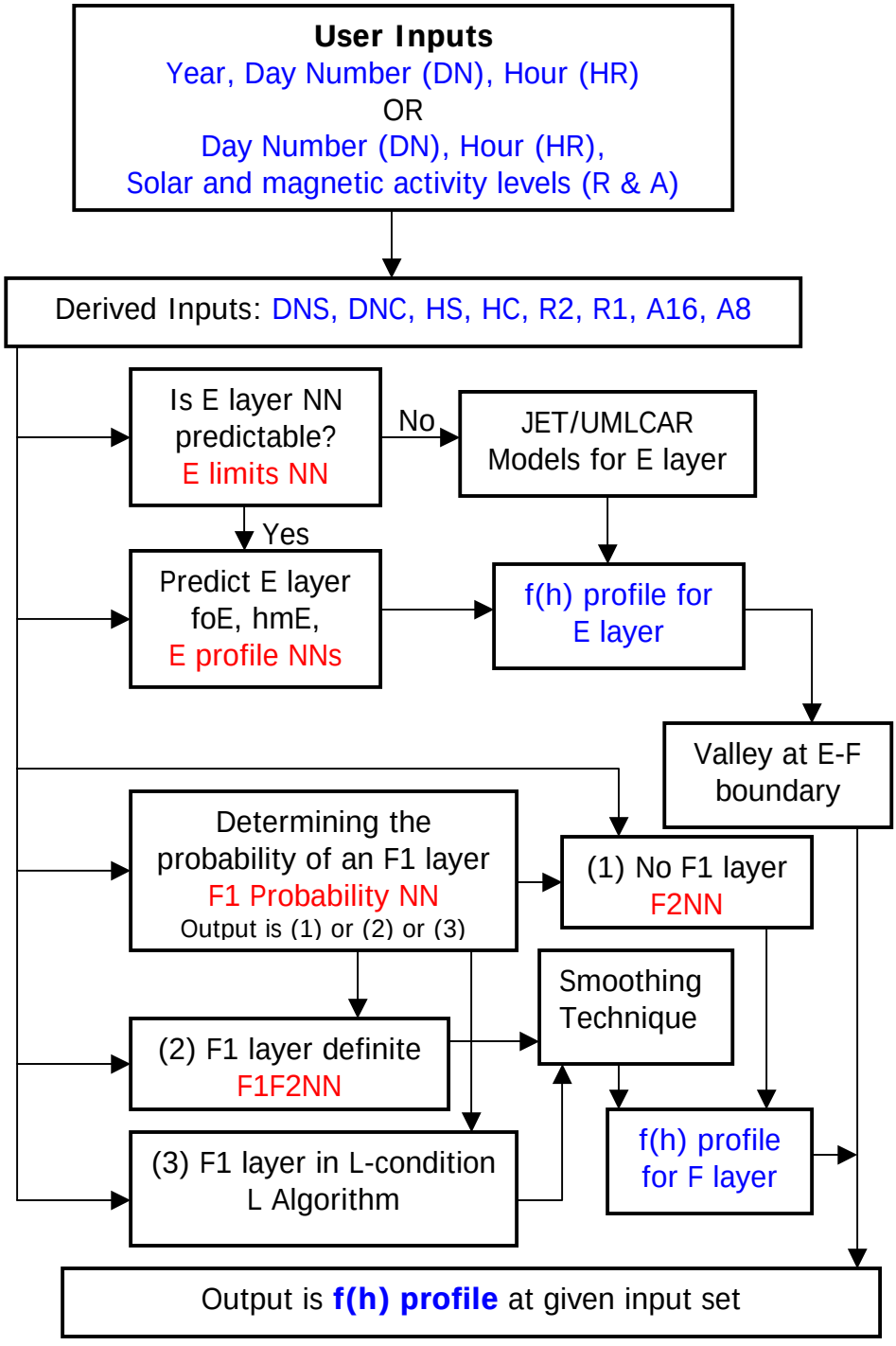

Figure 9-1: A block diagram depicting the process that the LAM model follows when predicting a profile for a particular set of inputs.

9.2 LAM Model Limitations

There are two main limitations that should be taken into account when using the LAM model. The first is the extent of the input space with which the model was developed. Two datasets were used for training and testing the neural networks (NNs) that contribute to this model, a 28-year dataset and a 5-year dataset. The difference between these two datasets arises from the ionospheric sounder and scaling methods that were used to record the data. To recap, the 28-year dataset consists of vertical chirpsounder (Verti) data that was manually scaled and only contains information on the critical frequencies and their virtual heights. In contrast, the 5-year dataset consists of Digisonde (DPS) data, which was scaled with the Artist scaling software and contains electron density profile information. Although the 28-year dataset was used wherever possible, the major contribution to the model came from using the 5-year dataset. The data from this 5-year dataset only covered one rising section of a solar cycle, from solar minimum to solar maximum and, therefore, the input space is particularly limited in the solar variation. This limitation does not affect the accuracy of the LAM model as long as the user remembers this limitation and does not interrogate the model with data for which it has not been trained.

The second limitation arises from the fact that the LAM model is a single station model. Only ionospheric data from the Grahamstown, South Africa ionospheric station were used in the development of the LAM model. Therefore, at this stage, the model is only valid for use in the Grahamstown area. In spite of this limitation, the LAM model can still provide a better indication of South African ionospheric behaviour than global ionospheric models. This is due to existing global empirical ionospheric models, such as the IRI, being based on little or no South African ionospheric data.

9.3 LAM Model Advantages

The LAM model is an empirical model that is neural network (NN) based. All available archived ionospheric data have been used in the development of this model. The major advantage of using NNs over other more conventional methods for ionospheric prediction lies in the ability of NNs to learn the relationships between the output and the input parameters without the need for additional user input.

Attempts to provide predictions of the more complicated ionospheric problems have proved successful in the LAM model. In particular, the F1 layer is predicted for the Grahamstown ionosphere with much more confidence than could be the case with the global ionospheric IRI model. The pioneering attempt to use NNs for predicting the probability of the existence of an F1 layer, as well as the prediction of the hours between which an E layer is measurable by a ground based ionosonde, have been very successful in the LAM model. These predictions are an additional advantage of the LAM model and prove the method of employing NNs to solve ionospheric prediction problems.

As well as predicting future ionospheric behaviour, the LAM model can also be used to investigate relationships between the input variables (day number, hour, solar and magnetic activity) and the electron density profile. Chapter 7 illustrated some of these relationships and compared the LAM model to the IRI. An aim in developing this model was to provide a better solution to predicting South African ionospheric behaviour than that of using the IRI model. It is clear from the results of chapter 7 that this aim has been met.

An additional advantage of the LAM model is that it is relatively easy to update the model when more data becomes available, thereby enlarging the input space and improving the ionospheric representation of the model.

9.4 Future Work and Conclusion

Future work includes updating the model as more data becomes available. The Grahamstown ionospheric station is continuing to collect and archive ionospheric data on a half-hourly basis. In order to improve the extent of the input space, the model requires updating with additional data from the Grahamstown station until at least 22 years of electron density profile data (one solar cycle) has been added.

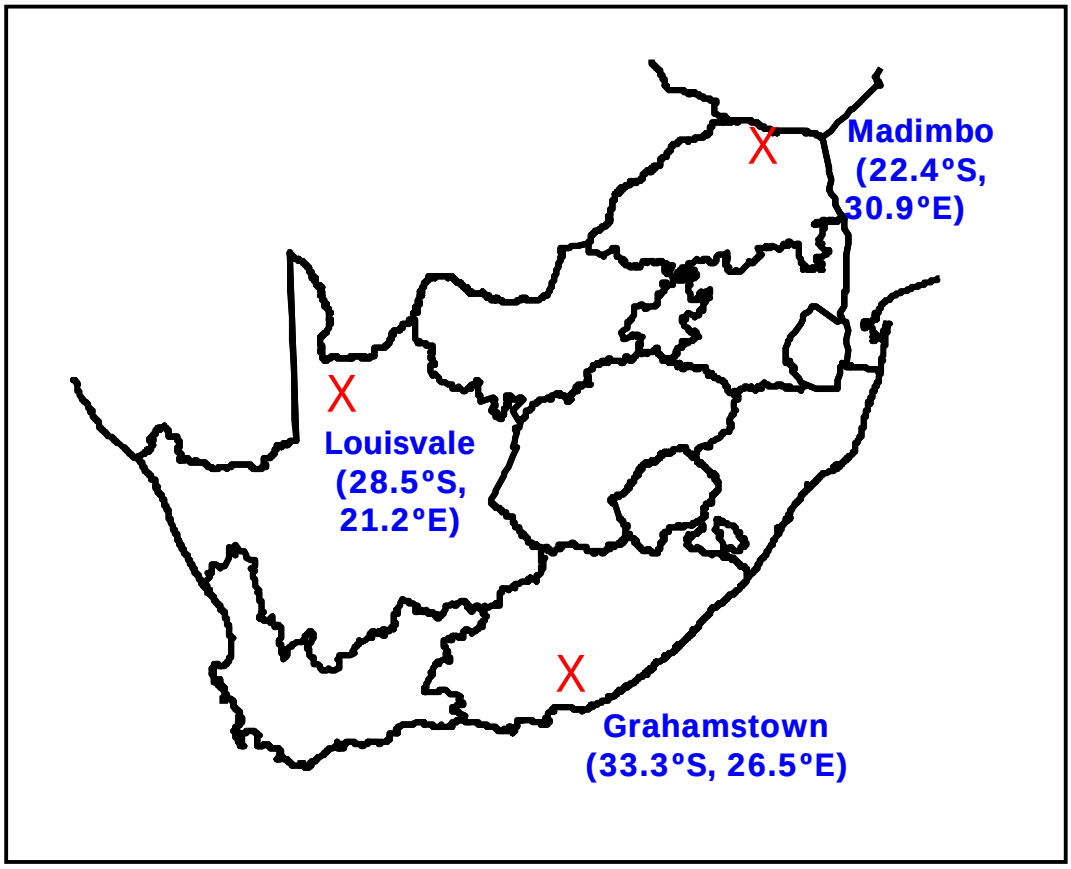

Figure 9-2: An illustration of a simple map of South Africa with the three South African ionospheric stations indicated. These stations are situated in such a way as to provide optimal coverage of the entire country.

As well as the Grahamstown station, South Africa has two additional ionospheric stations that are located in such a way as to optimize the ionospheric coverage over the entire country. These two stations are located at Louisvale (28.5ºS, 21.2ºE) in the Northern Cape province and Madimbo (22.4ºS, 30.9ºE) in the Limpopo province. The location of the three South African ionospheric stations is illustrated in figure 9-2.

The Louisvale and Madimbo stations have only been continuously collecting ionospheric data for one year. It is anticipated that as soon as sufficient data has been archived from these two stations, the LAM model will be expanded to include this data and will, therefore, become more representative of the entire South African ionosphere.

Future plans also include researching the F1 region in more detail. Although the LAM model provides an elegant solution to most of the F1 problems, it is felt that a research project that deals entirely with the scaling and predicting of the F1 layer is required. Working with the data while developing this LAM model, highlighted areas of the input space where the F1 layer is inadequately treated in the Artist scaling procedure. Since the Artist data was used in the development of the LAM model, all of the available F1 data requires re-scaling manually in order to check that the automatic scaling software has not compromised the model. This would also assist in improving the L algorithm and smoothing technique for future versions of the LAM model.

This new NN based ionospheric model, the LAM model, has been shown to provide more accurate descriptions for the electron density profile over Grahamstown than the global IRI model. Since the IRI is the most commonly used global ionospheric model, it is hoped that the LAM model can be used to assist the IRI community in improving the current model in the southern hemisphere. In particular, the method of employing NNs to the task of ionospheric prediction, as in the development of the LAM model, could be applied to any large ionospheric database where ionospheric prediction was required. Also, further relationships between potential input variables and an ionospheric

output could be investigated with relative ease. The IRI community has access to the worldwide data base of ionospheric records which would be required if this method is to be considered.

This thesis has described the development of a NN based ionospheric model for the bottomside electron density profile over Grahamstown, South Africa. This model provides accurate predictions of the electron density profile that are an improvement on the IRI. Allowance has been made for additions to the model that will ultimately expand and improve it even further. It is anticipated that the LAM model will prove invaluable to both the DF system operators of GrinTek Ewation and the worldwide ionospheric community.

REFERENCES

- Altinay O., Tulunay E., and Tulunay Y., Forecasting of ionospheric frequency using neural networks, *Geophys. Res. Let.*, **24**, pp.1467-1470, 1997.

- Bilitza D., *International Reference Ionosphere*, National Space Science Data Center, 1990.

- Bilitza D., International Reference Ionosphere – Status 1995/1996, *Adv. Space Res.*, **20**, 9, 1751-1754, 1997.

- Bilitza D., The E- and D- region in IRI, *Adv. Space Res.*, **21**, 6, pp.871-874, 1998.

- Bilitza D., Radicella S.M., Reinisch B.W., Adeniyi J.O., Mosert de Gonzalez M.E., Zhang S.R., and Obrou O., New B0 and B1 models for IRI, *Adv. Space Res.,* **25**, 1, pp. 89-95, 2000.

- Bilitza D., IRI-2001 now available from NSSDC, at URL http://nssdc.gsfc.nasa.gov/space/model/ionos/iri/irinfo/irinfo.html, retrieved August 2001.

- Bradley P.A., and Dudeney J.R., A simple model of the vertical distribution of electron concentration in the ionosphere, *J. Atmos. Terr. Phys.,* **35**, pp. 2131-2146, 1973.

- Chasovitin Y.K., Kashirin A.I., and Ivanova S.E., Algorithm for buildup of height profile of electron density in transition E-F region, *Adv. Space Res.,* **18**, 6, pp. 157-161, 1996.

- Davies K., *Ionospheric radio*, Peter Peregrinus Ltd, 1990.

- DuCharme E.D., Petrie L.E., and Eyfrig R., A method for predicting the F1 layer critical frequency, *Radio Science*, **6**, 3, pp. 369-378, 1971.

- Fausett L., *Fundamentals of neural networks*, Prentice-Hall Inc., 1994.

- Galkin I.A., *Standard Archiving Output (SAO) format,* at URL http://ulcar.uml.edu/~iag/SAO-4.htm, retrieved November 1998.

- Hafner J., Leitinger R., and Titheridge J., The E layer shape: the combination with existing models, *Phys. Chem. Earth (C)*, **26**, 5, pp.319-323, 2001.

- Haykin S., *Neural networks, a comprehensive foundation*, McMillan Publishing Company, Inc., 1994

- Huang X., and Reinisch B.W., Vertical electron density profiles from the digisonde network, *Adv. Space Res.*, **18**, 6, 121-129, 1996.

- Ivanov-Kholodny G.S., Kishcha P.V., and Zhivolup T.G., A mid-latitude E-layer peak height model, *Adv. Space Res.*, **22**, 6, pp.767-770, 1998.

- Kouris S.S., and Muggleton L.M., Diurnal variation in the E layer ionization, *J. Atmos. Terr. Phys.*, **35**, pp. 133-139, 1973.

- McKinnell L.A., *A new empirical model for the peak ionospheric electron density using neural networks*, Thesis approved for the Master of Science degree of Rhodes University, Grahamstown, 1996.

- McKinnell L.A., and Poole A.W.V., Ionospheric variability and electron density profile studies with neural networks, *Adv. Space Res.*, **27**, 1, pp.83-90, 2001.

- McKinnell L.A., and Poole A.W.V., A neural network based electron density model for the E Layer, *Adv. Space Res.*, submitted, 2002.

- McNamara L.F., *The ionosphere: communications, surveillance, and direction finding*, Krieger Publishing Company, 1991.

- McNamara L.F., and Reinisch B.W., Observations of the mid-latitude F1 region, *Adv. Space Res.,* **15**, 2, pp. 67-75, 1995.

- Muggleton L.M., A method of predicting foE at any time and place, *Telecommunications Journal*, 42, pp.413-418, 1975.

- Ohanian H.C., *Physics*, W.W. Norton & Company, Inc., 1985.

- Paul A.K., Use of virtual height slopes for determination of electron-density profiles, *Radio Science*, **2**, 10, 1967.

- Poole A.W.V., NHLO – A fortran program for converting vertical incidence ionograms into electron density profiles, *Private Notes*, 1985.

- Poole A.W.V., and McKinnell L.A., On the predictability of foF2 using neural networks, *Radio Science*, **35**, 1, pp.225-234, 2000.

- Radicella S.M., and Mosert de Gonzalez M., The calculation of the height of the characteristic point in the F1 layer, *Adv. Space Res.,* **11**, 10, pp. 93-95, 1991.

- Reinisch B.W., and Huang X., Automatic calculation of electron density profiles from digitial ionograms 3. processing of bottomside ionograms, *Radio Science*, **18**, 3, 477-492, 1983.

- Scotto C., Mosert de Gonzalez M., Radicella S.M., and Zolesi B., On the prediction of F1 ledge occurrence and critical frequency, *Adv. Space Res.,* **20**, 9, pp. 1773-1775, 1997.

- SNNS, Suttgart Neural Network Simulator user manual, Version 4.2, *University of Stuttgart, Institute for Parallel and Distributed High Performance Systems (IPVR)*, 1995a.

- SNNS, Suttgart Neural Network Simulator, retrieved 1998, at URL http://www-ra.informatik.uni-tuebingen.de/SNNS/, 1995b.

- Stanislawska I., Construction of the instantaneous n(h) profiles at single location, *Adv. Space Res.*, **25**, 1, pp.125-127, 2000.

- Titheridge J.E., Ionogram analysis with the generalised program POLAN, Report UAG-93, World Data Center A, Boulder, USA, 1985.

- Titheridge J.E., Starting models for the real height analysis of ionograms, *J. Atmos. Terr. Phys.*, 48, 5, 435-446, 1986.

- Titheridge J.E., Modelling the peak of the ionospheric E-layer, *J. Atmos. Solar-Terr. Phys.*, 62, 93-114, 2000.

- University of Massachusetts Lowell Center for Atmospheric Research (UMLCAR), *Digisonde Portable Sounder (DPS) system technical manual*, Version 4.0, 1996.

- Wakai N., Ohyama H., and Koizumi T., *Manual of ionogram scaling*, Radio Research Laboratories, Ministry of Posts and Telecommunications, Japan, 1985.

- Williscroft L.A., and Poole A.W.V., Neural networks, foF2, sunspot number and magnetic activity, *Geophys. Res. Let.,* **23**, 24, 3659-3662, 1996.

- Wintoft P., and Cander Lj.R., Short term prediction of foF2 using time-delay neural networks, *Physics and Chemistry of the Earth (C): Solar, Terrestrial, & Planetary Science*, **24**, 4, pp.343-347, 1999.